# AN INVESTIGATION OF SEISMIC FACE STABILITY OF DEEP TUNNELS BY USING AN AXISYMMETRIC FINITE ELEMENT MODEL

A THESIS SUBMITTED TO
THE GRADUATE SCHOOL OF NATURAL AND APPLIED SCIENCES
OF
MIDDLE EAST TECHNICAL UNIVERSITY

BY

HANNAH ELIZABETH HADLEY

IN PARTIAL FULFILLMENT OF THE REQUIREMENTS
FOR
THE DEGREE OF MASTER OF SCIENCE
IN
CIVIL ENGINEERING

MAY 2018

Approval of the thesis:

**AN INVESTIGATION OF SEISMIC FACE STABILITY OF DEEP TUNNELS BY USING AN AXISYMMETRIC FINITE ELEMENT MODEL**

submitted by **HANNAH ELIZABETH HADLEY** in partial fulfillment of the requirements for the degree of **Master of Science in Civil Engineering Department, Middle East Technical University** by,

Prof. Dr. Halil Kalıpçılar _____
Dean, Graduate School of **Natural and Applied Sciences**

Prof. Dr. İsmail Özgür Yaman _____
Head of Department, **Civil Engineering Dept., METU**.

Prof. Dr. Haluk Sucuoğlu _____
Supervisor, **Civil Engineering Dept., METU**.

Assoc. Prof. Dr. Mustafa Tolga Yilmaz _____
Co-Supervisor, **Engineering Sciences Dept., METU.**

**Examining Committee Members:**

Prof.Dr. Bahadır Sadık Bakır _____
Civil Engineering Dept., METU

Prof. Dr. Haluk Sucuoğlu _____
Civil Engineering Dept., METU

Prof.Dr. Ayşegül Askan Gündoğan _____
Civil Engineering Dept., METU

Assoc. Prof. Dr. Mustafa Tolga Yilmaz _____
Engineering Sciences Dept., METU

Dr. Ebru Akış _____
Civil Engineering Dept., Atılım Üniversity

**Date**: 8th of May 2018

**I hereby declare that all information in this document has been obtained and presented in accordance with academic rules and ethical conduct. I also declare that, as required by these rules and conduct, I have fully cited and referenced all material and results that are not original to this work.**

Name, Last name : Hannah Hadley

Signature :

# ABSTRACT

## AN INVESTIGATION OF SEISMIC FACE STABILITY OF DEEP TUNNELS BY USING AN AXISYMMETRIC FINITE ELEMENT MODEL

HADLEY, Hannah
Masters, Department of Civil Engineering
Supervisor: Prof. Dr. Haluk Sucuoğlu
Co-Supervisor: Assoc. Prof. Dr. Mustafa Tolga Yılmaz

May 2018, 96 pages

The static stability of tunnel faces has been widely studied, with the development of limit analysis and numerical modelling solutions. There has been limited research into seismic tunnel face stability. The aim of this study is to find the effect of seismic loading on tunnel face stability and suggest factors that could be used in design. A numerical model using the axisymmetric finite element method is developed to assess tunnel face stability under seismic loading. To verify the numerical analysis, it was compared with limit-analysis solutions of static tunnel face stability from literature. Earthquake forces were applied to the numerical model using the pseudo static method. Both drained and undrained behaviour of geological formations are considered in the numerical analyses. There was generally good agreement found between the numerical model and limit analysis solutions. The results suggest that seismic actions have a significant effect on tunnel face support pressure required for stability. The tunnel face support pressure necessary for stability was generally found to increase proportionally to the seismic coefficient. Using the results from the pseudo static analysis preliminary seismic design factors are proposed. The variation in tunnel face support pressure with seismic loading is generally small when compared to the uncertainty in the limit analysis solutions.

Keywords: Tunnel face stability, seismic loading, axisymmetric model, finite element.

# ÖZ

## DERİN TÜNEL AYNALARININ SİSMİK STABİLİTESİ ÜZERİNE EKSENEL SİMETRİK SONLU ELEMANLAR YÖNTEMİYLE BİR İNCELEME

HADLEY, Hannah
Yüksek Lisans Tezi, İnşaat Mühendislik Bölümü
Tez Danışmanı : Prof. Dr. Haluk Sucuoğlu
Yrd. Danışmanı: Doç.Dr. Mustafa Tolga Yılmaz

Mayıs 2018, 96 sayfa

Tünel aynalarının statik duraylılığı limit analizi ve sayısal yöntemlerle literatürde oldukça çalışılmıştır. Tünel aynalarının sismik duraylılığı üzerine ise çalışmalar oldukça kısıtlıdır. Bu çalışmanın amacı sismik yüklerin ayna stabilitesi üzerine etkilerinin anlaşılması ve tasarımda kullanılabilecek faktörlerin önerilmesidir. Bu amaçla eksenel simetrik sonlu elemanlar yöntemi ile sismik yükler altında ayna stabilitesi incelenmiştir. Doğrulama için sonuçlar literatürde sunulan limit analizi çözümleri ile karşılaştırılmıştır. Sayısal modele sismik yükler psödo statik olarak tesir ettirilmiştir. Jeolojik birimlerin hem drenajlı hem drenajsız davranış gösterdiği durumlar dikkate alınmıştır. Sayısal model ve limit analizi arasında uyumlu sonuçlar görülmüştür. Sonuçlar, tünel aynasının artan sismik yükler altında stabilitesinin sağlanabilmesi için ayna üzerindeki destek basıncının arttırılması gerektiği sonucuna varılmıştır. Psödo statik analizler sonucunda ön tasarım için sismik tasarım faktörleri belirlenmiştir. Ancak, destek basıncındaki bu değişimin limit analizleri sonuçlarında da görülen belirsizlikle de karşılaştırıldığında belirgin olmadığı sonucuna varılmıştır.

Anahtar kelimeler: Tünel ayna stabilitesi, sismik yükleme, eksenel simetrik model, sonlu elemanlar.

## ACKNOWLEDGEMENTS

I would like to especially thank:

My supervisors Assoc. Prof. Mustafa Tolga Yılmaz and Prof. Haluk Sucuoğlu for their support and trust supervising me during my thesis and, patiently assisting me to develop my research and writing abilities.

The MEEES institutions for all the opportunities and knowledge gained, this has widened and deepened my understanding of so many topics and made me feel more confident as an engineer

My colleagues in Prota Engineering, for their patience, assistance and contribution to my work. In particular, thanks to Ümit Kaçmaz, Serdar Karakoç, Başak Halaç and Göksu Hızıroğlu.

All my friends that I met during the MEEES program, for their joy and colour that they brought to my life during this program and the support that we gave to each other.

Finally, to my family for their support and encouragement to aim for my goals and achieve my dreams.

## TABLE OF CONTENTS

# LIST OF TABLES

TABLES

## LIST OF FIGURES

FIGURES

## LIST OF SYMBOLS

SYMBOLS

| | |
|---|---|
| $C$ | = Depth to top of tunnel (m) |
| $C/D$ | = Depth ratio |
| $c'$ | = Cohesion, drained analysis (kPa) |
| $C_S$ | = Coefficient for seismic design |
| $c_u$ | = Undrained shear strength(kPa) |
| $C_\varphi$ | = Coefficient for seismic design |
| $D$ | = Diameter of tunnel (m) |
| $D_0$ | = Disturbance factor of Hoek and Brown (1997) |
| $E$ | = Youngs Modulus (MPa) |
| $GSI$ | = Geological Strength Index of Hoek and Brown (1997) |
| $H$ | = Depth to centreline for tunnel |
| $K_A$ | = Active earth pressure coefficient |
| $k_h$ | = Seismic coefficient (g) |
| $K_O$ | = At rest earth pressure coefficient |
| $K_P$ | = Passive earth pressure coefficient |
| $m_i$ | = Strength parameter of Hoek and Brown (1997) |
| $N$ | = Stability ratio of Broms and Bennermark (1967) |
| $N_S$ | = Weighting coefficient of Leca and Dormieux (1990) |
| $N_S^{c-}$ | = Weighting coefficient for lower bound collapse of Leca and Dormieux (1990) |
| $N_S^{c+}$ | = Weighting coefficient for upper bound collapse of Leca and Dormieux (1990) |
| $N_\gamma$ | = Weighting coefficient of Leca and Dormieux (1990) |
| $N_\gamma^{c-}$ | = Weighting coefficient for lower bound collapse of Leca and Dormieux (1990) |
| $N_\gamma^{c+}$ | = Weighting coefficient for upper bound collapse of Leca and Dormieux (1990) |
| $Q_S$ | = Loading parameter of Leca and Dormieux (1990) |
| $Q_T$ | = Loading parameter of Leca and Dormieux (1990) |
| $Q_\gamma$ | = Loading parameter of Leca and Dormieux (1990) |
| $S_D$ | = Seismic design factor |
| $u$ | = Displacement (m) |
| $u_N$ | = Normalised displacement |
| $\alpha$ | = angle of failure cone to horizontal of Leca and Dormieux (1990) (°) |
| $\gamma$ | = Unit weight (kN/m$^3$) |

$\Sigma M_{stage}$ = PLAXIS stage multiplier

$\sigma_C$ = Unconfined compression strength (kPa)

$\sigma_{min}$ = Pressure below failure, used in FEM (kPa)

$\sigma_r$ = Radial stress (kPa)

$\sigma_S$ = Surcharge on ground surface (kPa)

$\sigma_T$ = Pressure on tunnel face (kPa)

$\sigma_{T_F}$ = Tunnel pressure at failure, used in FEM (kPa)

$\sigma_{T_N}$ = Normalised tunnel face support pressure

$\sigma_{T_{N\,Eq}}$ = Normalised tunnel face support pressure with earthquake loading

$\sigma_{T_{N\,Static}}$ = Normalised tunnel face support pressure with static loading

$\sigma_v$ = Confining pressure, used in FEM (kPa)

$\sigma_\theta$ = Tangential stress (kPa)

$\varphi$ = Friction angle (°)

$\varphi_0$ = Factor for frictional angle normalisation in seismic design

# CHAPTER 1

# INTRODUCTION

Tunnel face stability is an important consideration during the construction of tunnels (Leca and Dormieux, 1990). Damage can be caused inside the tunnel due to movement at the surface. There has been substantial investigation of static tunnel face stability. Earthquakes are also a major hazard in many areas. There are only a limited number of studies on the effects of seismic loading on tunnels and even less when looking at tunnel face stability specifically.

The typical layout of a tunnel heading is shown in Figure 1.1 (Mollon *et al*., 2013). The parameters used to describe the tunnel system are: $D$, the diameter of the tunnel, $C$, the depth from the ground surface to the top of the tunnel, $\sigma_T$, the pressure applied to the tunnel face during excavation, and $\sigma_S$, the surcharge on the ground surface. The depth and diameter are often combined into one dimensionless parameter, $C/D$, referred to as the depth ratio. Generally, two types of failure are considered. The first is collapse, shown in Figure 1.1a. This is when the material around the tunnel face moves into the tunnel. It is usually due to insufficient pressure applied to the tunnel face for stability during excavation. The second is blow out, shown in Figure 1.1b. In this case material in front of the tunnel face is pushed away towards a free boundary, the surface. This is usually due to excess tunnel face support pressure. For stability, the tunnel face support pressure must be between these two failure limits. Depending on the type of material and the speed of excavation the behaviour of the material can change. Two different types of material strength parameters are considered, for undrained and drained analysis (Atkinson, 2007). Undrained analysis is used for short term or fast loading and is based on the principles of constant-volume shearing of saturated geological materials. Total stress parameters, such as the undrained shear strength, $c_u$, are used with no seepage. Drained analysis is used for long term or slow loading. Effective stress parameters, such as effective friction, $\varphi$, and effective cohesion, $c'$, are used with steady state seepage. The distribution of pore-water

pressure around the tunnel is of concern in a drained analysis. The driving forces for instability are due to the weight of the geological mass above the tunnel face, which should be supported during excavation. Figure 1.1. The mobilization of this mass may cause severe ground subsidence in urban areas. Hence, the effect of a possible seismic event on face stability can be important for construction of tunnels beneath cities. There has been a substantial amount of investigation of tunnel face stability in the static case but there is very limited information on the effect of seismic loading on tunnel face stability (Saada *et al.*, 2013). Hence, this study aims to investigate tunnel face stability under seismic loading.

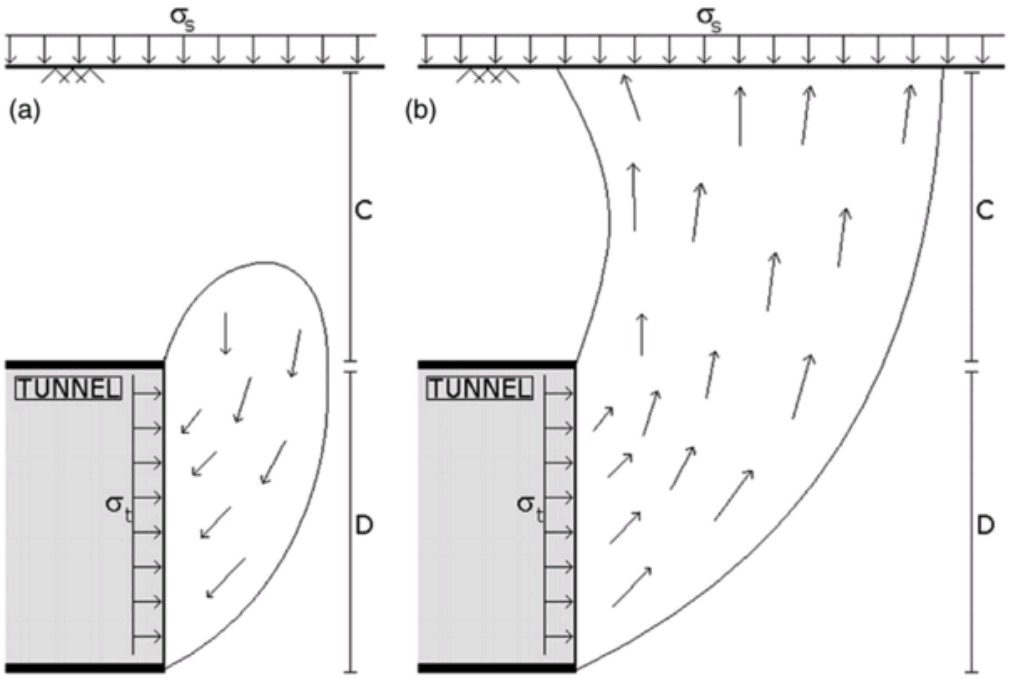


Figure 1.1 Typical tunnel face stability failure a) collapse, and b) blow out (Mollon et al., 2013)

In this study, the effect of seismic loading on tunnel face stability is investigated. An axisymmetric Finite Element Method (FEM) model has been developed to model the effect. It is important that the axisymmetric FEM model can adequately reflect tunnel face stability as any imprecision in the static solution can erroneously impact the seismic results. To ensure precision, a review of static limit analysis solutions has been

undertaken. The limit analysis solutions are used to verify the results from the static axisymmetric FEM solution. Inconsistencies found in the development and verification of the static solution are considered when discussing the seismic results. Seismic stability is investigated by applying a pseudo static force to the axisymmetric FEM model. The results from the seismic axisymmetric FEM solution are compared to previous results of seismic tunnel face stability using limit analysis. Finally, preliminary seismic design factors are proposed for tunnel face stability.

## 1.1 Literature Review

The static behaviour of tunnel face stability must be understood before the study of the dynamic response. To do this, existing solutions for tunnel face stability using limit analysis have been reviewed. These are also important to verify the outputs of the axisymmetric FEM model before seismic loading is applied. The use of numerical modelling for tunnel face stability has been revived. This is used as a guide in the development of the axisymmetric FEM model. Finally, a previous investigation on tunnel face stability behaviour under seismic conditions is reviewed.

### *1.1.1 Limit Analysis of Tunnel Face Stability*

The existing solutions for tunnel face stability using theoretical methods based on limit analysis are summarised below. The solution of plastic problems is mathematically very difficult to find. Limit analysis is used to reduce the problem, by considering static and kinematic equilibrium separately. In limit analysis, upper (kinematic equilibrium) and lower (static equilibrium) bounds are used to create a boundary within which failure will occur (Atkinson, 2007). A theoretical upper bound solution is calculated by ignoring equilibrium of forces and is a solution developed by considering the kinematics of collapse due to yielding material. A lower bound solution is calculated by ignoring the kinematic compatibility and is a solution developed by considering the limits of static equilibrium before collapse. In tunnel face stability the upper bound solution gives a smaller, or less safe, value for tunnel face support pressure than the lower bound solution. There are two main behaviours considered in tunnel face stability; drained and undrained. These are discussed below with proposed limit analysis solutions.

There have been many studies on the tunnel face stability in undrained, material since the development of Broms and Bennermark (1967)'s stability criteria (cited by Davis *et at.*, 1980). These criteria and the results of experimental testing by Mair (1979) were used in the analysis of Davis *et at.* (1980). They developed solutions for three cases of failure and proposed upper and lower bounds for failure. These solutions were limited to shallow tunnels with constant strength. More recent developments have been made to include more complexity in solutions. Wilson *et at.* (2011) developed a solution for unlined tunnels by considering linearly increasing shear strength with depth. Huang and Song (2013) suggest an upper bound solution for undrained geological materials by considering linearly increasing strength.

Leca and Dormieux (1990) developed upper and lower bound solutions for collapse in a drained, Mohr-Coulomb, material. The solution is developed for a tunnel in a uniform geological material above a water table. Chambon and Corté (1994) carried out centrifuge testing (cited by, Leca and Dormieux 1990). It was found that the mass mobilised during failure was typically bulb shaped. The tunnel face support pressure at failure was also found to be generally independent of depth. A number of improvements to the upper bound solution have been made. Sozio (2005) proposed 3D prism shapes that can be extended to φ'=0 conditions. Zhang *et at.* (2015) used 2D numerical modelling to propose an improved failure mechanism and then developed an updated lower bound limit analysis solution. The new proposed 3D failure mechanism consists of several cones and a load from an ellipsoid applied to the top of the cones. Typically, the improved solutions do not improve the upper bound significantly when compared to the gap between the lower and upper bound solutions of Leca and Dormieux (1990). Lee *et at.* (2003) included the aspects of seepage in the analysis by proposing to add seepage forces from ground water to the stability analysis developed by Leca and Dormieux (1990). The seepage forces from numerical modelling are added to the original solutions to get an updated solution for tunnel face stability. Perazzelli *et at.* (2014) investigate adding the results of seepage analysis to a limit equilibrium model. They developed dimensionless charts for quick analysis of tunnel face stability under seepage conditions. Lu *et at.* (2014) proposed a new upper bound solution. The failure shape was found using FEM. A new limit equilibrium solution was proposed for the updated failure shape. The application was widened to

include the addition of seepage forces and pore pressure distribution computed by FEM.

### *1.1.2 Numerical Modelling of Tunnel Face Stability*

Numerical models employ rigorous constitutive relationships of soil behaviour In the FEM it is assumed that the differential equations are solved approximately. Polynomials are used to approximate the displacement field in a finite section of continuum (Potts and Zdravkovic, 2001). All engineering problems are 3D problems, with axes in three directions, particularly tunnels. Simplification can be necessary to reduce the complexity and processing time of a problem. The assumption of plane strain or axisymmetric conditions can reduce the problem to a 2D problem.

The 3D FEM can be used to model the tunnel, the surface, and a circular tunnel face as well as interactions between them but requires larger amounts of computing cost, Lee *et at.* (2003) used the 3D FEM to investigate the effect of seepage on tunnel face stability. Plane strain is useful if multiple tunnels are being analysed, if ground effects are important or to model the tunnel face as a wall. It cannot be used to model multiple tunnels and the tunnel face at the same time. Lu *et at.* (2014) used the 2D FEM to investigate stability and seepage effects at the tunnel face. A Fourier series added FEM model builds a simplified 3D model where material properties, stresses and boundaries can vary with rotation (Shin, *et at.*, 2002). As well as the FEM, the finite-difference method can be used to model tunnels. Zhang *et at.* (2015) used the 3D finite difference method to model the failure shape at the tunnel face.

Axisymmetric FEM modelling can be used for tunnels if a single deep tunnel is being investigated and surface effects are not important (Potts and Zdravkovic, 2001). Hoek (2001) used an axisymmetric model to estimate the inward displacement of the tunnel face and radial displacement due to support pressure reduction of an unlined tunnel in squeezing ground. Shalabi (2005) used an axisymmetric model to analyse the effects of two soil creep models on tunnel behaviour. Suzuki (2000) used axisymmetric FEM to model the seismic interactions between a tunnel body, isolation layer and surrounding soil.

### *1.1.3 Seismic Stability of Tunnels*

The investigations of seismic design and response of tunnels is limited compared with the studies on the static case. A number of studies of seismic stability of tunnels have been completed. These often consider the stability of the tunnel lining after construction is completed. Suzuki (2000) investigated seismic interactions between a tunnel, isolation layer and surrounding material. Hashash *et al.* (2001) and Hashash *et al.* (2005) summarised and improved the practical methods used in the estimation of seismic effect on underground structures. Sahoo and Jyant (2012) analysed the stability of a long unsupported circular opening with pseudo static forces using a plane strain FEM model. Argyroudis *et al.* (2007) developed a methodology for vulnerability assessment in shallow metro tunnels. A few case studies of tunnel collapse due to earthquake have been carried out. One is an investigation of the Bolu tunnel collapse, caused during construction by the 12 November 1999 Düzce earthquakes (Üçer, 2012). However, there is very limited information available for seismic effects specifically on tunnel face stability. The paper by Saada *et al.* (2013) is one of the few available studies investigating the effects of seismic loading on tunnel face stability. They estimate a lower bound for collapse load using the kinematic limit analysis methods and the pseudo static approach. The Hoek-Brown failure criterion can be used to define the shear strength of rock (Hoek and Brown, 1997, Hoek *et al.*, 2002). The effect of the Hoek-Brown failure criterion on tunnel stability for static and seismic loading is investigated.

## 1.2 Scope

The scope of this thesis is to investigate the effects of seismic load on tunnel face stability. To investigate this effect an axisymmetric FEM model has been developed in PLAXIS[1]. The major stages of this investigation are:

- A review of exiting literature, focusing on two tunnel face stability solutions using limit analysis, axisymmetric FEM modelling of tunnels, and seismic tunnel face stability.

[1] PLAXIS Version 2017.01

- Development of a spreadsheet for the calculation of tunnel face stability using limit analysis solutions.

- Development of an axisymmetric FEM model of tunnel face stability in PLAXIS.

- Verification of the model by comparing static results from the axisymmetric FEM solution with static limit analysis solutions.

- Application of seismic loading to the axisymmetric FEM model. Seismic loading is applied using pseudo static analysis.

- Comparison of pseudo static results from the seismic tunnel face stability solution and axisymmetric FEM solution.

- Development of seismic design parameters for tunnel face stability.

Analysis has been completed for both drained and undrained analysis. For simplicity, and to exclude confounding effects, the material strength parameters are taken as constant in each model. The tunnel is assumed to be above the water table in the drained analysis. The effects of any seepage are ignored in the undrained analysis. The simplification of the problem to an axisymmetric solution is only valid for deep tunnels. Pseudo-static analysis has been used to estimate earthquake effects. Vertical seismic forces are neglected.

# CHAPTER 2

# THEORY REVIEW

In this section a detailed review of selected tunnel face stability solutions, axisymmetric FEM modelling of tunnels and seismic tunnel face stability has been completed. First two limit analysis solutions are reviewed, one undrained and one drained. It is important to ensure that the axisymmetric FEM solution accurately models tunnel face stability. The limit analysis solutions are important for the verification of the axisymmetric FEM solution. The set up and assumptions used to develop previous axisymmetric FEM models of tunnels are summarised. Finally, there is a review of a previous investigation of seismic tunnel face stability.

## 2.1 Limit Analysis Solutions for Tunnel Face Stability

Two limit analysis solutions have been reviewed. They are used in the verification of the static results from the axisymmetric FEM solution. One is for the undrained case and the other is for the drained case. Only the failure due to collapse has been covered in detail.

### *2.1.1 Review of Davis et at. (1980)'s Solution*

Davis *et at.* (1980) present a lower and an upper bound solution for undrained analysis of tunnel face stability, giving both collapse and blow out solutions. The geological material surrounding the tunnel was assumed to be uniform. The problem was idealised as shown in Figure 2.1. It was defined using the dimensionless parameters $C/D$ , $P/D$ , $\gamma D/c_u$ , and $(\sigma_s - \sigma_T)/c_u$ The solution was presented for $C/D \leq 5$ but it is stated that solutions may be used with confidence when $C/D \leq 3$. The stability ratio, $N$, developed by Broms and Bennermark (1967), and cited by Davis *et at.* (1980), was used to represent tunnel stability;

$$N = [\sigma_s - \sigma_T + \gamma(C + D/2)]/c_u \qquad (2.1)$$

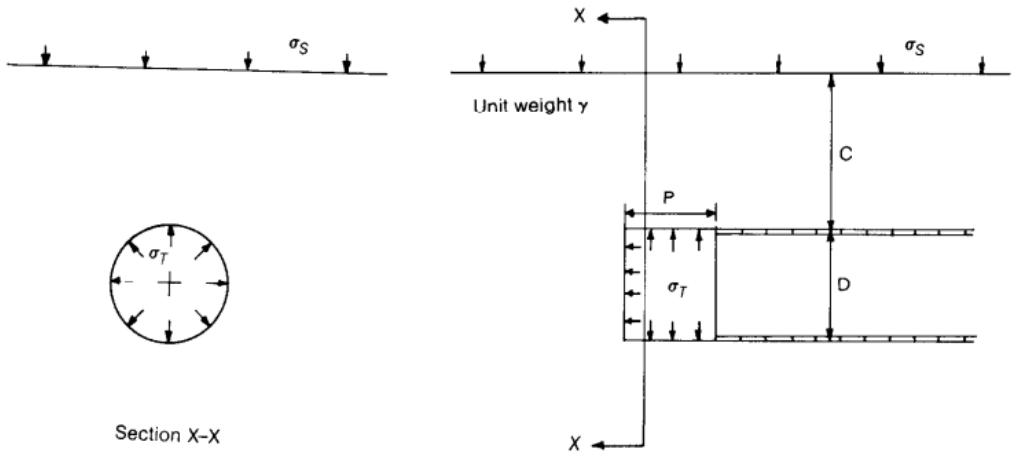


Figure 2.1 Idealisation of tunnel (Davis et at., 1980)

The solution was presented for collapse and blow out. For collapse, three cases were considered as well as local failure of the face. Lower and upper bounds were presented for each solution. Only the solutions for the case of collapsing face are reviewed.

Case 1 was a plane strain unlined tunnel, configuration shown in Figure 2.2a. This is the case of a long unlined cylindrical cavity. This case is only partly related to tunnel pressure stability. It is the critical case when $P/D$ in Figure 2.1 is very large. Two lower bound stress fields were considered. The first had weightless soil. An axially symmetric stress field was created around the opening, with the outer boundary touching the ground surface. Outside this the stress field was isotropic. The second stress field had a unit weight greater than zero and the stress field was developed using a computer programme. The upper bound considered four mechanisms of roof and side wall collapse. Figure 2.2b shows the upper and lower bounds for different values of $\gamma D/c_u$, the stability ratio is plotted against $C/D$ for case-1. It can be seen that there was a wider spread with $\gamma D/c_u$ at lower values of $C/D$.

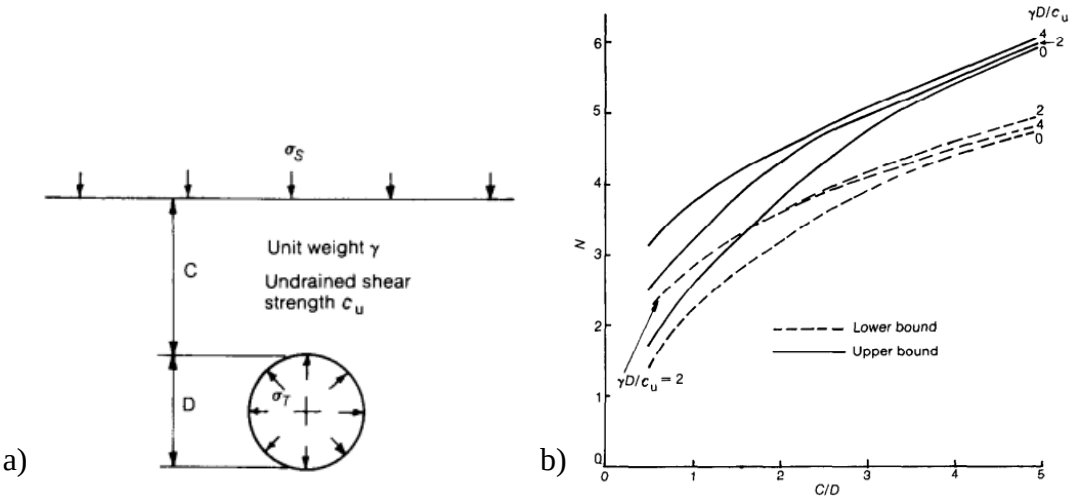


Figure 2.2 Case-1 – plane strain unlined tunnel a) configuration, and b) upper and lower bound stability solution (Davis et at., 1980)

Case 2 was solved by a plane strain model, configuration shown in Figure 2.3a. This is the case of an underground wall excavation. In the longitudinal section, the model is the same as the pertinent section in a three-dimensional model of a tunnel. But due to the prismatic continuity of the section's geometrical properties in out-of-plane direction, the face extends as a long wall, it is not circular. Lower and upper bound solutions were found for the case where $\gamma D/c_u = 0$. The lower bound solution was constructed of three and four sided areas of constant stress at or below yield. These are extended outward from the top and bottom of the heading. The shear load is transmitted from the soil to the lining. Using a smooth lining a lower bound solution for support pressure at failure was found to be;

$$(\sigma_s - \sigma_T)/c_u = 2 + 2\ln(C/D + 1) \qquad (\ 2.2\ )$$

A lower bound solution using a rough tunnel lining was also found. This was calculated for a number of values of $C/D$. The relationship was interpolated between these points.

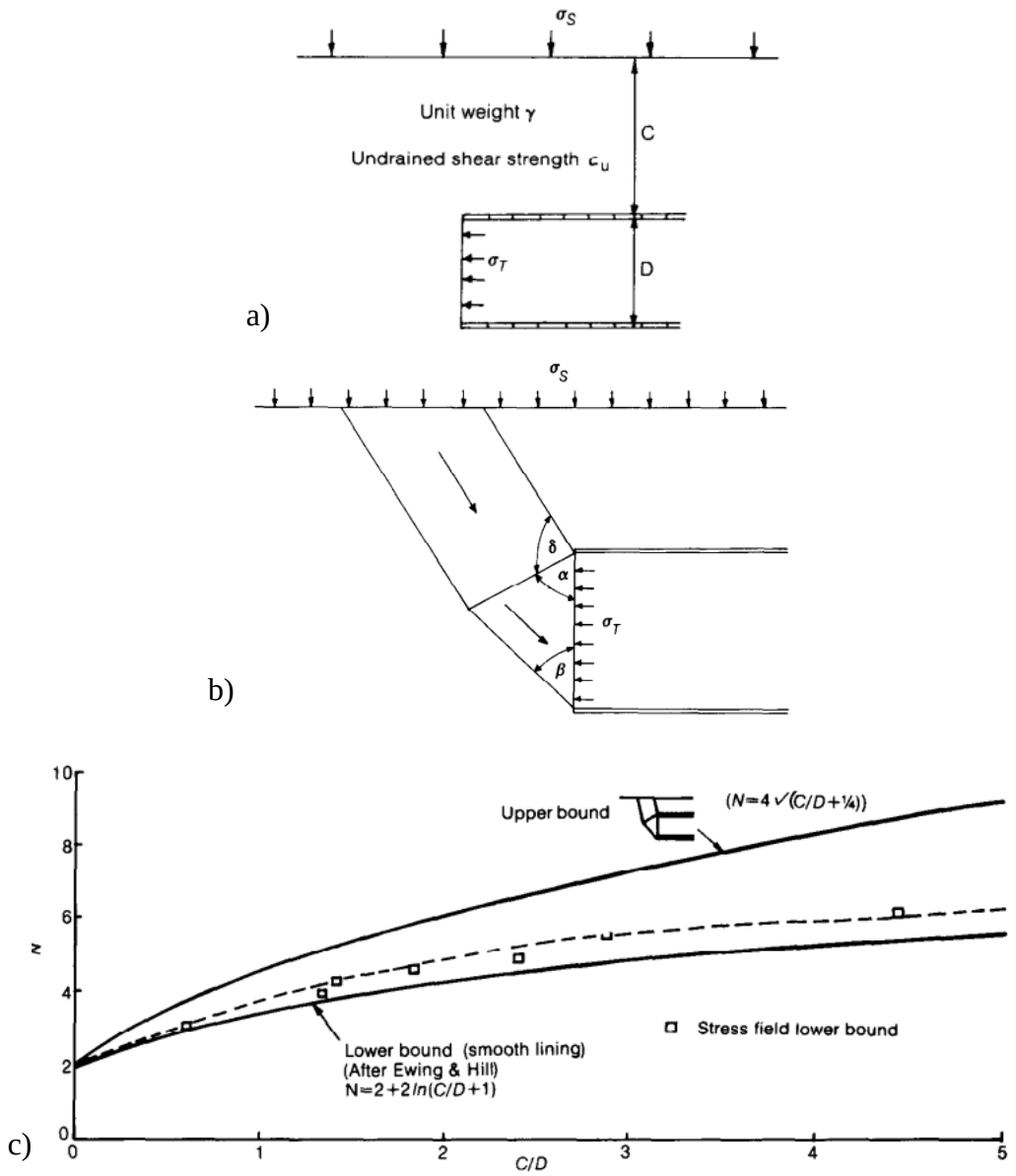


Figure 2.3 Case-2 – plane strain heading a) configuration, b) upper bound failure mechanism, and c) upper and lower bound stability solution (Davis et at., 1980)

The upper bound was comprised of a two block mechanism as shown in Figure 2.3b. It was optimised with respect to the three angles. An upper bound solution for support pressure during collapse was found to be;

$$(\sigma_s - \sigma_T)/c_u = 4\sqrt{(C/D + \frac{1}{4})} \qquad (\ 2.3\ )$$

A lower bound solution using a rough tunnel lining was also found. This was calculated for a number of values of $C/D$. The relationship was interpolated between these points. The upper bound was comprised of a two block mechanism as shown in Figure 2.3b. It was optimised with respect to the three angles. An upper bound solution for support pressure during collapse was found to be;

$$(\sigma_s - \sigma_T)/c_u = 4\sqrt{(C/D + \frac{1}{4})} \qquad (\ 2.4\ )$$

The solutions were extended to include the case where $\gamma D/c_u > 0$. A lower bound solution was found to be;

$$N = 2 + 2\ln(C/D + 1) \qquad (\ 2.5\ )$$

And an upper bound solution was found to be;

$$N = 4\sqrt{(C/D + \frac{1}{4})} \qquad (\ 2.6\ )$$

The results of the extension to $\gamma D/c_u > 0$ are shown in Figure 2.3c. The case-2 lower and upper bounds of $N$ as $C/D$ is varied are plotted. It can be seen that the bounded area for failure increases as $C/D$ increases. Also, the lower bound solution found using a rough lining gave slightly higher values of $N$.

Case-3 was a tunnel with a circular heading. This is considered the Broms and Bennermark problem as cited by Davis *et at.* (1980). The configuration is the same as Figure 2.1 when $P/D = 0$. This case is the closest to the real tunnel face stability problem. Two lower bound stress fields were considered. The first stress field was referred to as thick cylinder. The solution consisted of two cylinders with an axis at

the centre of the tunnel. The stress field of the inner cylinder had an axial stress of $\sigma_T$ and radial stress of $\sigma_T + 2c_u$, so that the ground was at yield everywhere. This was surrounded by the second cylinder. A solution with radial stress of $\sigma_r$, tangential stress of $\sigma_\theta$ , and longitudinal stress of $\sigma_z$ were derived assuming the ground was at yield. Outside the second spherical stress field there was an isotropic stress field of $\sigma_s$. A lower bound solution for support pressure at failure was found to be;

$$(\sigma_s\text{-}\sigma_T)/c_u = 2+2\ln(2\,C/D+1) \qquad (\ 2.7\ )$$

The second stress field was referred to as a thick sphere. The mechanism was spherically symmetrical around the centre of the tunnel face. Stresses were isotropic inside a hemispherical cap on the tunnel face, $\sigma_T$. This was surrounded by a sphere. The radial stresses of $\sigma_r$ and tangential stress of $\sigma_\theta$ were derived assuming the ground was at yield as with SII. Outside the sphere there was an isotropic stress field of $\sigma_s$. A lower bound solution was found to be;

$$(\sigma_s - \sigma_T)/c_u = 4\ln(2\,C/D + 1) \qquad (\ 2.8\ )$$

An upper bound solution consisted of a two block mechanism. This is the same mechanism as shown in Figure 2.3b but with elliptical cross sections. It was optimised with respect to the three angles. The solutions were extended to include the case where $\gamma D/c_u > 0$. Lower bound solutions were found to be;

$$N = 2 + 2\ln(2\,C/D + 1) \qquad (\ 2.9\ )$$

And;

$$N = 4\ln(2\,C/D + 1) \qquad (\ 2.10\ )$$

The results of the extension to $\gamma D/c_u > 0$ are shown in Figure 2.4. The case-3 lower and upper bounds of $N$ as $C/D$ is varied are plotted. It can be seen that there was a wider spread with $\gamma D/c_u$ at lower values of $C/D$ . The bounded area for failure increases as $C/D$ increases. This larger gap is attributable to the increased complexity of extending the problem to 3D.

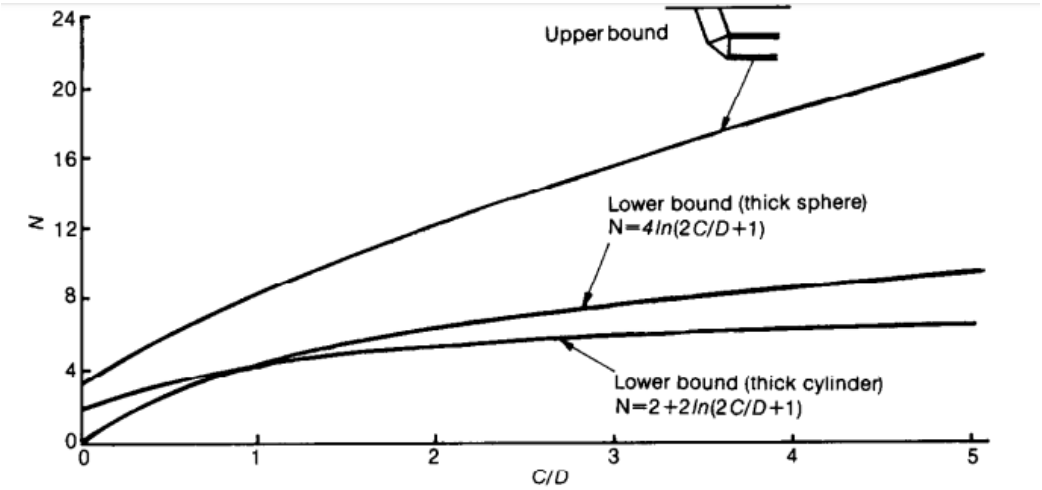


Figure 2.4 Case-3 – circular tunnel heading upper and lower bound stability solution (Davis et at., 1980)

The final collapse case was local collapse. When the ratio $\gamma D/c_u$ is large enough, partial collapse of the tunnel face will occur for any tunnel face support pressure. An optimised upper bound solution for $\gamma D/c_u$ was found to be 8.71, 8.28 and 10.96 for the mechanisms a, b, and c respectively in Figure 2.5. Failure would not cause immediate settlement at the surface but progressive failure that propagates to the surface is likely to occur. The best lower bound solution proposed was developed using Pastor (1978)'s lower bound for a vertical cut in cohesive soil as cited by Davis *et at.* (1980). The stress field is shown in Figure 2.5d. The heading was found to be stable for;

$$\gamma D/c_u \leq 5.63. \qquad (2.11)$$

When;

$$\sigma_T = \gamma(C + 0.355D) \qquad (2.12)$$

The tunnel dimensions when failure occurs are independent of $C/D$.

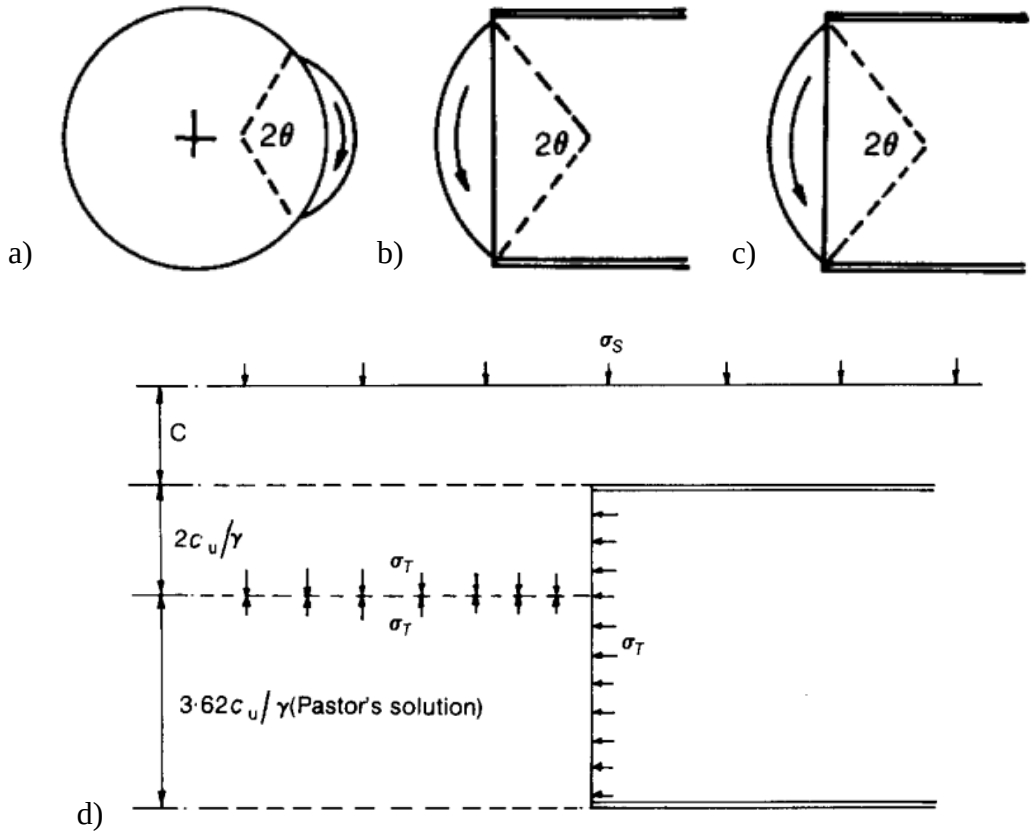


Figure 2.5 Local collapse– upper bound collapse a) plane strain circular tunnel, b) plane strain tunnel heading c) 3D circular tunnel heading, and d) lower bound stress field for local collapse (case-2) using Pastor's solution (Davis et at., 1980)

The results suggest that higher tunnel pressure is required for an unlined tunnel than a tunnel excavated using a TBM or shield. Case-1 requires a higher pressure than case-2 or case-3. It was found that the critical value of $N$ varies significantly with $C/D$. The results were compared to experimental testing carried out by Mair (1979). It was found that the tunnel face failure pressure on unlined tunnels was within the upper and lower bound solutions found in case-1. Testing on model tunnel headings showed that tunnel face failure pressures were generally close to the lower bound solution of case-3. The experimentally observed failure mechanisms were only similar for shallow unlined tunnels (case-1). The assumption of equal settlement at the tunnel and surface was not observed in deeper, $C/D > 2$, unlined tunnels (case-1). For most experimental results of tunnel face failure (case-3) the equal settlement at the face and surface assumed in the failure mechanisms was also not observed. This is likely due to arching effects

around the tunnel. The authors however suggest that the solution is appropriate for tunnels when $C/D < 3$.

### *2.1.2 Review ofLeca and Dormieux (1990)'s Solution*

Leca and Dormieux (1990) present lower and upper bound solutions for drained analysis of tunnel face stability, giving solutions for both collapse and blow out mechanisms. Groundwater is not included and the geological material surrounding the tunnel was assumed to be uniform. The effective friction was limited to between 20° and 45° and effective cohesion must be larger than zero. The solution was presented for $C/D \leq 3$. The tunnel was assumed to have a fixed lining with a free face supported by a uniform tunnel face support pressure.

The problem was idealised in the same way as by Davis *et at.* (1980), shown in Figure 2.1. One additional geometric parameter was used;

$$H = C + \frac{D}{2} \qquad (2.13)$$

The geological material was modelled as a Mohr-Coulomb material with $\varphi$ and $c'$. The unconfined compressive strength;

$$\sigma_C = 2\frac{c' \cos\varphi}{1 - \sin\varphi} \qquad (2.14)$$

And Rankine earth pressure coefficients were also used;

$$K_A = \frac{1 - \sin\varphi}{1 + \sin\varphi} \qquad (2.15)$$

$$K_P = \frac{1 + \sin\varphi}{1 - \sin\varphi} \qquad (2.16)$$

For active and passive failure respectively.

Leca and Dormieux (1990) arrange the capacity problem in a form similar to bearing capacity. For collapse the form was;

$$N_S Q_S + N_\gamma Q_\gamma \leq Q_T \qquad (2.17)$$

Where;

$$Q_S = (K_P - 1)\frac{\sigma_S}{\sigma_C} + 1 \qquad (\ 2.18\ )$$

$$Q_T = (K_P - 1)\frac{\sigma_T}{\sigma_c} + 1 \qquad (\ 2.19\ )$$

$$Q_\gamma = (K_P - 1)\frac{\gamma D}{\sigma_c} \qquad (\ 2.20\ )$$

$N_S$ and $N_\gamma$ are weighting coefficients.

Upper and lower bound solutions of $N_S$ and $N_\gamma$ were calculated for collapse. Two mechanisms were considered for an upper bound solution and three stress fields for a lower bound solution. ${N_\gamma}^{c+}$ and ${N_S}^{c+}$ were used to refer to the best upper bound collapse results and ${N_\gamma}^{c-}$ and ${N_S}^{c-}$ for the best lower bound collapse results.

An upper bound solution was found by calculating the power (force times velocity) mobilised along the axis of the cones in the proposed mechanisms. It consisted of the external loads, retaining pressure, surcharge and weight, and the dissipation power of the lateral surface of the cone. Where the cone intersects the tunnel face the failure area is in the shape of an ellipse, as shown in Figure 2.6, implying that only a part of the tunnel face is failing.

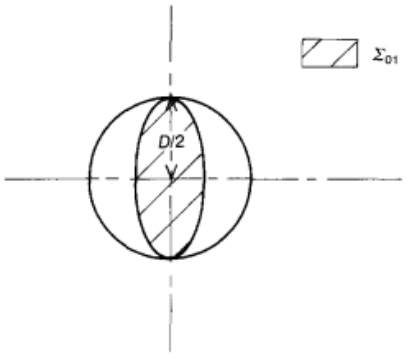


Figure 2.6 Area of tunnel face at failure (Leca and Dormieux, 1990)

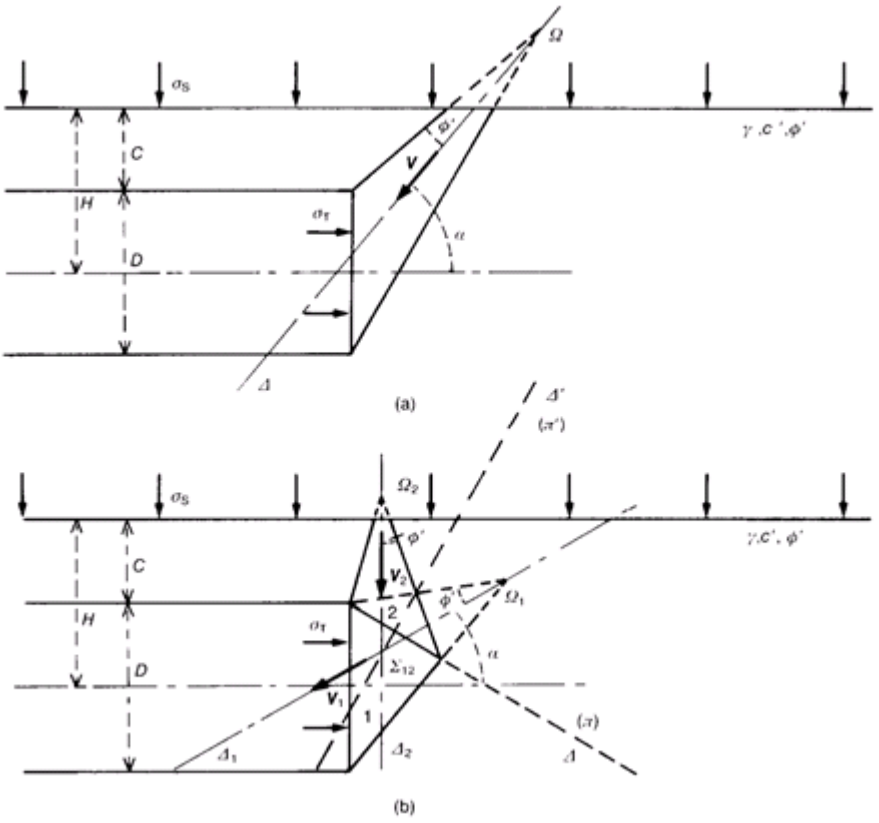


Figure 2.7 Upper bound collapse mechanisms a) MI and b) MII (Leca and Dormieux, 1990)

Figure 2.7 shows the two collapse mechanisms for an upper bound solution. Mechanism MI was formed by one cone from the tunnel face towards the surface, and mechanism MII by two cones, one from the face of the tunnel and one perpendicular to the ground surface. The failure cones do not necessarily reach the surface. The geometry was characterised by one parameter, the angle between the axis of the cone and the horizontal, α. For mechanism MI it was found that;

$$N_S{}^{c+} = \frac{1}{\cos 2\varphi - \cos 2\alpha} \frac{{R_D}^2}{R_E} \tan\alpha \qquad (2.21)$$

And;

$$N_\gamma{}^{c+} = \frac{1}{3} R_B \left(1 - \frac{{R_D}^3}{{R_E}^3}\right) \tan\alpha \qquad (2.22)$$

Where $R_B, R_D,$ and $R_E$ were derived from the geometric properties of the loading mechanism. They were;

$$R_B = \frac{\sqrt{\cos(\alpha-\varphi)\cos(\alpha+\varphi)}}{\cos\varphi} \qquad (2.23)$$

$$R_D = \sin 2\alpha - \frac{2H}{D}\sin 2\varphi \qquad (2.24)$$

$$R_E = \sqrt{\sin 2(\alpha-\varphi)\sin 2(\alpha+\varphi)} \qquad (2.25)$$

The formulas only apply where mechanism MI reaches the ground surface; this occurs when;

$$2\frac{C}{D} + 1 \leq \frac{\sin 2\alpha}{\sin 2\varphi} \qquad (2.26)$$

If this is not so then $R_D$ must be set to zero for equation 2.21 and equation 2.22 to remain valid. For mechanism MII it was found that;

$${N_S}^{c+} = \frac{1}{\cos\alpha - \cos^2\varphi}\frac{\sin(\beta-\varphi)}{\sin(\beta+\varphi)}\frac{{R_E}^2}{R_A} \qquad (2.27)$$

And;

$${N_\gamma}^{c+} = \frac{1}{3}\left[\tan\alpha\, R_B + \frac{\cos\varphi\cos(\beta+\varphi)}{2\sin\varphi\sin(\beta+\varphi)}\frac{{R_C}^3}{R_A} - \frac{1}{2\sin\varphi\cos\alpha\cos^2\varphi}\frac{\sin(\beta-\varphi)}{\sin(\beta+\varphi)}\frac{{R_E}^2}{R_A}\right] \qquad (2.28)$$

Where $\beta, R_A, R_B, R_C,$ and $R_E$ are derived from the geometric properties of the loading mechanism. They were;

$$\beta = \left(\frac{\pi}{2} + \alpha\right)/2 \qquad (2.29)$$

$$R_A = \frac{\sqrt{\cos(\alpha-\varphi)\cos(\alpha+\varphi)}}{\cos\varphi} \qquad (2.30)$$

$$R_B = \frac{\cos(\alpha-\varphi)\cos(\alpha+\varphi)}{\sin 2\varphi} \qquad (2.31)$$

$$R_C = \frac{\cos(\alpha+\varphi)}{\cos\varphi}\left[\frac{\sin(\beta-\varphi)}{\sin(\beta+\varphi)}\right]^{\frac{1}{2}} \quad (2.32)$$

And;

$$R_E = \frac{\cos^2\varphi}{\cos(\alpha+\varphi)}\ R_C - \frac{2C}{D}\sin\varphi \quad (2.33)$$

These only apply where mechanism MII reaches the ground surface; this occurs when;

$$\frac{C}{D} \leq \frac{\cos(\alpha+\varphi)}{2\sin\varphi}\frac{\sin(\beta-\varphi)}{\sin(\beta+\varphi)} \quad (2.34)$$

If this is not so then $R_E$ must be set to zero for equation 2.27 and equation 2.28 to remain valid. The upper bound collapse mechanisms are optimised when α is chosen so that $N_S$ and $N_\gamma$ are maximised. This critical value of α for collapse was found to be;

$$\alpha^{c+} \cong 49° - \frac{\varphi}{2} \quad (2.35)$$

Mechanism MII typically provides the best mechanism for collapse except for very shallow tunnels ($C/D \leq 0.25$) or material with a low effective friction angle ($\varphi \leq 30$). Results from the two mechanisms are similar when $C/D > 1.0$. ${N_\gamma}^{c+}$ is typically greater than ${N_S}^{c+}$. ${N_S}^{c+}$ is equal to zero when $C/D \geq 0.6$ indicating that any surcharge will only affect a very shallow tunnel and that in most conditions failure will not reach the ground surface.

A lower bound solution was found using the three stress fields derived by Leca and Panet (1988) (cited by Leca and Dormieux, 1990). These are similar to those presented by Davis *et at.* (1980) for the lower bound. Lower bound conditions were found by assuming that the yield criterion is not exceeded in the soil mass. Figure 2.8 shows the stress fields of the three mechanisms. In stress field solution SI the soil weight was greater than zero. The area in front of the tunnel was divided into three layers, with isotropic stresses above and below the tunnel and a horizontal stress of $\sigma_T$ in front of the tunnel. For stress field solution SI it was found that;

$${N_S}^{c-} = K_A \quad (2.36)$$

And;

$$N_\gamma{}^{c-} = K_A\left(\frac{C}{D}+1\right) \qquad (\ 2.37\ )$$

In stress field solution SII the soil weight is zero. The solution was comprised of two cylinders with an axis at the centre of the tunnel. The stress field of the inner cylinder had an axial stress of $\sigma_T$ and radial stress of $\sigma_0$, a constant, so that the ground was at yield everywhere. This was surrounded by the second cylinder. A solution with radial stress $\sigma_r$, tangential stress of $\sigma_\theta$ , and longitudinal stress of $\sigma_z$ was derived assuming the ground was at yield. Outside the second cylinder there was an isotropic stress field of $\sigma_s$. For stress field solution SII it was found that;

$$N_S{}^{c-} = K_A\left(2\frac{C}{D}+1\right)^{1-K_P} \qquad (\ 2.38\ )$$

In stress field solution SIII the soil weight was zero. The solution was spherically symmetrical around the centre of the tunnel face. Stresses were isotropic inside a hemispherical cap on the tunnel face, $\sigma_T$. This was surrounded by a sphere. The radial stresses of $\sigma_r$ and tangential stress of $\sigma_\theta$ were derived assuming the ground is at yield as with stress field solution SII. Outside the sphere there was an isotropic stress field of $\sigma_s$. For stress field solution SIII it was found that;

$$N_S{}^{c-} = \left(2\frac{C}{D}+1\right)^{2(1-K_P)} \qquad (\ 2.39\ )$$

$N_\gamma{}^{c-}$ is equal to zero for the stress field solutions SII and SIII. Therefore, $N_\gamma{}^{c-}$ from stress field solution SI was used in the lower bound solution. The best lower bound solution for collapse was found when $N_S{}^{c-}$ was minimised. As in Davis *et at.* (1980)'s solution the best lower bound solution was SII for shallow tunnels and SIII for deeper tunnels.

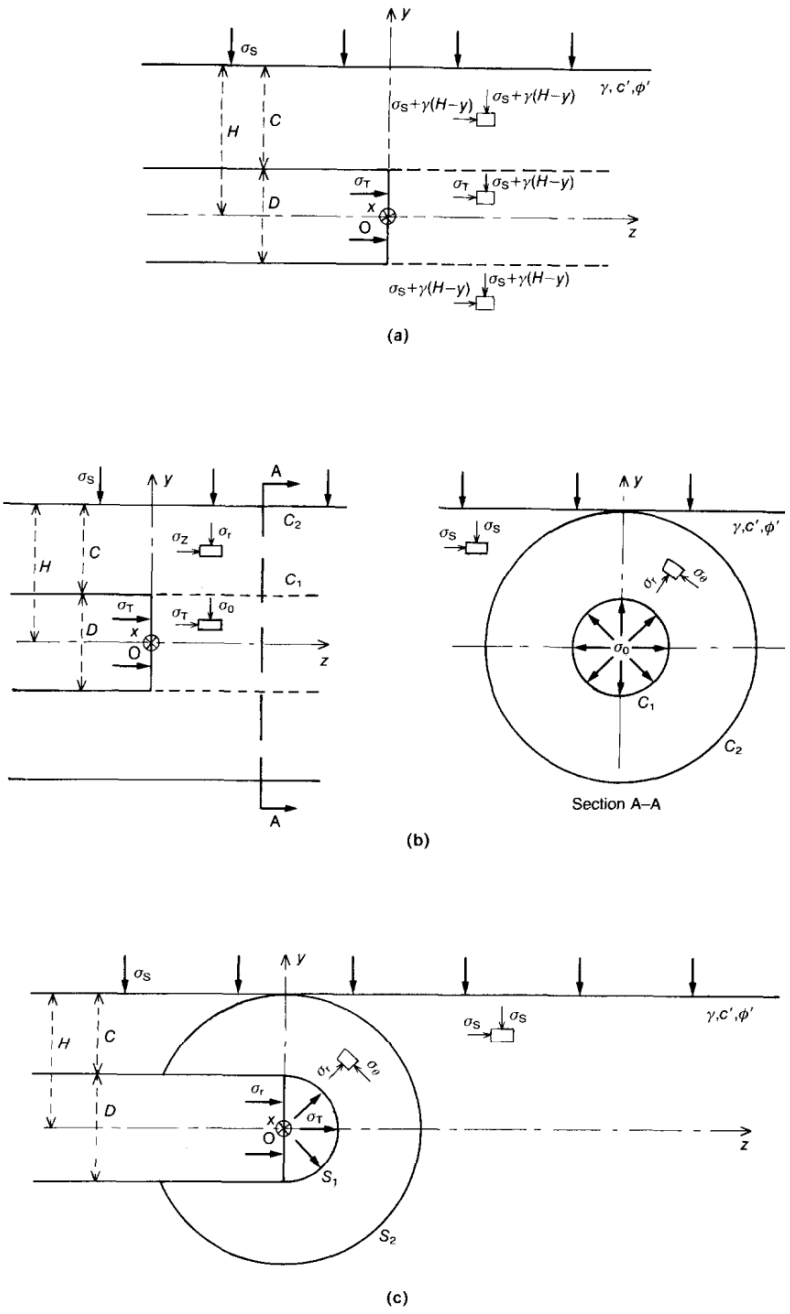


Figure 2.8 Stress fields a) SI, b) SII and c) SIII (Leca and Dormieux, 1990)

The solutions were compared with experimental results from centrifuge tests by Chambon and Corté (1994) (cited by Leca and Dormieux, 1990). The centrifuge test used two different depth ratios, $C/D$ = 1.0 and 2.0, and two soil conditions, a loose sand and a dense sand. The experiments showed that failure was sudden, occurred at a low tunnel face support pressure, that the depth ration had little influence on results for the range considered, the failure geometry was a bulb shape and failure (i.e., mobilized mass) did not reach the surface for $C/D > 1.0$. It was found that the measured pressure at failure was near the upper bound solution from the limit analysis.

## 2.2 Axisymmetric FEM Modelling of Tunnel Face Stability

Axisymmetric FEM models of tunnels require a number of assumptions and simplifications. To use an axisymmetric FEM model the tunnel failure must be "deep", not reach the surface, as the surface is not explicitly expressed (Potts and Zdravkovic 2001). Limit analysis indicates that when $C/D > 1$ for drained analysis, the failure does not reach the surface (Leca and Dormieux, 1990). Experimental results indicate that the surface is not reached when $C/D > 2.5$ for undrained analysis (Davis *et at.*, 1980).

FEM simplifies a boundary-condition problem in mechanics by splitting the solution domain into smaller finite solution domains, namely the finite elements, with nodes defined on the boundaries and sometimes within the elements (Potts and Zdravkovic 2001). The displacement any point between nodes can be found using interpolation functions, namely the shape functions. In an axisymmetric problem, the displacement field can be characterised by u and v respectively in the radial ($r$) and vertical ($z$) directions. Due to symmetry there is no displacement in the circumferential ($\theta$) direction. For instance, the displacement equations for a (constant-strain) three noded triangular element are;

$$u = \beta_1 + \beta_2 r + \beta_3 z \qquad (2.40)$$

$$v = \beta_4 + \beta_5 r + \beta_6 z \qquad (2.41)$$

where $\beta_i$ are generalised coordinates. Values of $\beta_i$ can be expressed as nodal displacements by substituting the nodal coordinates into equations 2.40 and 2.41 and

solving two sets of three simultaneous equations. The displacement components *u* and *v* can be expressed in terms of the nodal displacements using;

$$\begin{Bmatrix} u \\ v \end{Bmatrix} = [N] \begin{Bmatrix} u \\ v \end{Bmatrix}_{nodes} \quad (2.42)$$

Where $[N]$ is the matrix of shape functions. The incremental displacement can be computed by;

$$\{\Delta d\} = \begin{Bmatrix} \Delta u \\ \Delta v \end{Bmatrix} = [N] \begin{Bmatrix} \Delta u \\ \Delta v \end{Bmatrix}_{nodes} = [N]\{\Delta d\}_{nodes} \quad (2.43)$$

The incremental strains corresponding to the incremental displacements by the relationships;

$$\Delta\varepsilon_r = -\frac{\delta \Delta u}{\delta r} \quad (2.44)$$

$$\Delta\varepsilon_z = -\frac{\delta \Delta v}{\delta z} \quad (2.45)$$

$$\Delta\gamma_{rz} = -\frac{\delta \Delta v}{\delta r} - \frac{\delta \Delta v}{\delta z} \quad (2.46)$$

$$\Delta\varepsilon_\theta = -\frac{\Delta u}{r} \quad (2.47)$$

These relationships can be substituted in Equation 2.43 to yield;

$$\{\Delta\varepsilon\} = [B]\{\Delta d\}_{nodes} \quad (2.48)$$

where $[B]$ contains the derivatives of the shape functions, *N*. The constitutive model is used to define material behaviour. The general constitutive relationship is usually;

$$\{\Delta\sigma\} = [D]\{\Delta\varepsilon\} \quad (2.49)$$

where $\{\Delta\sigma\}$ are the stress increments in the material, and $[D]$ is the constitutive relationship between incremental strains and incremental stresses on any point of an finite element. In geotechnical engineering the constitutive relationship is typically non-linear, such that the behaviour of the material is dependent on displacement history. A stiffness matrix is developed for each element to define relationship between external loads acting on nodes of an element and nodal displacements. The principal

of minimum potential energy is used to develop the general form for the elemental stiffness matrix (Potts and Zdravkovic 2001), such as;

$$[K_E] = \int_{Vol} [D]^T [D][B] dVol \qquad (\ 2.50\ )$$

So that, the equilibrium for an element will be met if;

$$[K_E]\{\Delta d_E\} = \{\Delta R_E\} \qquad (\ 2.51\ )$$

where $[K_E]$is the elemental stiffness matrix, $\{\Delta d_E\}$ is incremental displacements of all nodes of element, and $\{\Delta R_E\}$ is all incremental nodal forces acting on nodes of element. The elemental stiffness matrices are combined to develop a global stiffness matrix to be used in global equations of equilibrium, such as;

$$[K_G]\{\Delta d_G\} = \{\Delta R_G\} \qquad (\ 2.52\ )$$

where $[K_G]$is the global stiffness matrix, $\{\Delta d_G\}$ is all incremental nodal displacements and $\{\Delta R_G\}$ is all incremental nodal forces acting on all nodes of a solution domain, namely on finite-element mesh. Boundary conditions, typically imposed loading or displacement, are defined by modifying the global equations for known variables. Finally, the global equations are solved using integration to evaluate the stiffness matrix and displacement vector. Numerical integration is generally required as explicit integration cannot be performed except in special cases (Potts and Zdravkovic 2001).

Due to the circular nature of the axis symmetric model the tunnel has the same stress conditions and material properties around the circumference. Therefore, equal stresses are calculated on the top and the bottom of the tunnel. For this to be a suitable assumption the difference between the confining pressure at the top and the bottom of the tunnel must be significantly smaller than the confining pressure. This means that the tunnel must be deep (Potts and Zdravkovic 2001). Also due to the radial symmetry the stresses at any perpendicular distance from the tunnel axis are constant. Therefore, the stresses in the vertical direction and perpendicular horizontal direction are equal. To extend this to the horizontal direction parallel to the tunnel axis an at rest earth pressure coefficient, $K_0 = 1.0$ can be used. This is an acceptable assumption for many

rocks and weathered rocks/residual soils but may not be realistic for some geological formations (Ladd *et al.*, 1997).

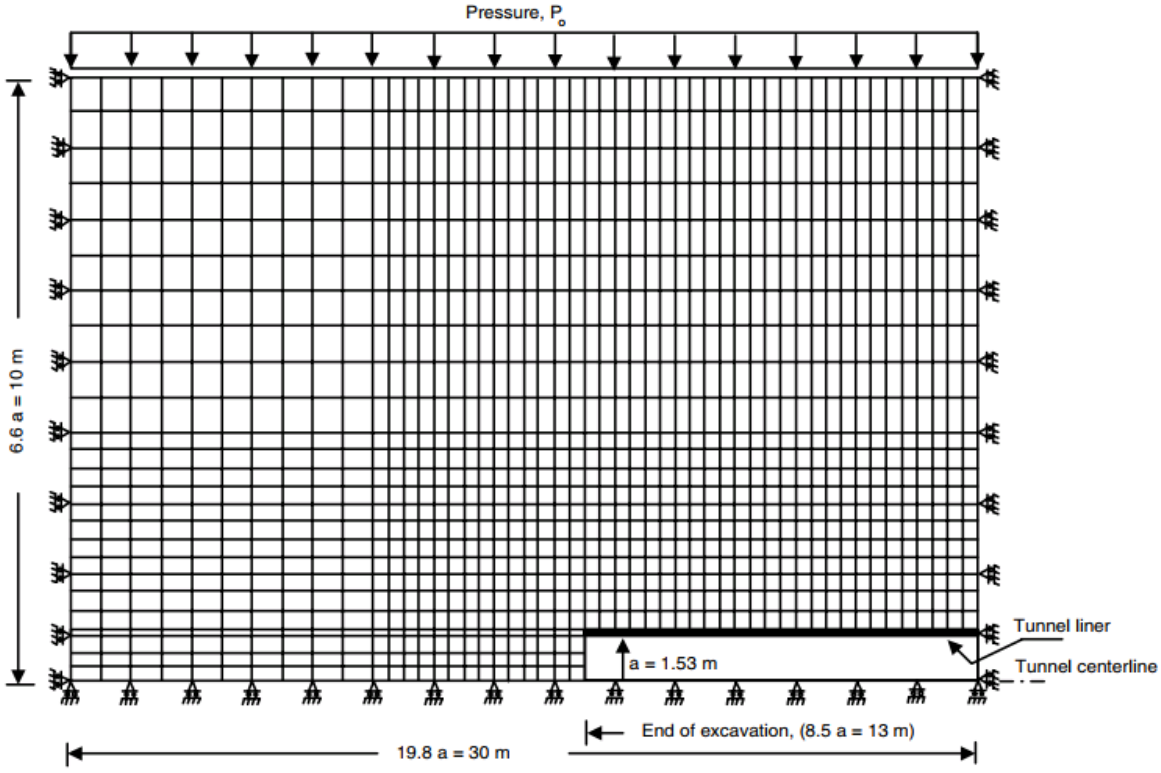


Figure 2.9 Example of axisymmetric FEM model with finite element mesh and boundaries from Shalabi (2005)

An example of the boundaries and finite element mesh for an axisymmetric FEM model is shown in Figure 2.9 (Shalabi, 2005). The model is set up so that the tunnel axis is along the axis of symmetry, the central axis. Boundaries along the central axis and perpendicular to the tunnel are normally fixed. The final boundary, on the outside of the cylinder created by the model, is free and a confining pressure is applied. The mesh is typically finer around the parts of the tunnel that are being investigated (Suzuki, 2000, Shalabi, 2005). Excavation of the tunnel is done by deactivation of the soil elements within the tunnel and lining is applied as required (Shalabi, 2005). When the focus of a study is tunnel face stability the lining of the tunnel can be modelled as a line with no displacement (Lu *et at.*, 2014). This is done to reduce the influence of

everything except the tunnel pressure on results. The tunnel pressure is generally modelled as uniform. This is consistent with limit analysis solutions of Davis *et at.*, (1980), Leca and Dormieux (1990), and Lu *et al.*, (2014) amoung others.

### 2.3 Seismic Analysis of Tunnel Face Stability

Seismic analysis of tunnel face stability has previously been undertaken by Saada *et al.* (2013). The influence of seismic load on the upper bound kinematic analysis was investigated using a modified Hoek-Brown failure condition. The strength of the material was specified using rock uniaxial strength, $\sigma_c$, geological strength index, $GSI$, strength parameter $m_i$, and disturbance factor, $D_0$. The stability of the tunnel face was characterised using six dimensionless parameters;

$$\frac{\sigma_T}{\gamma D}, \quad k_h, \quad \frac{\sigma_c}{\gamma D}, \quad m_i, \quad GSI \text{ and } D_0 \qquad (2.53)$$

Two failure mechanisms were considered, shown in Figure 2.10. It was assumed that neither mechanism reaches the ground's surface and the mechanisms are independent of depth. Figure 2.10a shows the cone failure mechanism developed by Leca and Dormieux (1990), mechanism MI described in section 2.1. Figure 2.10b shows the horn failure mechanism, developed by Cuvillier (2001). The horn failure is a single horn shaped block with rotational movement.

The horn failure mechanism was found to be closer to experimental and numerical results and tended to give slightly larger tunnel face failure pressure. The effect of rock uniaxial strength, geological strength index and strength parameter $m_i$ on static tunnel face support pressure were presented, shown in Figure 2.11. it was concluded that there is a significant increase in tunnel face support pressure for low values of $\sigma_c/\gamma D$, the other parameters have similar but less pronounced effect on the tunnel face support pressure. It was suggested that there is moderate influence of the two rock parameters when compared to the uniaxial rock strength.

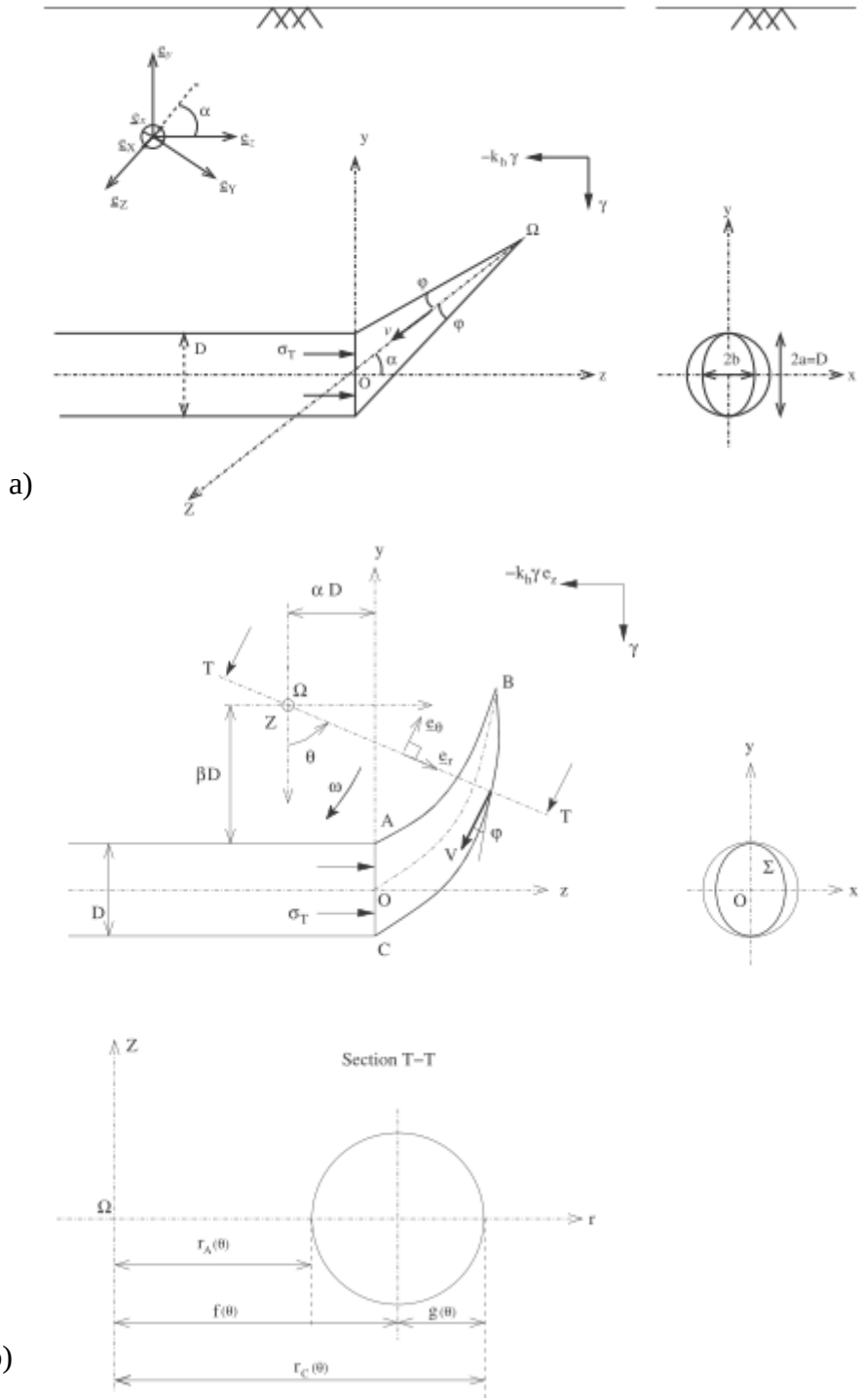


Figure 2.10 a) Cone and b) horn failure mechanisms considered in (Saada et al., 2013)

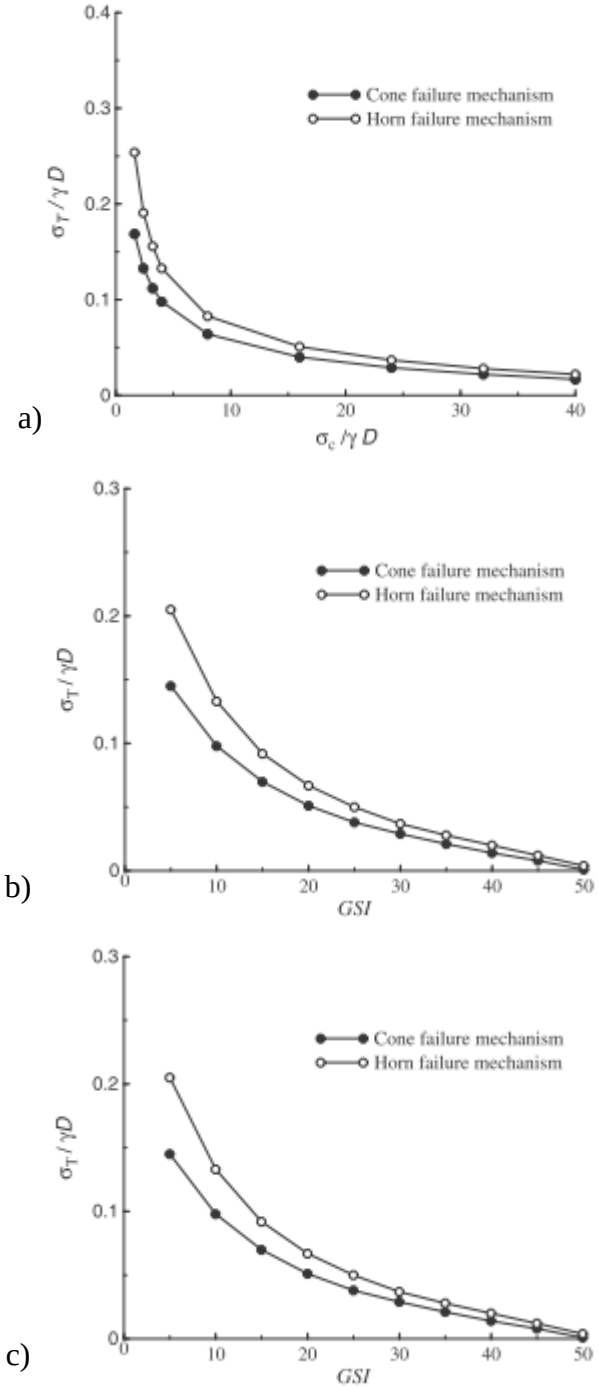


Figure 2.11 effect of a) rock uniaxial strength, b) geological strength index, and c) strength parameter $m_i$ on tunnel face failure pressure (Saada et al., 2013)

Earthquake effects were investigated using pseudo static analysis and the application of the seismic coefficient, $k_h$. Figure 2.12a shows the effect of $k_h$ on the tunnel face support pressure found for the two mechanisms. For both mechanisms the increase in support pressure with $k_h$ was approximately linear, it was found that the tunnel face support pressure is sensitive to seismic loading. A suggested relationship was;

$$\frac{\sigma_T}{\gamma D}\ (k_h = 0.4) \cong 2.5\frac{\sigma_T}{\gamma D}\ (k_h = 0) \qquad (\ 2.54\ )$$

As with the static case the horn mechanism gave higher values of tunnel face support pressure. Figure 2.12b shows how the tunnel face stability was affected by the strength of the material for the horn failure mechanism.

It was concluded that there is a significant reduction of tunnel face stability when seismic forces are applied and that the reduction in stability is greater for larger values of $k_h$. The relationship between the increase in tunnel face support pressure and $k_h$ appeared to be linear. Saada *et al.* (2013) assumed that the vertical force from the earthquake could be neglected, this is true when the horizontal acceleration is small compared to gravity (Chen and Liu, 1990). It was also suggested that using a single conical block may not be appropriation for upper bound tunnel face stability analysis of tunnel for material with a Hoek-Brown failure criterion.

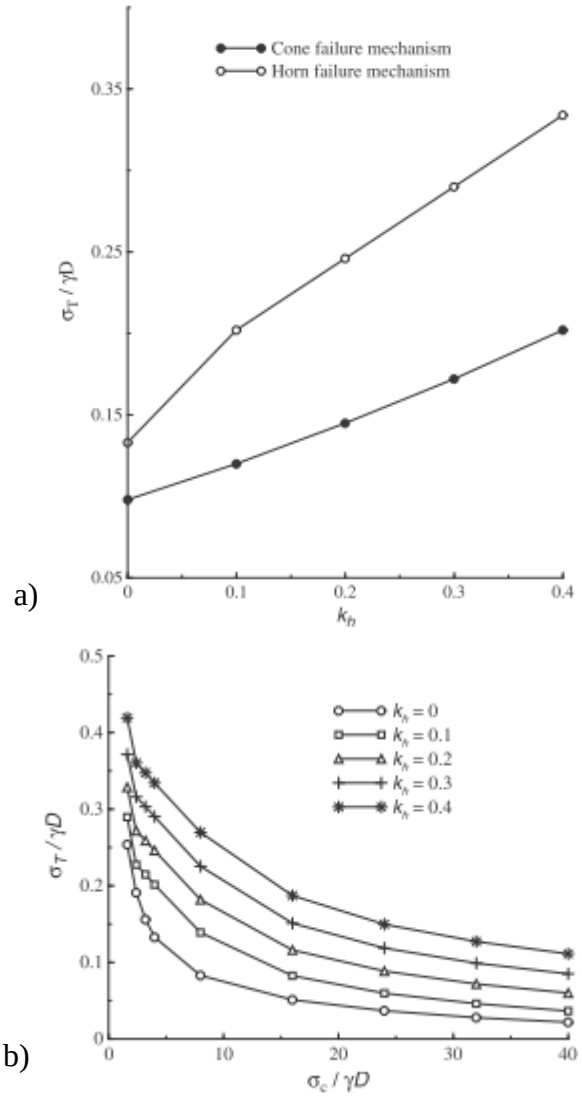


Figure 2.12 effect of a) $k_h$ on tunnel face failure pressure, and b) earthquake on tunnel face stability (Saada et al., 2013)

## 2.4 Procedure of Analysis

The theory outlined above is used to develop and verify the axisymmetric FEM solution. The spreadsheet developed to verify the static response for tunnel face stability of the axisymmetric FEM solution. Equation 2.1 to equation 2.12 are used for the calculation of Davis *et at.* (1980)'s solution. Equation 2.13 to equation 2.39 are used for the calculation of Leca and Dormieux (1990)'s solution. The axisymmetric FEM model was developed based on previous investigations outlined in section 2.2. The results from previous analysis of seismic tunnel face stability, presented in section 2.3, are compared to the seismic results of the axisymmetric FEM solution.

### *2.4.1 Parameters and Normalisation*

To compare different solutions' predictions of tunnel face support pressure the same model parameters must be applied. It is also important to investigate the effect of changing parameters on tunnel face stability. The different parameters considered in the axisymmetric FEM solution are effective friction angle, effective cohesion, undrained shear strength, unit weight, confining pressure, $\sigma_v$, tunnel diameter and Young's Modulus, $E$. The limit analysis solutions generally use the same parameters. Exceptions are; the depth ratio is used rather than the confining pressure, no Young's Modulus is included, and a separate surface surcharge can be included. The parameters chosen for analysis are presented in Table 2.1: The quantities in bold are the default values of the parameters used in simulations. These values have been chosen such that they are within the bounds provided by the solutions of limit analyses, and the numerical modelling gives reasonable results.

Table 2.1. Parameters used in modelling, Bold parameters denote default values.

| Parameter | Values |
|---|---|
| $\varphi$ (°) | 20, **27**, 35 |
| $c'$ (kPa) | **0.1**, 10 |
| $c_u$ (kPa) | 50, **200**, 500 |
| $\gamma$ (kN/m$^3$) | **20**, 25 |
| $\sigma_v$ $(C/D)$ (kPa) | **700** (3), 1100 (5) |
| $D$ (m) | 5, **10** |
| $E$ (MPa) | **100**, 200 |
| $\sigma_S$ (kPa) | **0** |

To compare tunnel face failure between different simulations, normalisation has been used for the tunnel face support pressure and the displacement. Normalised values are denoted with a subscript "N"; $\sigma_{T_N}$ and $u_N$ respectively. For normalisation of the tunnel face support pressure, the same normalisation as Saada *et al.* (2013) has been used;

$$\sigma_{T_N} = \frac{\sigma_T}{\gamma D} \qquad (2.55)$$

This is a dimensionless parameter. This normalisation removes the influence of unit weight and tunnel diameter, particularly on drained limit analysis solutions. The formulation used for normalisation of the displacement in the axisymmetric FEM solution is;

$$u_N = \frac{uE}{D\sigma_v} \qquad (2.56)$$

This is a dimensionless parameter. This normalisation reduces the influence of elastic modulus on numerical modelling results.

# CHAPTER 3

# ASSESSMENT OF STATIC TUNNEL FACE STABILITY

An axisymmetric FEM model in PLAXIS was developed to use in the assessment of tunnel face stability under seismic loading. For analysing the seismic stability of the tunnel face a model that can reflect the face stability adequately is required. Any imprecision in the static solution can erroneously impact the seismic results. To ensure that the axisymmetric FEM solution is adequately reflecting tunnel face stability, the static results have been verified using limit analysis solutions. To do this a spreadsheet for calculations has been developed, using Davis *et at.* (1980)'s solution for undrained behaviour and Leca and Dormieux (1990)'s solution for drained behaviour. The trends in behaviour when parameters are varied and tunnel face support pressure at failure for the different solutions have been compared.

## 3.1 Limit Analysis Spreadsheet

This section presents the development of the limit analysis spreadsheet using the undrained and drained solutions reviewed in section 2.1. It outlines why these solutions were selected, how the equations referred to in section 2.1 were used in the development, and an investigation of the effects of important parameters on tunnel face stability.

The spreadsheet was developed in Microsoft Excel[2]. It requires the input parameters of the tunnel; depth and diameter, the ground; strength parameters, unit weight, and surcharge. The outputs of the spreadsheet are upper and lower bounds for the tunnel face support pressure at collapse. The spreadsheet can be found in APPENDIX A.

[2] Microsoft Excel 2016 (16.0.9029.2016) 32-bit

### *3.1.1 Undrained Limit Analysis Solution*

The solution of Davis *et at.* (1980) was selected for undrained analysis. It has the same simplifying assumptions as in the scope, constant material parameters and no water seepage. Although the paper is old there has been little expansion of undrained analysis for the constant strength and no water flow condition. Therefore, it was considered that Davis *et at.* (1980)'s solution was appropriate for checking that the FEM results were within an acceptable range.

The undrained part of the spreadsheet was developed to calculate lower and upper bound pressures for tunnel face stability using Davis *et at.* (1980)'s solution for case-1, case-2, case-3, and local collapse. The stability ratio $N$ was calculated for each case and then the tunnel face support pressure was found by equation 2.1. Case-1 lower and upper bound solutions were calculated using Figure 2.2b. The best fit power or polynomial trendline was found for each line and then $\gamma D/c_u$ interpolating between lines. The $R^2$ value for all trendlines was greater than 0.97 indicating excellent fit (Mendenhall, 1979). Case-2 lower and upper bound solutions were calculated by using the two equations presented on Figure 2.3c. The lower bound was chosen as the smooth lining as this is slightly more conservative and easier to implement. The lower bound solution was calculated using equation 2.7. The upper bound solution was calculated using equation 2.8. Case-3 lower and upper bound solutions were calculated using Figure 2.4. The lower bound solution was calculated using the maximum of equation 2.13 and equation 2.14. The upper bound solution was calculated by finding the best fit power trendline from Figure 2.4. The $R^2$ value was greater than 0.97 indicating excellent fit (Mendenhall, 1979). Local collapse was checked to ensure the conditions equation 2.11 were met. If conditions were not met the results were flagged.

The spreadsheet was used to investigate the theoretical effects of different values for the undrained shear strength, tunnel diameter, unit weight and depth ratio in the undrained case using Davis *et at.* (1980)'s solution. The default parameters and normalisation in section 2.4.1 are used where no values are specified. Comparisons of the simulation results are presented in Figure 3.1. It can be seen that the lower bound gives a higher tunnel face failure pressure than the upper bound. It can also be seen that case-1 gives the highest tunnel face failure pressure while case-3 gives the lowest.

This behaviour is typically constant across all cases. All figures use normalised tunnel face failure pressure. Negative normalised tunnel face pressure values indicate that the tunnel face is stable with no support pressure applied. For collapse to occur a negative pressure would have to be applied to the tunnel face. Figure 3.1a shows the effect of undrained shear strength on the tunnel face support pressure. It can be seen that increasing the undrained shear strength reduces the tunnel face failure pressure. The upper bound decreases faster than the lower bound, making the boundary for the failure larger with increased undrained shear strength. Figure 3.1b shows the effect of the unit weight on the tunnel face support pressure. It can be seen that there is a small increase in the normalised tunnel face support pressure with unit weight. Figure 3.1c shows the effect of the tunnel diameter on the tunnel face support pressure. It can be seen that the normalised tunnel face support pressure increases with tunnel diameter. The effect is greater at smaller tunnel diameters. Figure 3.1d shows the effect of the cover to depth ratio on the tunnel face support pressure. It can be seen that the case-3 upper bound decreases with $C/D$ . The case-3 lower-bound and case-2 upper-bound predictions for tunnel face support pressure initially decrease. At higher values of $C/D$ there is very little change in tunnel face support pressure. Finally, case-1 and case-2 lower bound predictions of tunnel face support pressure change very little with $C/D$. It was found that local collapse did not occur with any of the parameters used, such that the conditions in equation 2.11 were always met. As case-1 does not consider the tunnel face stability, but the radial stability, it is not included in any further comparisons. It was included in this section to show that the results are comparable with the other cases.

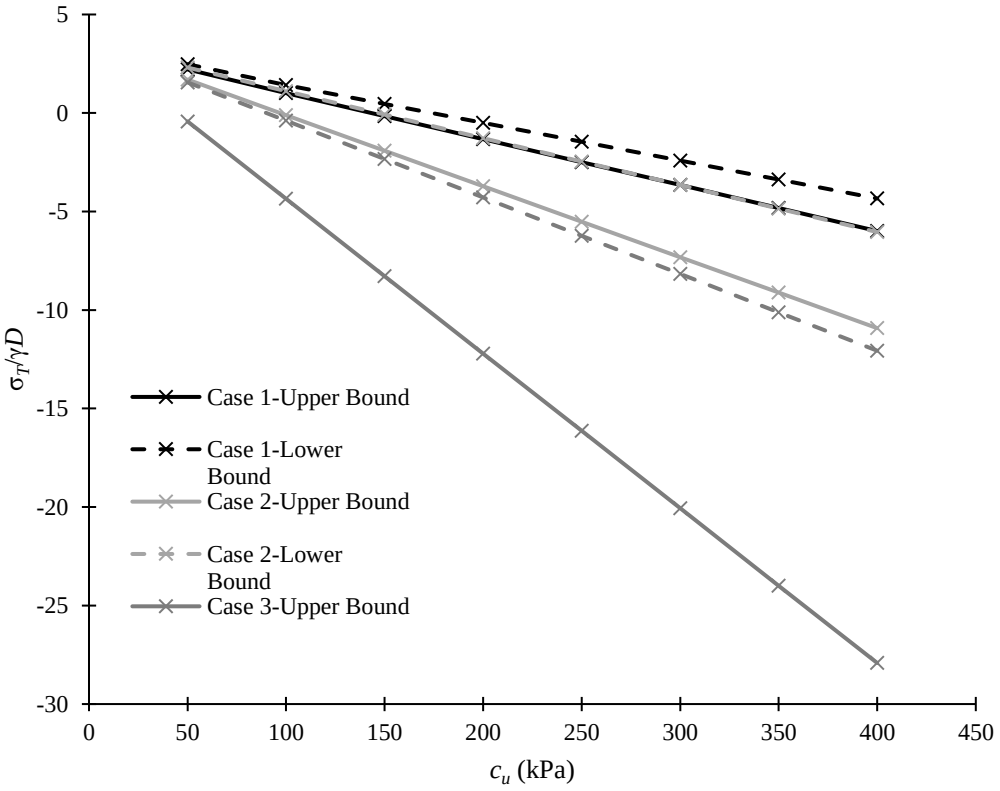


a)

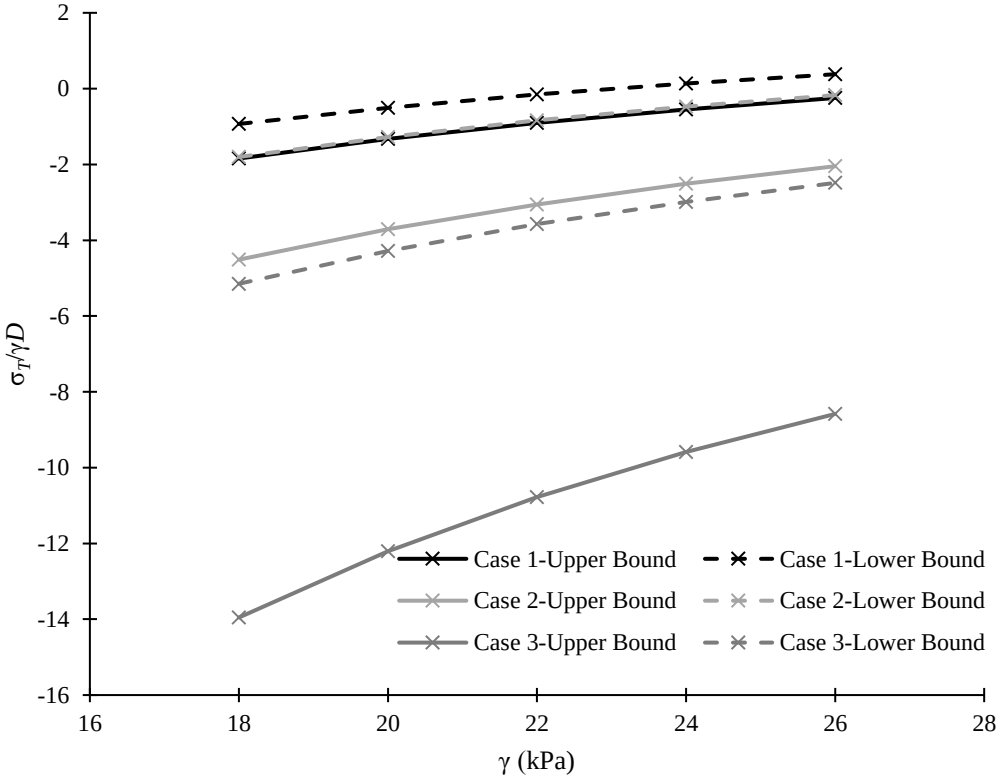


b)

Figure 3.1 Effect of a) undrained shear strength, b) unit weight, c) tunnel diameter, and d) cover to depth ratio on tunnel face stability using Davis et at. (1980)'s solution

c)

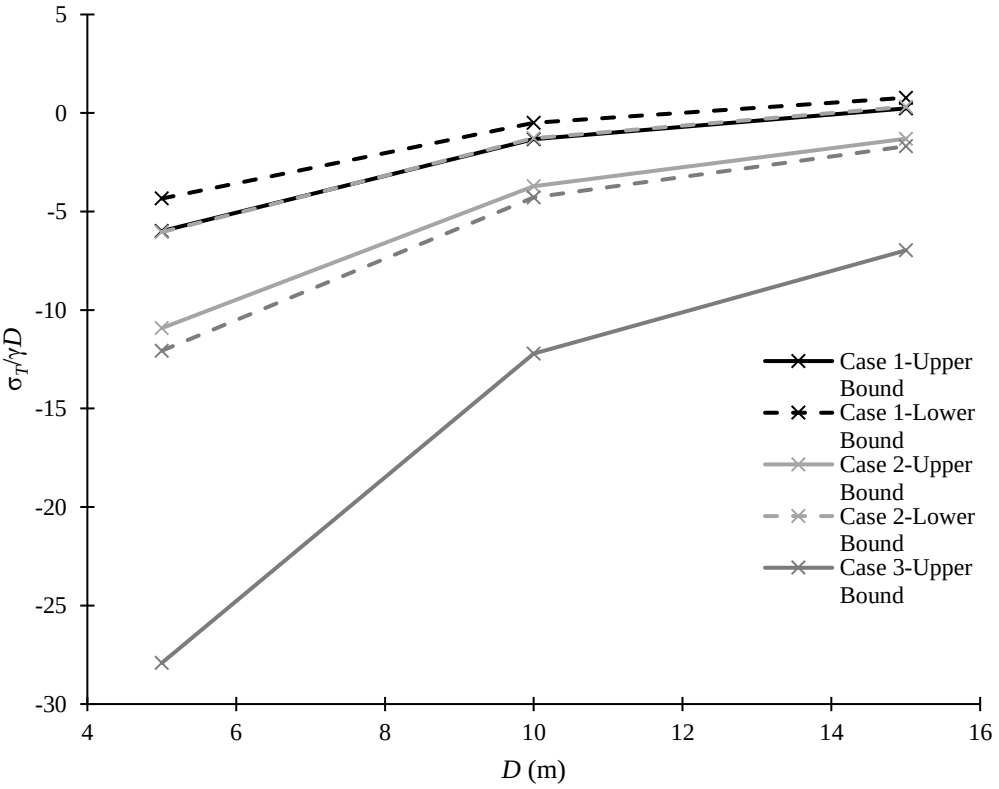


d)

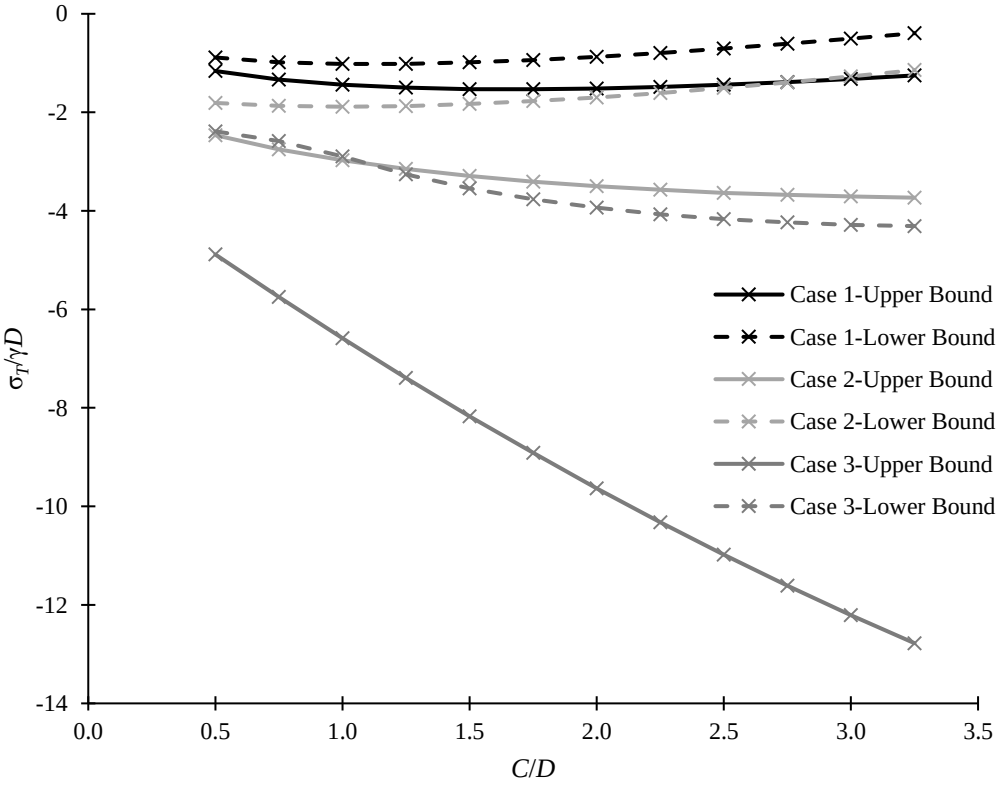


Figure 3.1 Continued

### *3.1.2 Drained Limit Analysis Solution*

The solution of Leca and Dormieux (1990) was selected for drained analysis. It has the same simplifying assumptions as in the scope, constant material parameters and being above the water table. A number of refinements have been made to the drained models for tunnel face designs since the paper of Leca and Dormieux (1990). Most of these refinements have focused on the upper bound solution. These refinements offer some improvement in results. The improvements are limited compared to the gap between upper and lower bound. They are also limited when compared with the additional computing power and unknowns that must be optimised for a solution. It was considered that Leca and Dormieux (1990)'s solution was appropriate for checking the FEM results were within an acceptable range.

The drained part of the spreadsheet was developed to calculate the lower and upper bound pressures for tunnel face stability using Leca and Dormieux (1990)'s solution. For the upper bound solution mechanisms MI and MII were included and for the lower bound solution collapse stress fields SI, SII and SIII were included. For each mechanism or stress field the loading parameter $Q_T$ was calculated and then the tunnel face support pressure was found by rearranging equation 2.19.The unconfined compressive strength and earth pressure coefficients were calculated using equation 2.14 to equation 2.16. The other loading parameters, $Q_S$ and $Q_\gamma$, were calculated using equation 2.18 and equation 2.20 respectively. For the upper bound solution mechanism MI $Q_T$ was calculated by applying equation 2.17 and equation 2.21 to equation 2.25. Interaction with the ground surface was checked using equation 2.26. For mechanism MII $Q_T$ was calculated by applying equation 2.17 and equation 2.27 to equation 2.33. Interaction with the ground surface was checked using equation 2.34. Initial values of $\alpha^{c+}$ were calculated using equation 2.35 and input. The values were optimised using the inbuilt solver in Microsoft Excel. The variation $\alpha^{c+}$ from the initial value was found to be larger with smaller values of effective friction angle. For the lower bound solution stress field SI $Q_T$ was calculated using equation 2.17, equation 2.36, and equation 2.37. For stress field SII $Q_T$ was calculated using equation 2.17, and equation 2.38. For stress field SIII $Q_T$ was calculated using equation 2.17, and equation 2.39. The spreadsheet was used to investigate the theoretical effects of different values for

the effective friction angle, effective cohesion, tunnel diameter, unit weight and depth ratio in the drained case using Leca and Dormieux (1990)'s solution. The default parameters and normalisation in section 2.4.1 are used where no values are specified. Comparisons of the simulation results are presented in Figure 3.2. It can be seen that the lower bound gives a higher tunnel face failure pressure at failure than the upper bound. All figures use normalised tunnel face failure pressure. Figure 3.2a shows the effect of the effective friction angle on the tunnel face support pressure. It can be seen that increasing the effective friction angle reduces the tunnel face failure pressure. There is a larger effect on the lower bound than the upper bound, making the boundary for the failure smaller with increasing effective friction angle. Figure 3.2b shows the effect of the effective cohesion on the tunnel face support pressure. It can be seen that increasing the effective cohesion slightly reduces the tunnel face failure pressure. The lower and upper bound decrease at similar rates. Figure 3.2c shows the effect of the unit weight on the tunnel face support pressure. It can be seen that there is no change to the normalised tunnel face failure pressure with the unit weight. This is due to the normalisation; the increase in tunnel face support pressure is proportional to the increase in unit weight. Figure 3.2d shows the effect of the tunnel diameter on the tunnel face support pressure. It can be seen that there is no change to the normalised tunnel face failure pressure with the tunnel diameter. This is due to the normalisation, the increase in tunnel face support pressure is proportional to the increase tunnel diameter. Figure 3.2e shows the effect of the cover to depth ratio on the tunnel face support pressure. It can be seen that increasing the cover to depth ratio increases the lower bound tunnel face failure pressure and causes no change to the upper bound tunnel pressure, making the boundary for the failure larger.

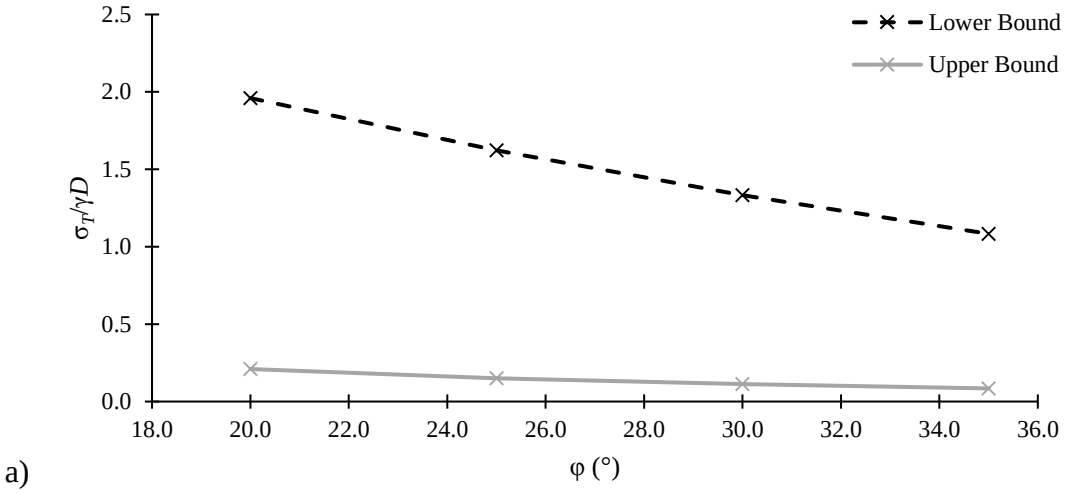


a)

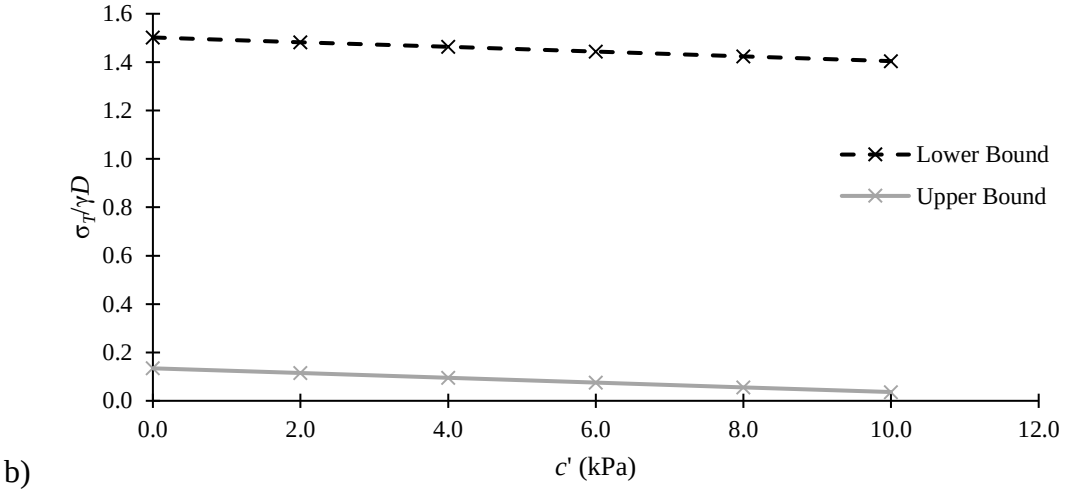


b)

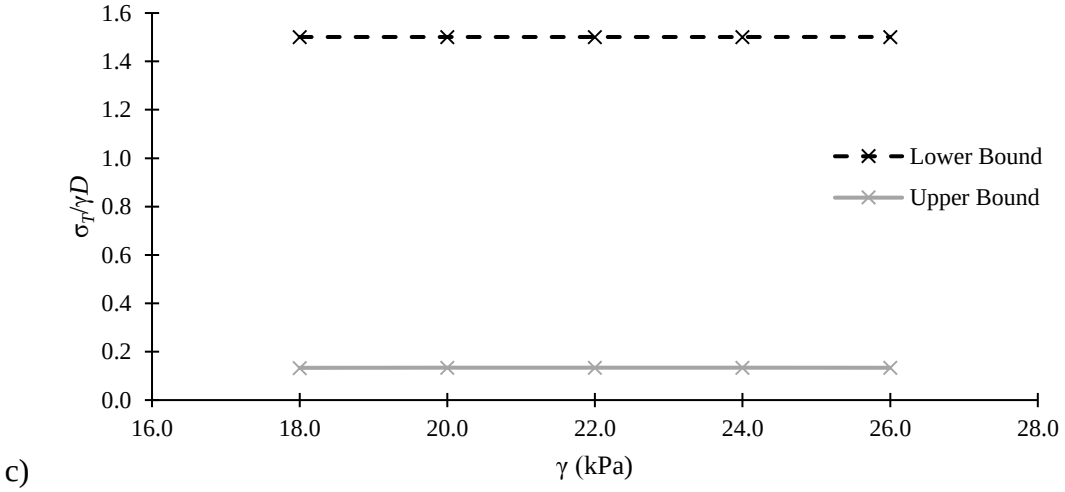


c)

Figure 3.2 Effect of a) effective friction angle, b) effective cohesion, c) unit weight, d) tunnel diameter and e) cover to depth ratio on tunnel face stability using Leca and Dormieux (1990)'s solution

d)

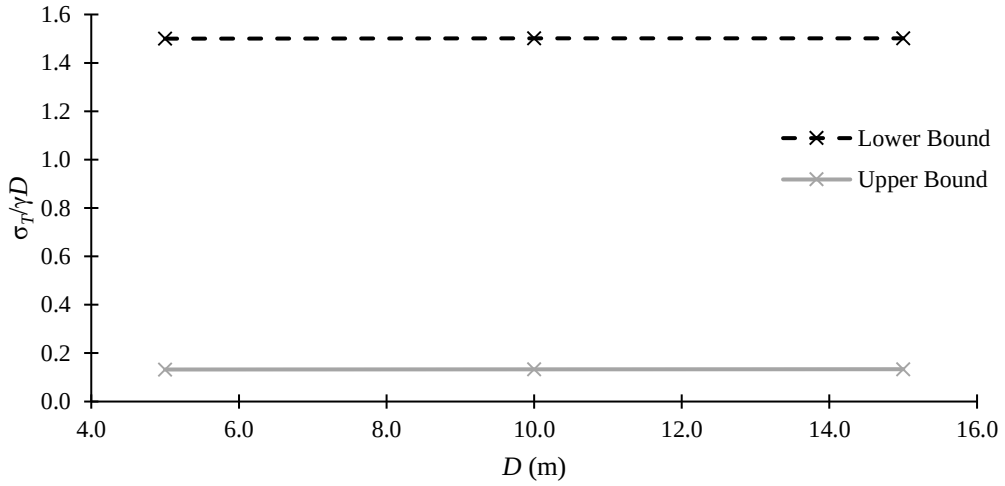


e)

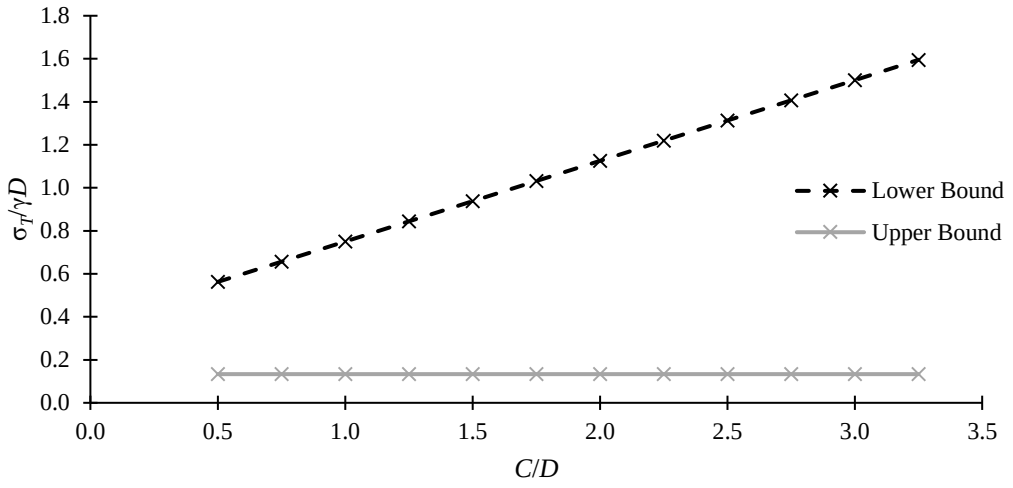


Figure 3.2 Continued

## 3.2 Axisymmetric FEM Model for Tunnel Face Stability

An Axisymmetric FEM model for tunnel face stability has been developed for both undrained and drained analysis. The tunnel face stability results of the axisymmetric FEM solution are compared to the results of the limit analysis solutions, highlighting where there are agreements and differences. The failure point for the Axisymmetric FEM model is also defined. The default parameters and normalisation in section 2.4.1 are used in simulations where no values are specified.

### *3.2.1 Development of Axisymmetric FEM Model*

This section outlines the development of the Axisymmetric tunnel face stability FEM model. The computer program PLAXIS has been used for FEM analysis (Brinkgreve *et al.*, 2017). It follows the methodology set out in section 2.2. For any model parameters not mentioned the default values in PLAXIS have been used.

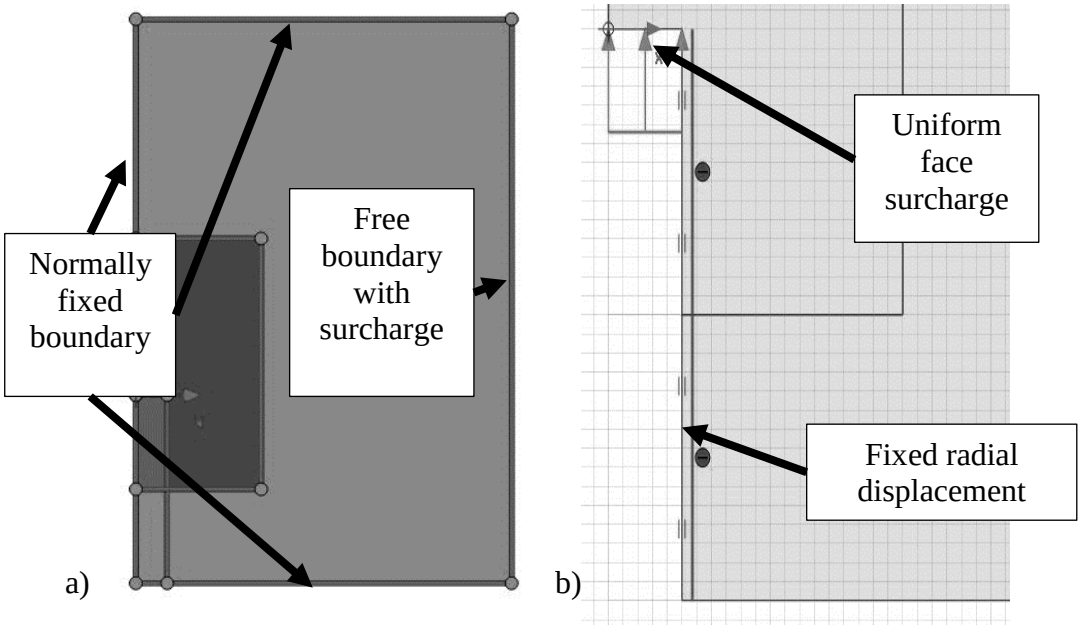


Figure 3.3 Axisymmetric FEM model set up a) boundaries and mesh coarseness and b) tunnel configuration

To use the axisymmetric FEM model in PLAXIS the axis of the tunnel was rotated; the central axis of the tunnel is at $x = 0$ and in the $y$-direction. As the vertical direction at the tunnel is no longer in the $y$-axis gravity in the model is working in the wrong direction and the weight multiplication factor was set to zero. The default boundaries were changed for the new orientation with $x$-min, $y$-min and $y$-max boundaries set to normally fixed and the $x$-max boundary set to free with a surcharge applied. These are the same boundary conditions as used in the paper of (Shalabi, 2005). 15-node triangular axisymmetric elements were used for the finite-element mesh. The Mohr Coulomb failure criterion was used to model soil behaviour. The mesh has been refined

around the face of the tunnel to increase the density of calculations. The boundaries and courses of the mesh are shown in Figure 3.3a; darker grey indicates refinement of the mesh. The model needs to be large enough that the boundaries do not affect the results of the model (Potts and Zdravkovic 2001). The focus of the investigation is tunnel face stability. The tunnel lining was included as a line with a prescribed inwards displacement of 0m, $x$-direction, and free displacement parallel to the tunnel axis, $y$-direction. The tunnel lining was modelled with no unsupported length. The pressure on the tunnel face was modelled using a uniform surcharge. Figure 3.3b shows the tunnel in the model with uniform face surcharge and fixed radial displacement. This is similar to the conditions encountered when a tunnel is constructed using a tunnel boring machine. Due to the radial nature of the model, the stresses at any perpendicular distance from the tunnel axis are constant. To extend this to the direction parallel to the tunnel axis $K_0 = 1.0$ has been used in the drained soil model. All other material parameters have been used as presented in section 2.4.1.

Three phases have been used for the model; the first is the confining pressure, the second is the excavation of the tunnel and the third is the tunnel face failure. Due to the weight factor being zero there is no loading in the initial stage. In the confining phase the confining pressure is applied to the $x$-max boundary as a uniform load. This sets up the stresses in the soil before construction. As the stage weight is set to zero the confining pressure needed to be applied separately. This was done by applying a uniform load to the free $x$-max boundary. This load was equal to the confining pressure at the centreline of the tunnel;

$$\sigma_v = \left(C + \frac{D}{2}\right) \times \gamma \qquad (3.1)$$

The layout of the confining phase in PLAXIS is shown in Figure 3.4a. In the tunnel excavation phase the tunnel is excavated by turning off the soil elements, the fixed radial displacement is prescribed along the tunnel lining, and the confining pressure is applied to the face of the tunnel. These steps are carried out so that the only loading in the final phase will be the change in tunnel pressure. The deformations and small strains are reset for the phase. The layout of the excavation phase in PLAXIS is shown in Figure 3.4b. In the tunnel face failure phase the tunnel face support pressure is

reduced to $\sigma_{min}$; a pressure lower than the failure tunnel pressure, $\sigma_F$. In calculation the tunnel face support pressure is reduced from the confining pressure until failure. The deformations and small strains are reset for the phase. The layout of the tunnel face failure phase in PLAXIS is shown in Figure 3.4c. The reduction of tunnel face support pressure runs as a single

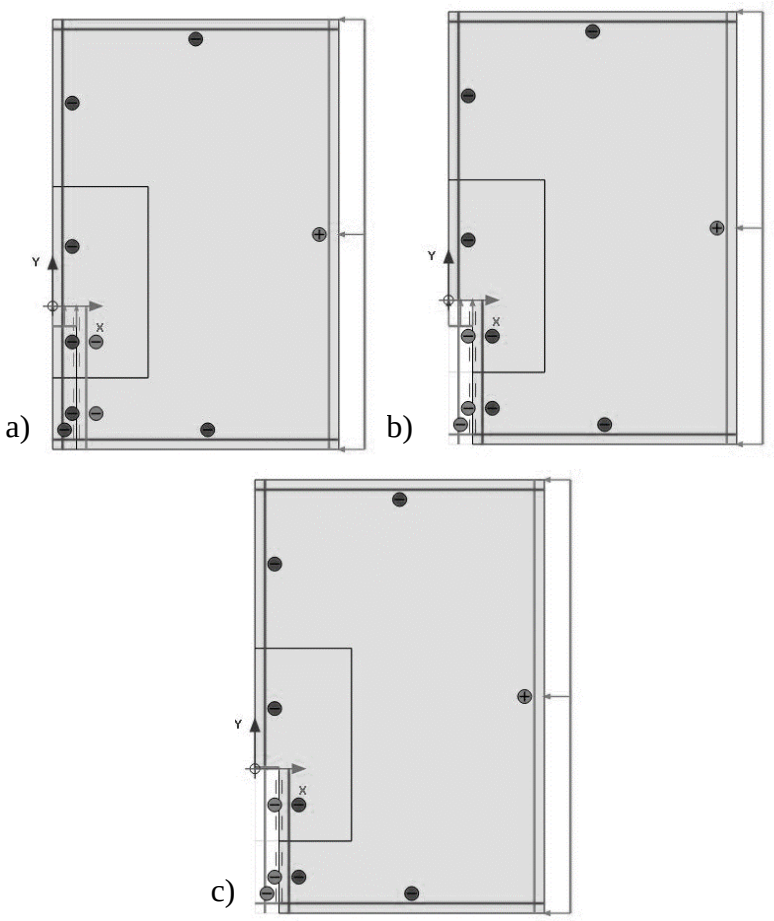


Figure 3.4 Axisymmetric FEM model phase configuration a) confining phase, b) excavation of tunnel phase, and c) tunnel face failure phase

phase to model the behaviour of the tunnel face, which is faster than running multiple stepping stages. The output used is from phase three of the model; the tunnel failure phase. The displacement at the tunnel face is recorded using a strain point on the tunnel face at the axis. The stage factor, $\Sigma M_{stage}$, from PLAXIS is used to find the tunnel face support pressure during each simulation using;

$$\sigma_T = \Sigma M_{stage} \times (\sigma_v - \sigma_{min}) \quad (3.2)$$

From this the elastic and plastic behaviour that occurs at the tunnel face can be seen.

A number of the assumptions that have been used in creating the model were checked. These included the size of the model, the failure shape, the influences of the number of phases on tunnel face failure, the normalisation of displacement to remove the influence of Young's Modulus and the coarseness of the mesh.

Figure 3.5 shows comparisons of the results from the model size that was selected, and a model half the size for the undrained and drained axisymmetric FEM solutions. Dashed lines show the results from the smaller model. It can be seen that the results for both the drained and undrained simulations are consistent between the two sizes for a range of parameters.

It was found that the failure shape of the tunnels did not represent what was typically found in literature for shallow tunnels. Most literature shows the development of the failure surface slightly above the tunnel, as seen in the discussion in section 2.1. The axisymmetric FEM model only has a cone shaped failure at the face if the tunnel, as seen in Figure 3.6. This is likely due to the uniform confining pressure. Leca and Dormieux (1990) and Davis *et at.* (1980) both indicate that as $C/D$ increases the height of the failure above the tunnel becomes smaller. The exact failure shape is not followed but it is similar. The comparison between the axisymmetric FEM and limit analysis solutions shown in section 3.2.2 shows similar results, therefore it is considered acceptable.

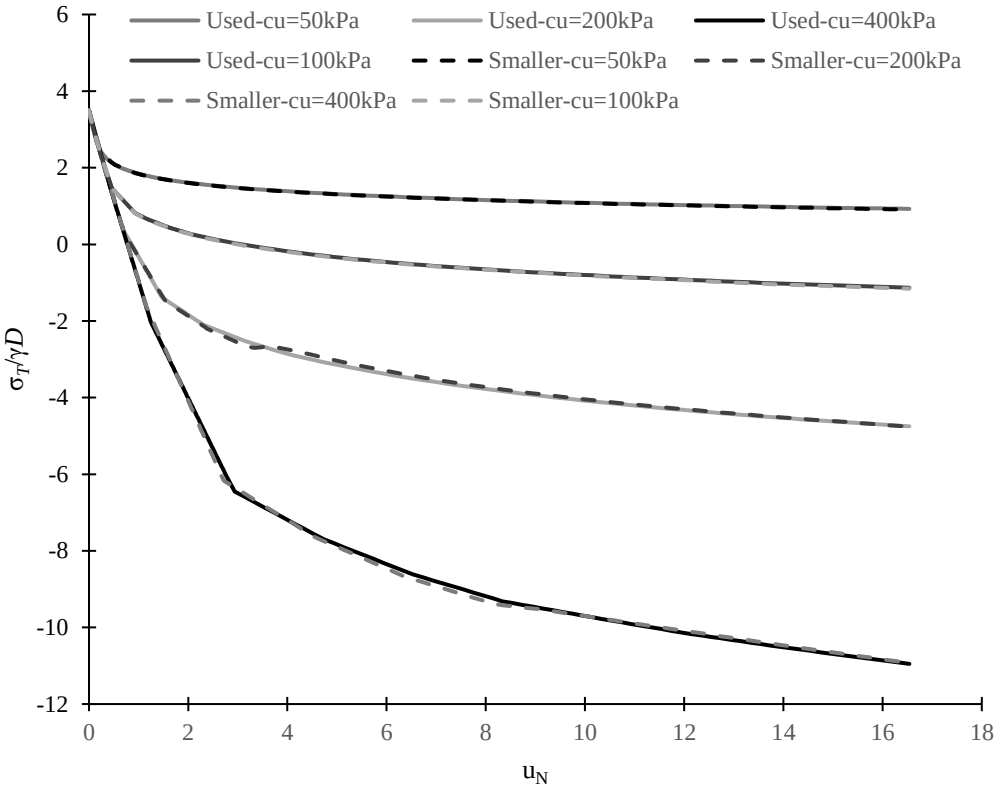


a)

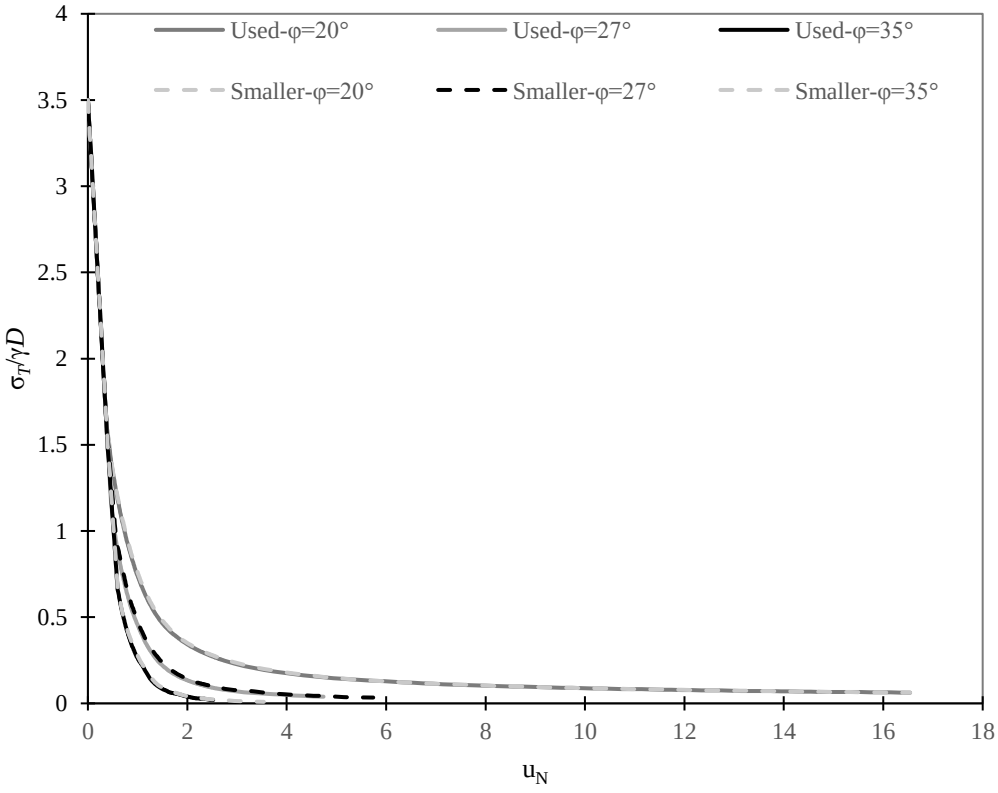


b)

Figure 3.5 Comparison of the chosen a) undrained and b) drained axisymmetric FEM solution, and a smaller model (default parameters)

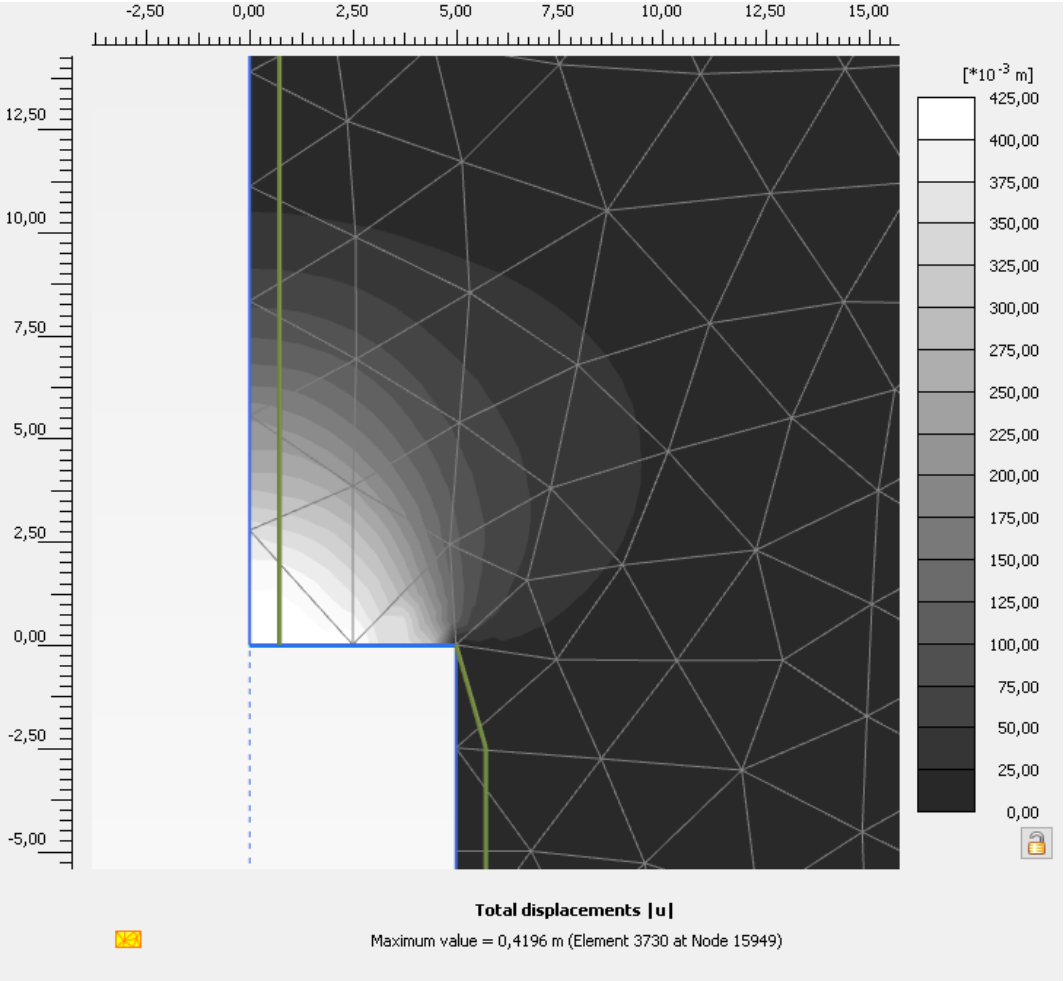


Figure 3.6 tunnel face deformation at failure in axisymmetric FEM model (default drained parameters)

In the axisymmetric FEM model, the tunnel failure has been run in one phase. The sensitivity of the model to being run in one or multiple phases was checked. Figure 3.7a shows a comparison of the tunnel face support pressure computed by single and multi-phase reduction of tunnel face support pressure. It can be seen that the behaviour throughout the single stage, dashed line, is very similar to the behaviour of the multiple stages, solid lines. The normalisation of the displacement in section 2.4.1 was chosen so that different Young's Modulus values do not influence the displacement. Figure 3.7b shows a comparison of the tunnel face pressure computed by two simulations with different Young's Modulus. The largest difference in normalised tunnel face support pressure between the two simulations was less than 0.0001. With the default parameters this is a difference of 0.00003kPa.

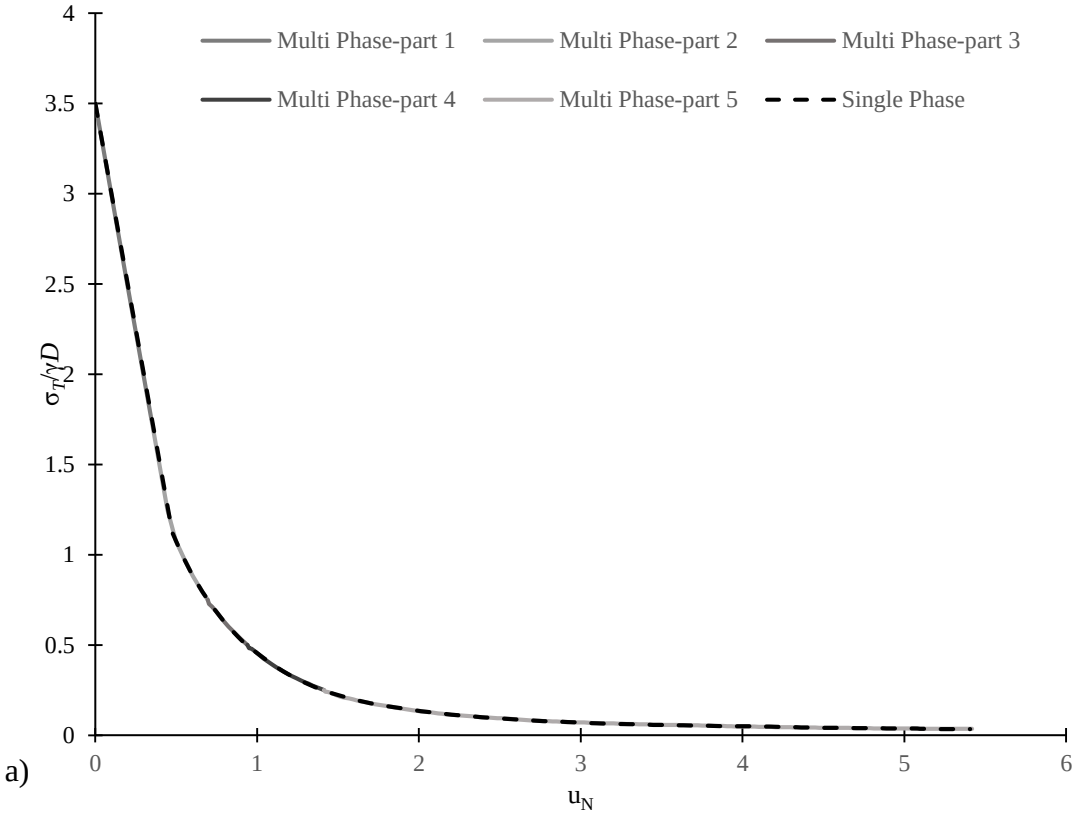


a)

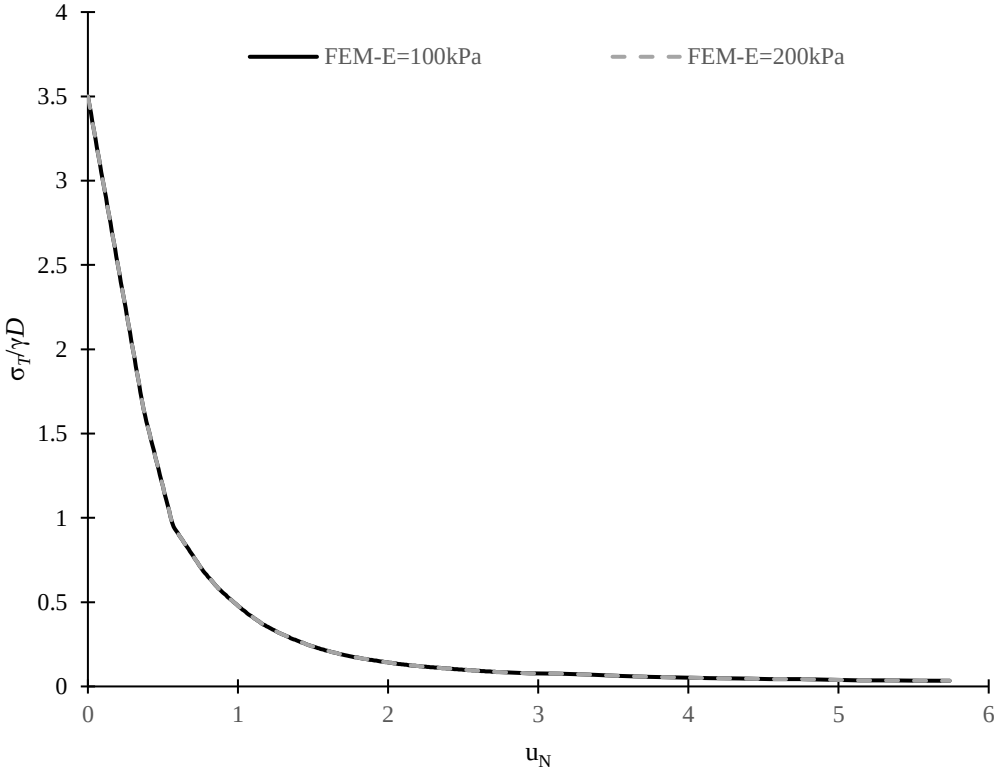


b)

Figure 3.7 Comparison of a) single phase, and multiple phase tunnel face support pressure reduction, and b) *E*=200MPa, and *E*=100Mpa tunnel pressure reduction (default drained parameters)

a)

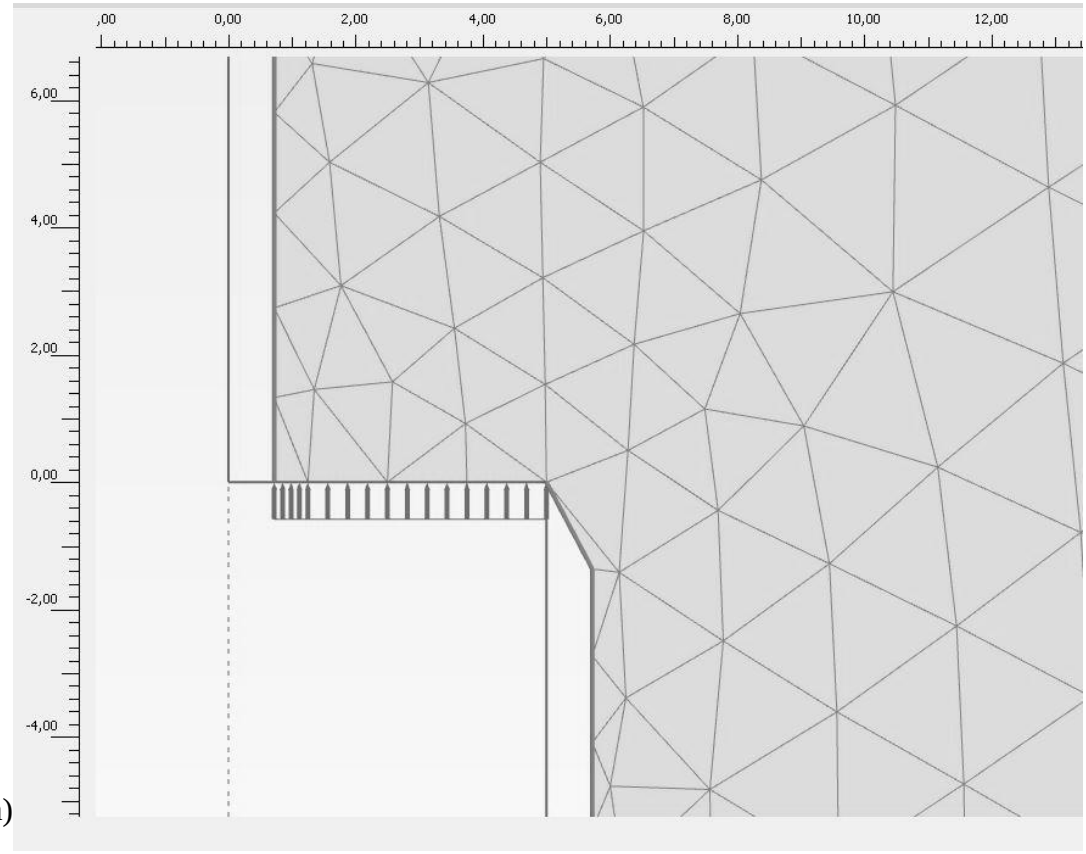


b)

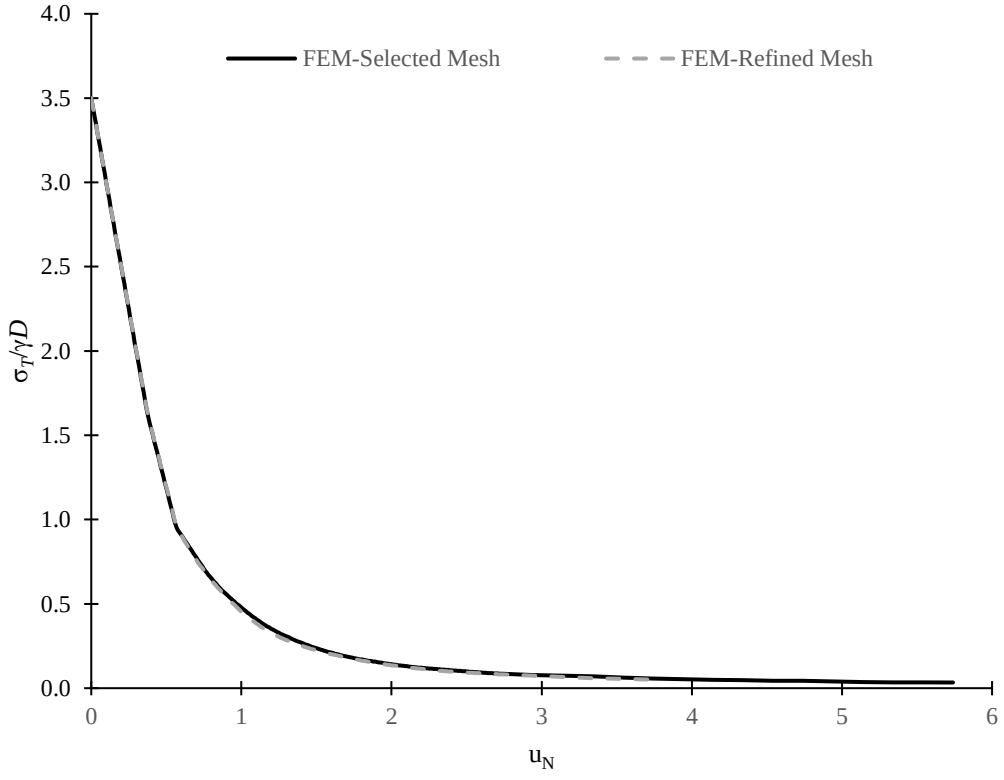


Figure 3.8 Analyses for mesh sensitivity (a) refined mesh, (b) comparison face support pressure computed by selected mesh for analyses of this study with that computed by the refined mesh (default drained parameters)

Sensitivity analysis of mesh refinement was undertaken. The axisymmetric FEM model used in analysis was compared to a model with a refined mesh. The axisymmetric FEM model used in analysis has 3,941 elements, with two elements across the tunnel face. Additional refinement of the mech around the tunnel to have four elements across the face resulted was undertaken. This resulted in 4,339 elements. The refined mesh at the tunnel face is shown in Figure 3.8a. The resulting calculations took almost twice the time to complete. Figure 3.8b shows a comparison of the tunnel face support pressure computed by the mesh used in the analyses, with that computed by the refined mesh using the default drained parameters. It can be seen that there is no significant change in computed face support pressure with the mesh refinement. The largest difference in normalised tunnel face support pressure between the two models was 0.025. With the default parameters this is a difference of 0.007kPa.

### *3.2.2 Comparison of Static Limit State and Axisymmetric Solutions*

The results from the axisymmetric FEM solution and the limit analysis solutions from section 3.1 have been compared. Firstly, the behaviour during the failure phase is compared to the results from the limit analysis solutions. Secondly the trends shown by the application of different parameters on the behaviour of the axisymmetric FEM solution are compared to the trends from the limit analysis solutions.

The static undrained axisymmetric FEM solution has been compared with the tunnel face failure pressure from Davis *et at.* (1980)'s solution. The effect of changing parameters is also compared between the axisymmetric FEM and limit analysis solutions. Only case- 2 and case-3 of Davis, *et al.* (1980)'s solution are presented.

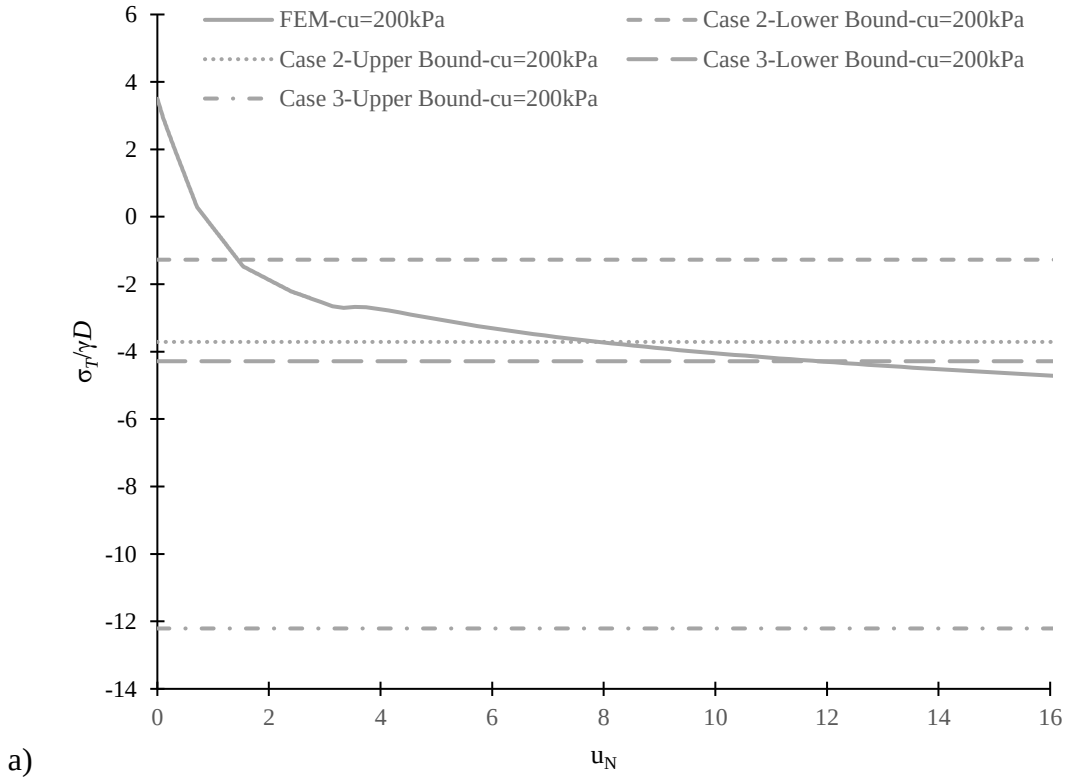


a)

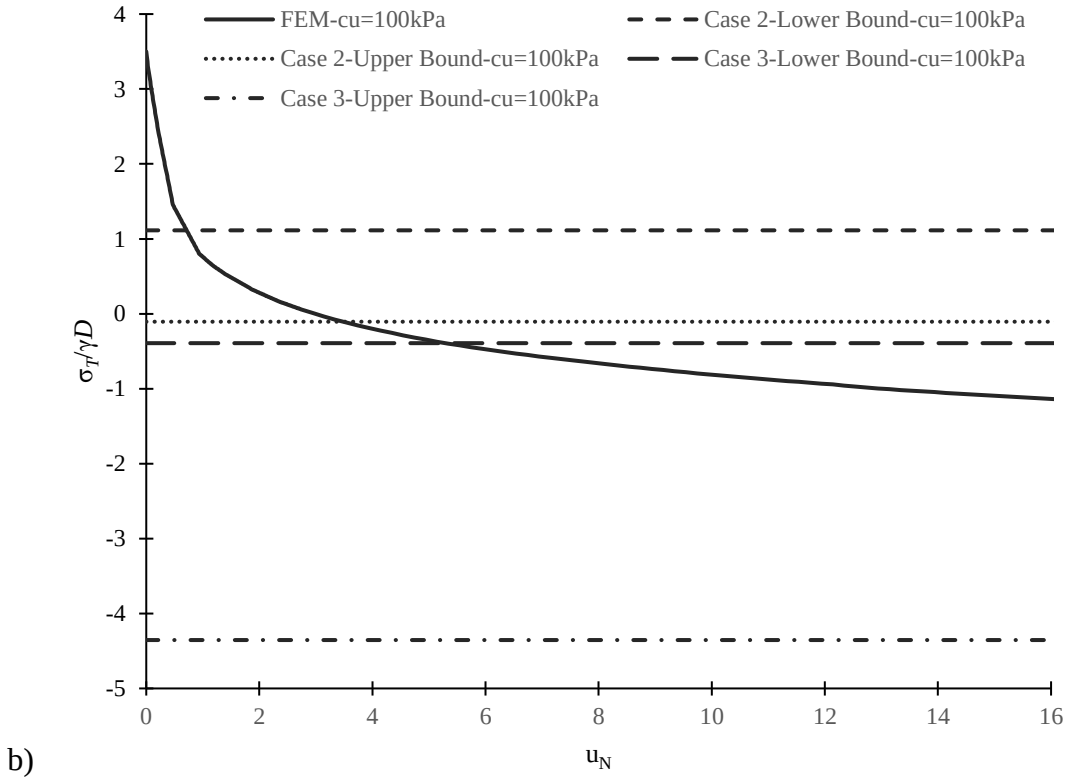


b)

Figure 3.9 Comparison of undrained axisymmetric FEM and Davis et at. (1980)'s solution for a) default parameters, b) $c_u$=100kPa, c) γ=25kN/m3, and d) $\sigma_v$=1100kPa (*C/D*=5)

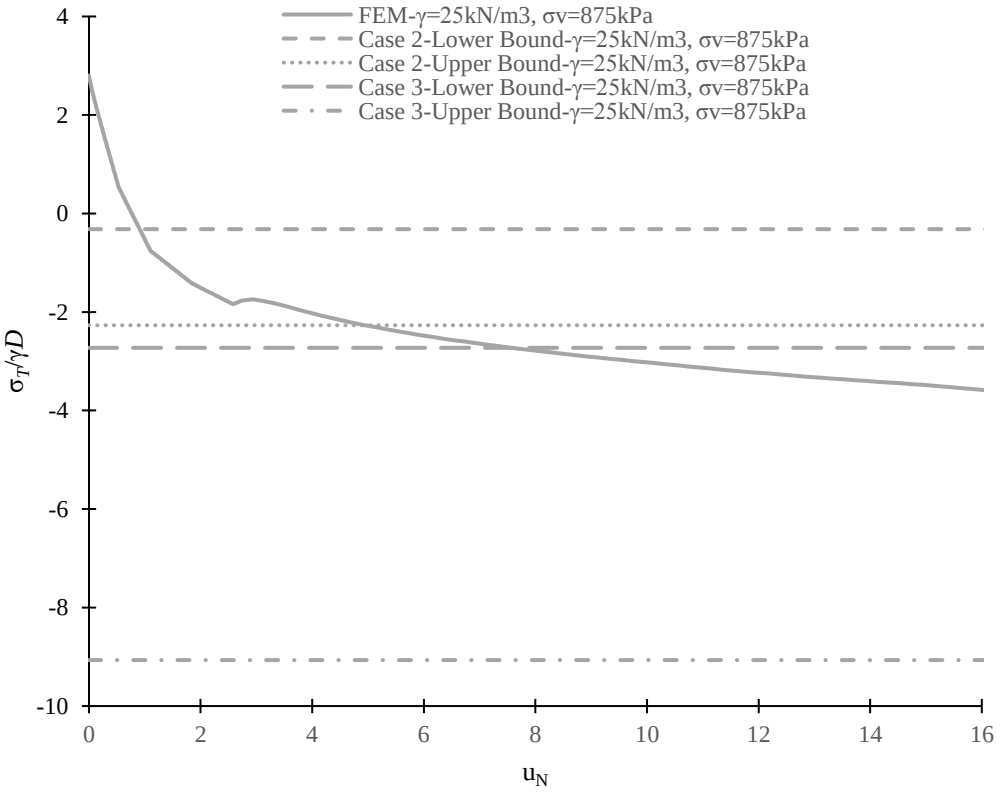


c)

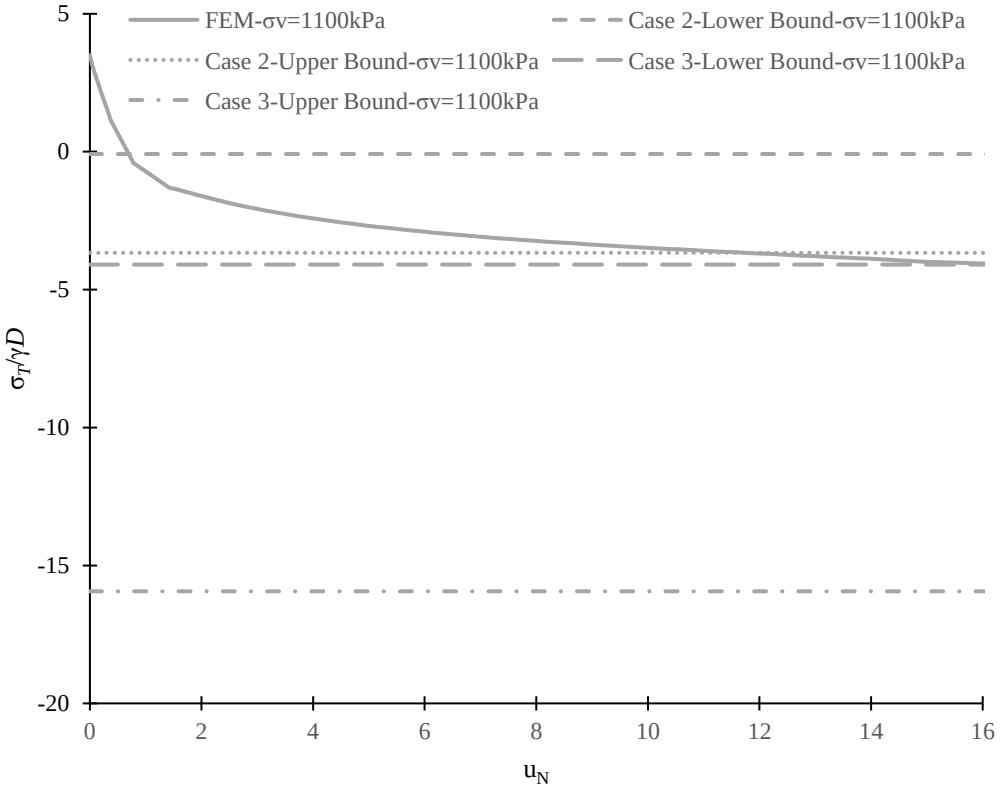


d)

Figure 3.9 Continued

The behaviour from a number of undrained simulations using the axisymmetric FEM and Davis *et at.* (1980)'s solutions are compared in Figure 3.9. The results for the simulations with default parameters are shown in Figure 3.9a. It can be seen that the final value for very large normalised displacement, is between the case-3 bounds, while elastic to plastic behaviour transitions around the case-2 lower bound. The results for the simulations with an undrained shear strength of 100kPa are shown in Figure 3.9b. The comparison is consistent with the default parameters. The results for the simulations with a unit weight of 25kN/m$^3$ and confining stress of 875kPa, $C/D = 3$, are shown in Figure 3.9c. The comparison is consistent with the default simulation. The solutions for the simulations with a confining stress of 1100kPa, $C/D = 5$, are shown in Figure 3.9d. The comparison is consistent with the default parameters. This $C/D$ ratio is outside the limitations of the study by Davis *et at.* (1980).

The effects of undrained shear strength, confining stress and unit weight on the undrained axisymmetric FEM simulation results are shown in Figure 3.10. Figure 3.10a shows the effect of undrained shear strength on the tunnel face support pressure. It can be seen that increasing the undrained shear strength reduces the tunnel face failure pressure. This is consistent with Davis *et at.* (1980)'s solution. Figure 3.10b shows the effect of unit weight on the tunnel face support pressure. It can be seen that increasing the unit weight while keeping the $C/D$ ratio the same increases the tunnel face failure pressure. This increase in pressure is similar to Davis *et at.* (1980)'s solution but of a much larger magnitude. Figure 3.10c shows the effect of confining pressure on the tunnel face support pressure. It can be seen that there is a slight increase in tunnel face failure pressure with the increase in confining pressure. The confining pressure is related to $C/D$ ratio and the unit weight used in Davis *et at.* (1980)'s solution. The variation in behaviour of the undrained axisymmetric FEM solution results are consistent with Davis *et at.* (1980)'s solution when different values of undrained shear strength are compared. The effect of both unit weight and confining pressure on the axisymmetric solution are generally similar to Davis *et at.* (1980)'s solution.

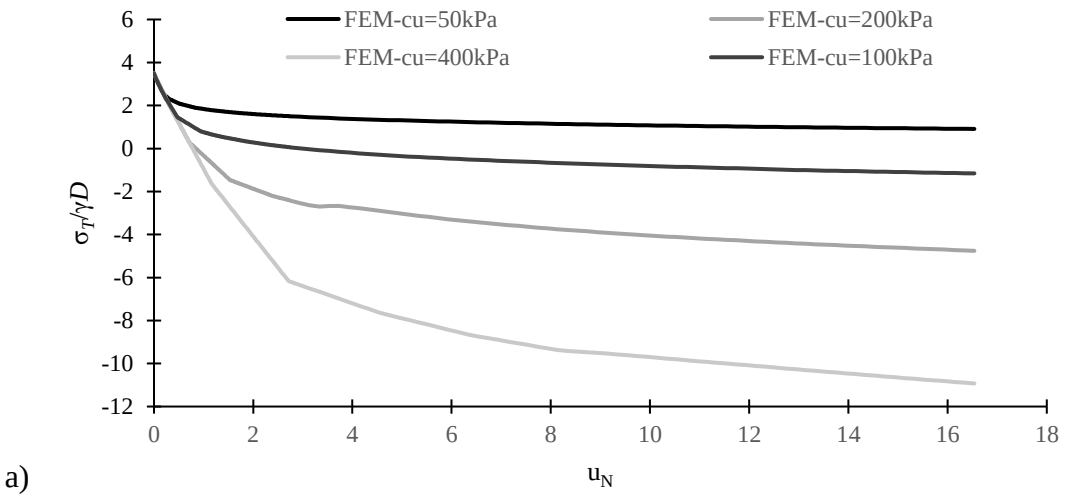


a)

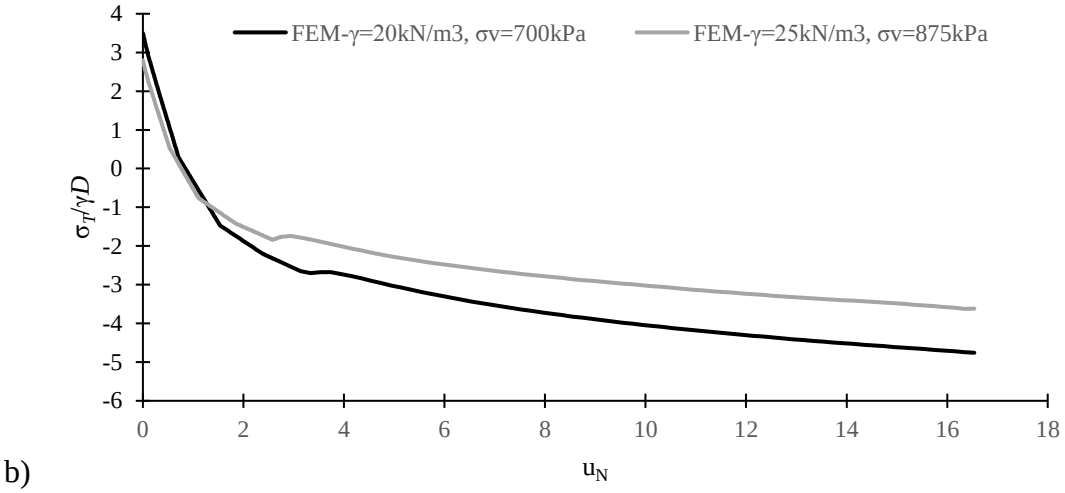


b)

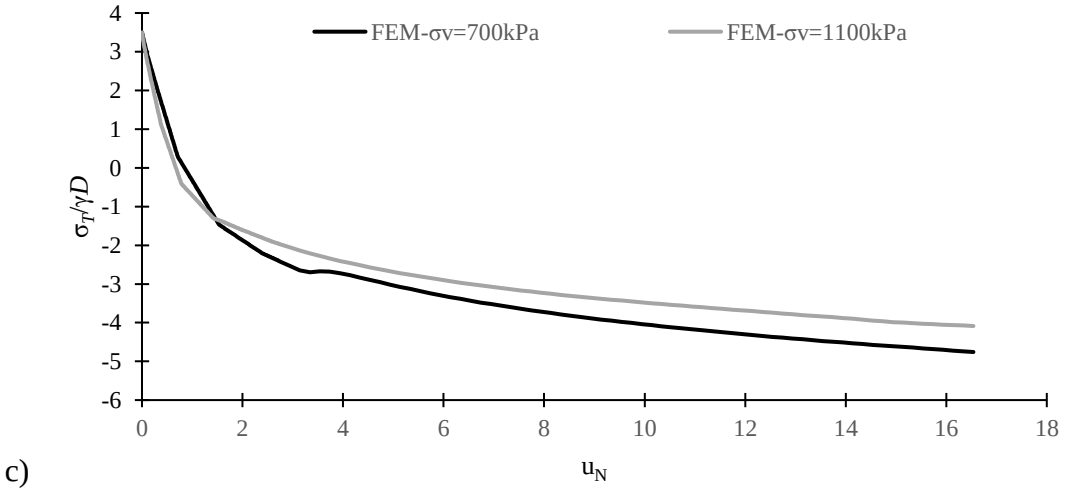


c)

Figure 3.10 Effect of a) undrained shear strength, b) unit weight, and c) confining pressure on tunnel face stability using axisymmetric solution

The static drained axisymmetric FEM solution has been compared against the tunnel face failure pressure from Leca and Dormieux (1990)'s solution. The effect of changing parameters is also compared between the axisymmetric FEM and limit analysis solutions.

The behaviour from a number of drained simulations using the axisymmetric FEM and Leca and Dormieux (1990)'s solutions are compared in Figure 3.11.The results for the simulations with default parameters are shown in Figure 3.11a. It can be seen that the behaviour transitions from elastic to plastic behaviour slightly below the lower bound. The upper bound is near but slightly larger than the failure point of the axisymmetric simulation. The results for the simulations with an effective friction angle of 35° are shown in Figure 3.11b. The comparison is consistent with the default parameters. The results for the simulations with an effective cohesion of 10kPa are shown in Figure 3.11c. The comparison is consistent with the default parameters. The results for the simulations with a unit weight of 25kN/m$^3$ and confining stress of 875kPa, $C/D = 3$, are shown in Figure 3.11d. The comparison is relatively consistent with the default simulation. The distance from the lower bound to the end of elastic behaviour and from the upper bound to failure is larger when compared to the results using default parameters. The results for the simulations with a confining stress of 1100kPa, $C/D = 5$, are shown in Figure 3.11e. The comparison is similar to the unit weight comparison. This $C/D$ ratio is outside the limitations of the study by Leca and Dormieux (1990).

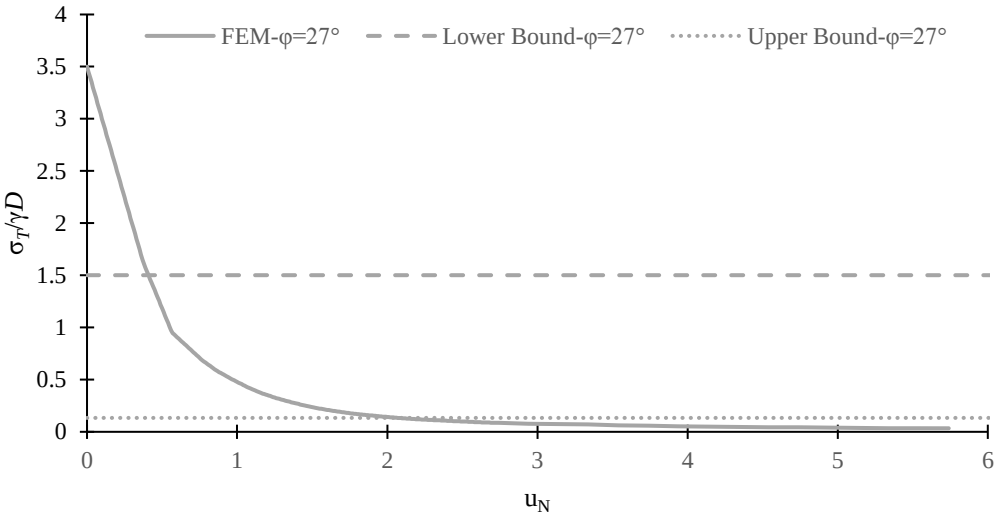


a)

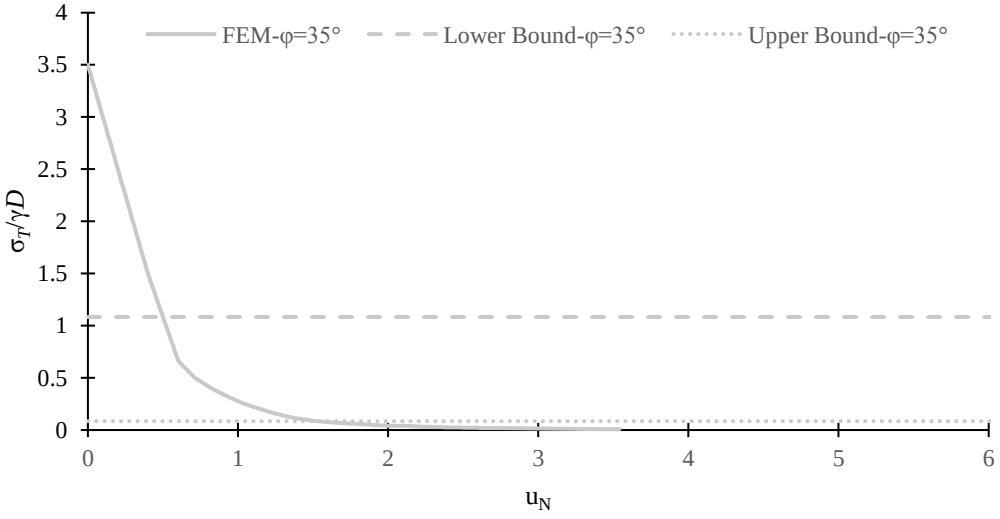


b)

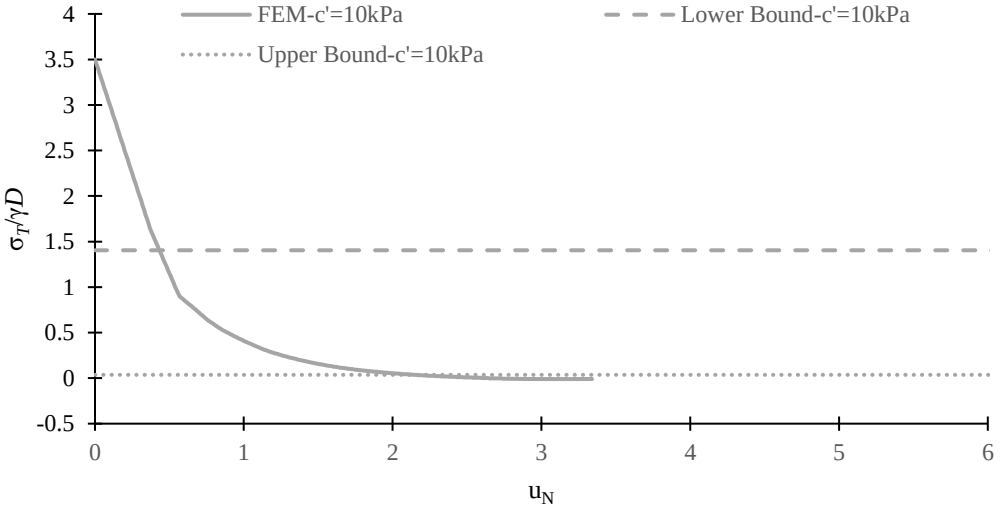


c)

Figure 3.11 Comparison of drained axisymmetric FEM and Leca and Dormieux (1990)'s solutions for a)default parameters, b) ϕ=35°, c) *c*'=10kPa, d) γ=25kN/m3, and d) $\sigma_v$=1100kPa (*C/D*=5)

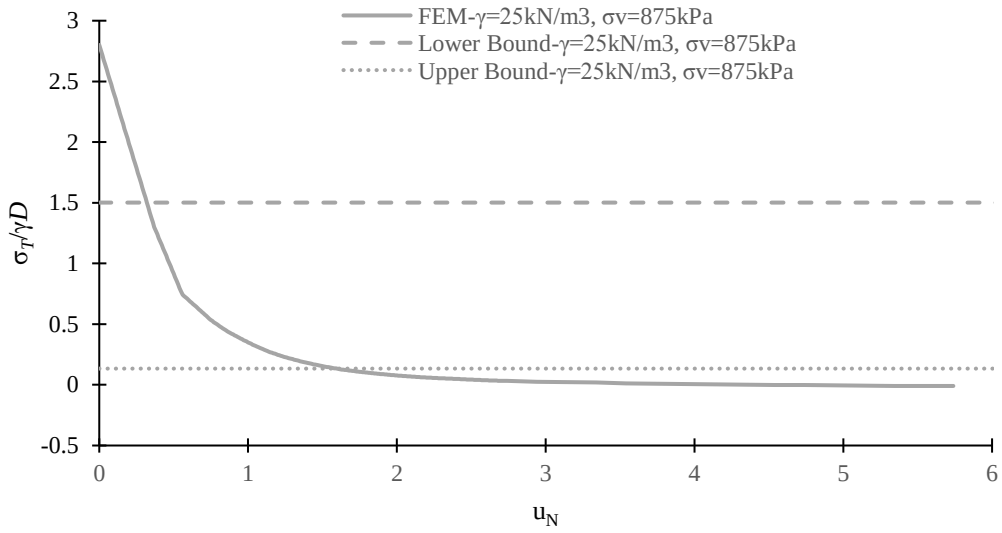


d)

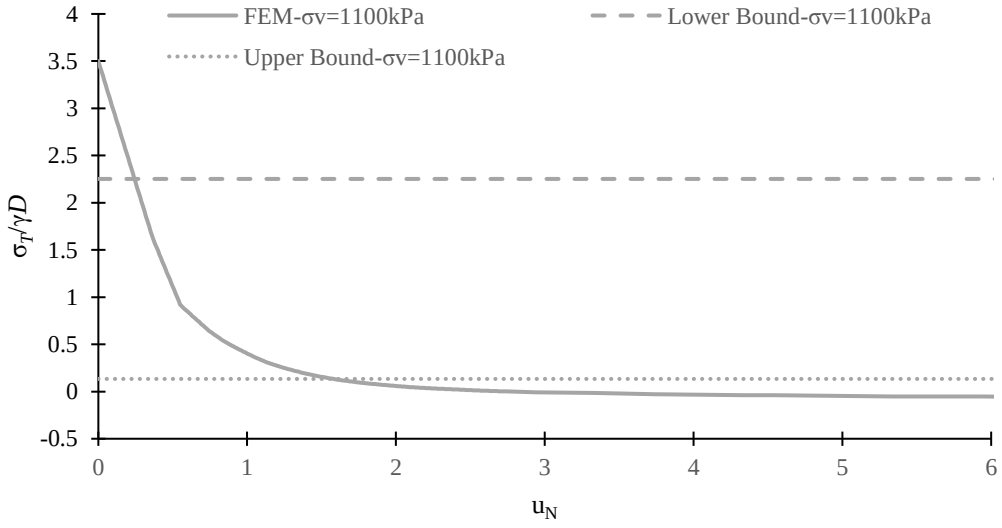


e)

Figure 3.11 Continued

The effects of effective friction angle, effective cohesion, confining stress and unit weight on the drained axisymmetric simulation results are shown in Figure 3.12. Figure 3.12a shows the effective friction angle on the tunnel face support pressure. It can be seen that increasing the effective friction angle reduces the tunnel face failure pressure. This is consistent with Leca and Dormieux (1990)'s solution. Figure 3.12b shows the effective cohesion on the tunnel face support pressure. It can be seen that increasing the effective cohesion reduces the tunnel face failure pressure. This is consistent with Leca and Dormieux (1990)'s solution. Figure 3.12c shows the effect of unit weight on the tunnel face support pressure. It can be seen that increasing the unit weight while keeping the $C/D$ ratio the same reduces the tunnel face failure pressure. This is not the same as Leca and Dormieux (1990)'s solution where there is no change in the normalised tunnel face failure pressure due to unit weight. Figure 3.12d shows the effect of confining pressure on the tunnel face support pressure. It can be seen that there is a reduction in tunnel face failure pressure with the increase in confining pressure. The confining pressure is related to $C/D$ ratio and the unit weight used in Leca and Dormieux (1990)'s solution. The axisymmetric comparison is not consistent with the paper of Leca and Dormieux (1990), which shows no variation in normalised tunnel face failure pressure with variation in unit weight and only a lower bound increase with $C/D$ ratio.

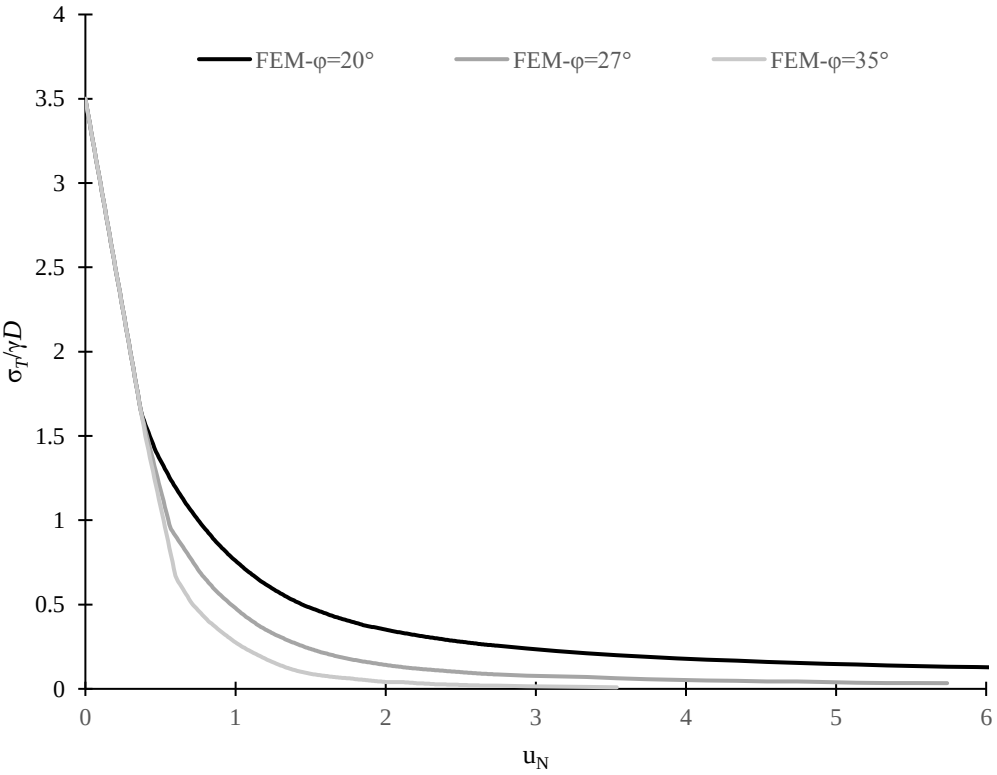


a)

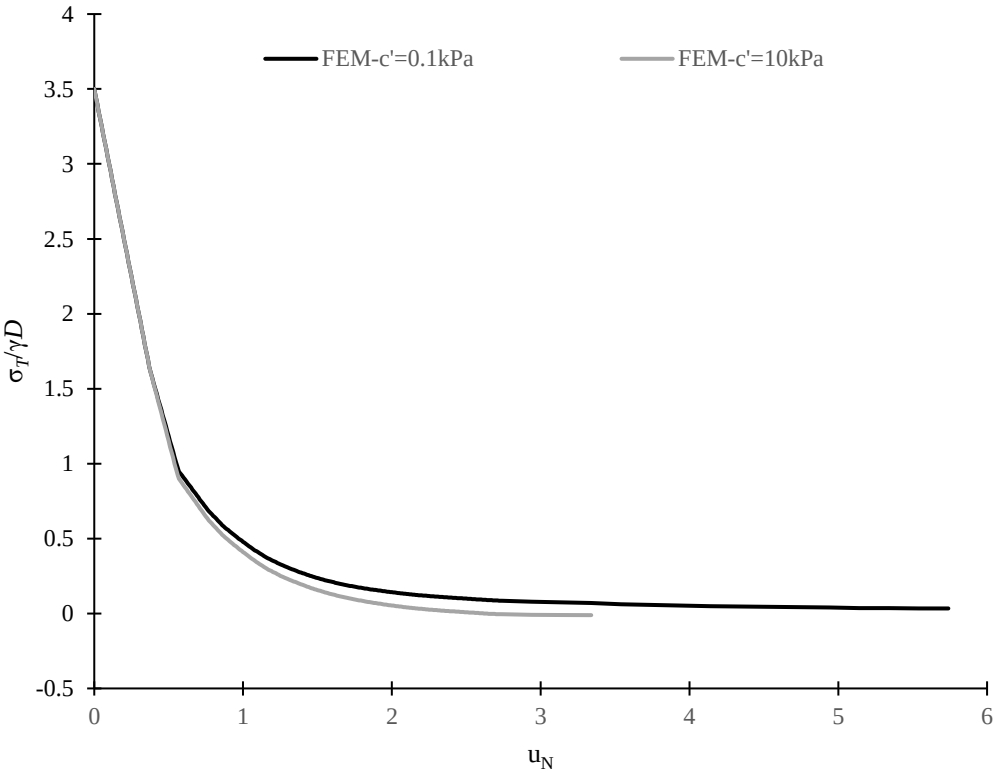


b)

Figure 3.12 Effect of a) effective friction angle, b) effective cohesion, c) unit weight, and d) confining pressure on tunnel face stability using axisymmetric solution

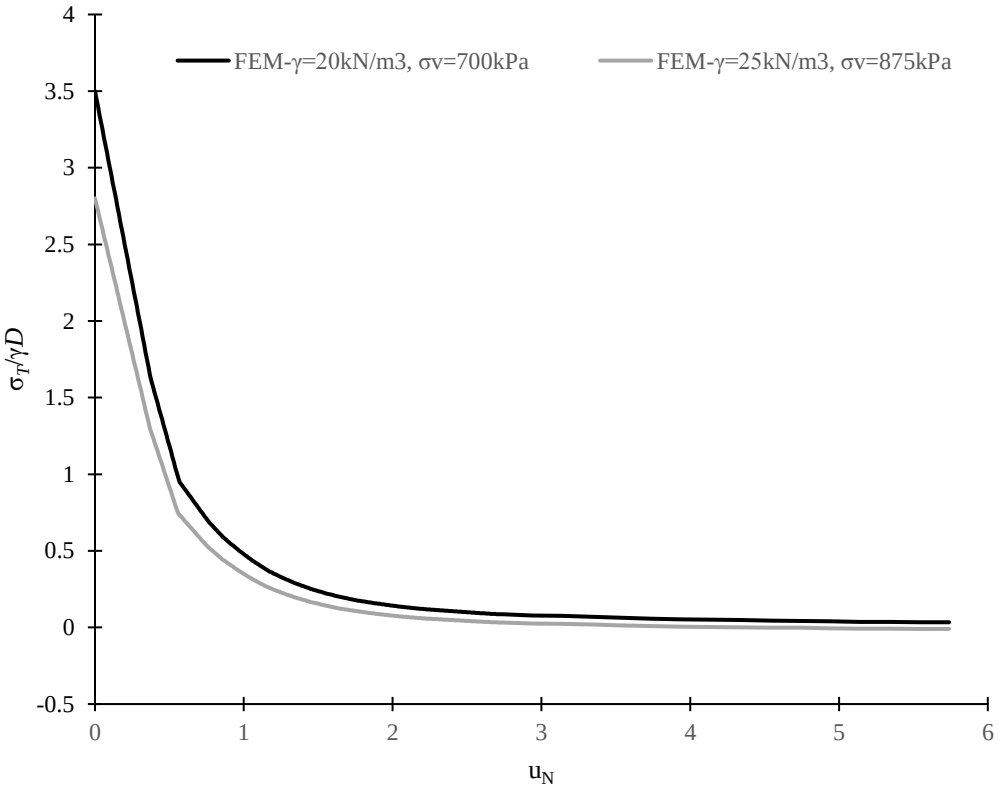


c)

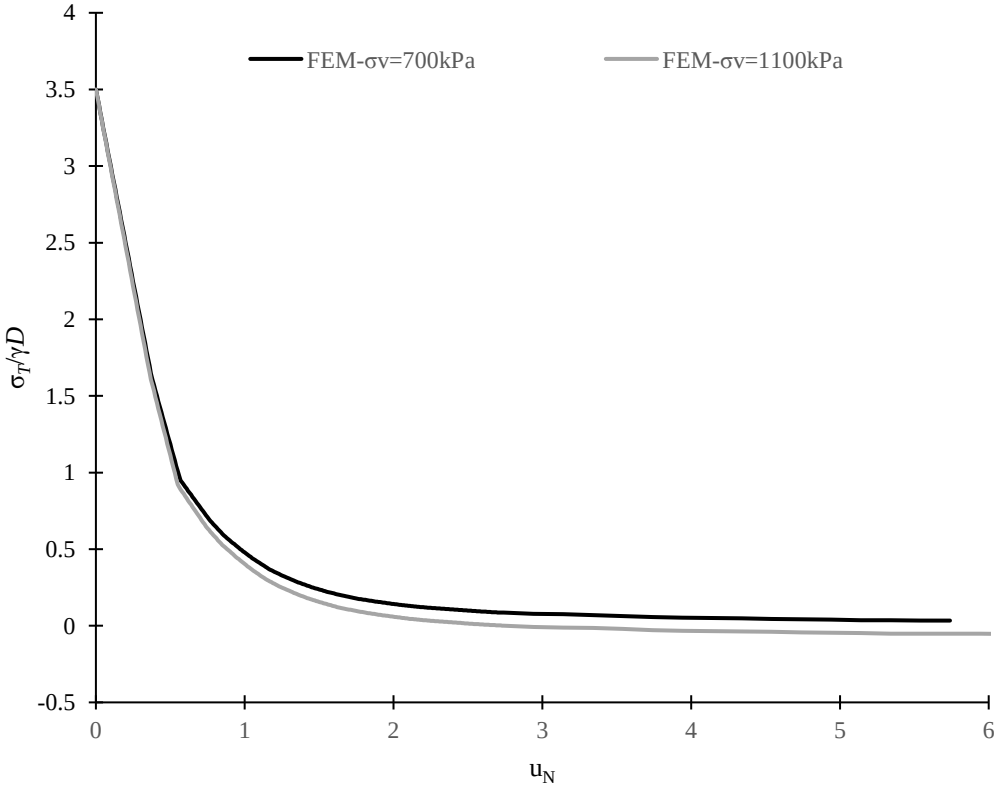


d)

Figure 3.12 Continued

The variation in behaviour with the drained axisymmetric FEM solution gives consistent results when compared to Davis *et at.* (1980)'s solution for different values of effect friction angle and effective cohesion. The effect of both unit weight and confining pressure on the axisymmetric solution is not consistent with Leca and Dormieux (1990)'s solution.

### *3.2.3 Definition of Failure*

To be able to compare the results of different axisymmetric FEM simulations it is necessary to define a point of failure. An examination of the simulation results shows that the behaviour typically results in an initial elastic stiffness and then transitions into plastic failure. The final failure of a simulation was very sensitive to small changes in the model. It also occurred at very large values in the undrained analysis, in some cases $u_N > 50$ . This was not considered an appropriate failure point for comparison. To quantify failure a set normalised deformation, $u_{N_F}$, between the axisymmetric FEM analysis and the initial elastic behaviour has been chosen. This is demonstrated in Figure 3.13. The solid black line shows the results from the axisymmetric simulation while the dashed grey line shows the elastic behaviour. When the distance between the two lines reaches $u_{N_F}$ this is considered failure. The normalised tunnel face support pressure and normalised displacement at failure can then be found; the dotted grey and black lines respectively. The tunnel pressure at this point is used as the normalised failure tunnel pressure, $\sigma_{T_F}$. The value chosen for the deformation must be large enough that significant plastic deformation occurs but small enough that all simulations did not reach final failure before this point.

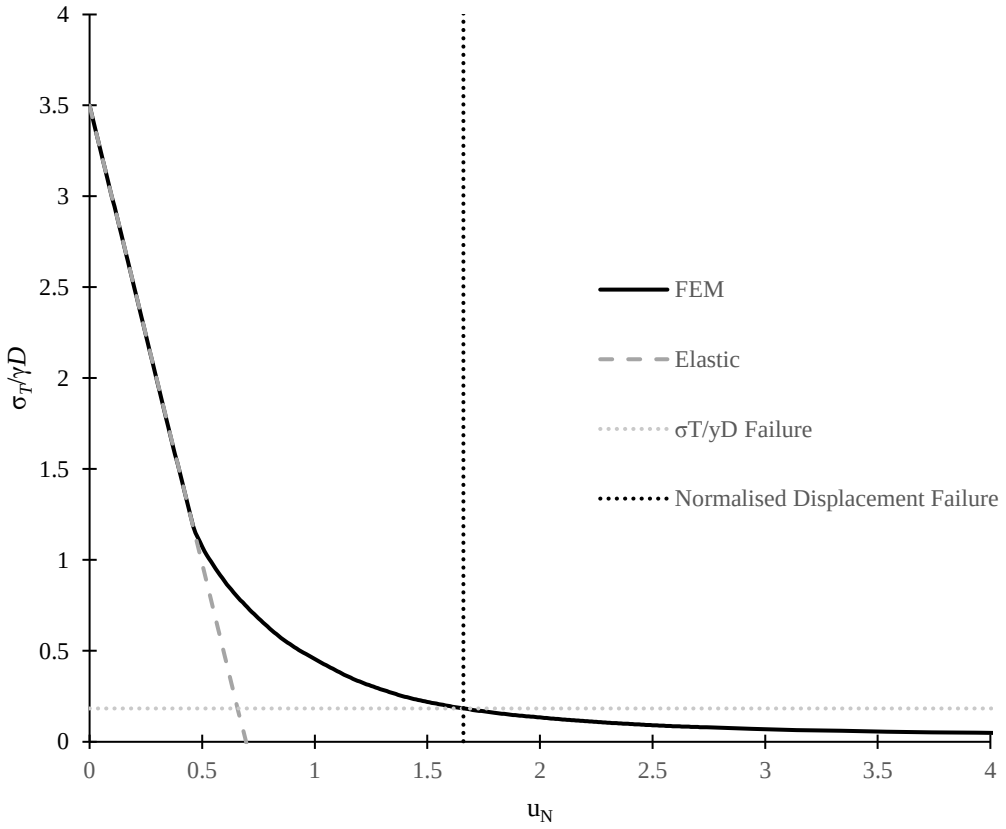


Figure 3.13 Definition of failure for axisymmetric FEM solution (default drained parameters)

For this study $u_{N_F} = 5$ has been used for the displacement gap in the undrained analysis. Figure 3.14 shows the tunnel face failure pressure from the axisymmetric FEM and Davis *et at.* (1980)'s solutions for a number of different parameters. The results are consistent with the comparisons above. Figure 3.14a shows the comparison for undrained shear strength. It can be seen that using this failure criteria the axisymmetric FEM solution failure pressure is close to the upper bound of case-2 and the lower bound of case-3. It can be seen that at greater undrained shear stress values the FEM solution requires a slightly larger tunnel face support pressure. Figure 3.14b shows the comparison for unit weight. It can be seen that the FEM results are around the same limit analysis solutions. They follow a similar trend. Figure 3.14c shows the comparison for depth ratio, or confining stress. It can be seen that the FEM results are around the same limit analysis solutions. They follow a similar trend. In all the comparisons the axisymmetric FEM solution failure results are similar to the lower

bound of case-3 from the limit analysis solution. This is consistent with experimental results from the paper of Davis *et at.* (1980). When comparing the failure points from the axisymmetric FEM solution to Davis *et at.* (1980)'s solution the differences in results for variation of unit weight and confining stress, identified above, are reduced. This is because the variation at moderate normalised displacement is smaller. From these comparisons the prediction of tunnel face support pressure using the undrained axisymmetric FEM solution is generally consistent with Davis *et at.* (1980)'s solution.

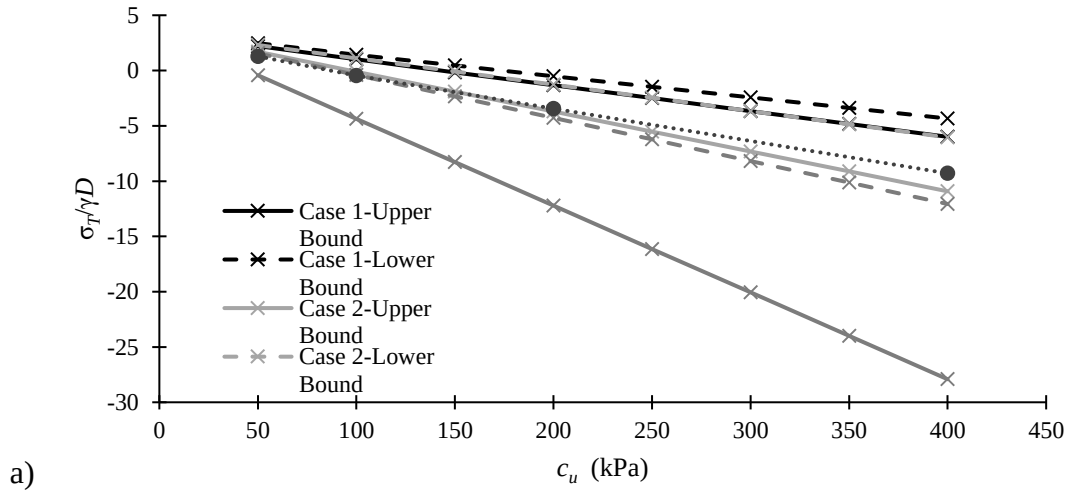


a)

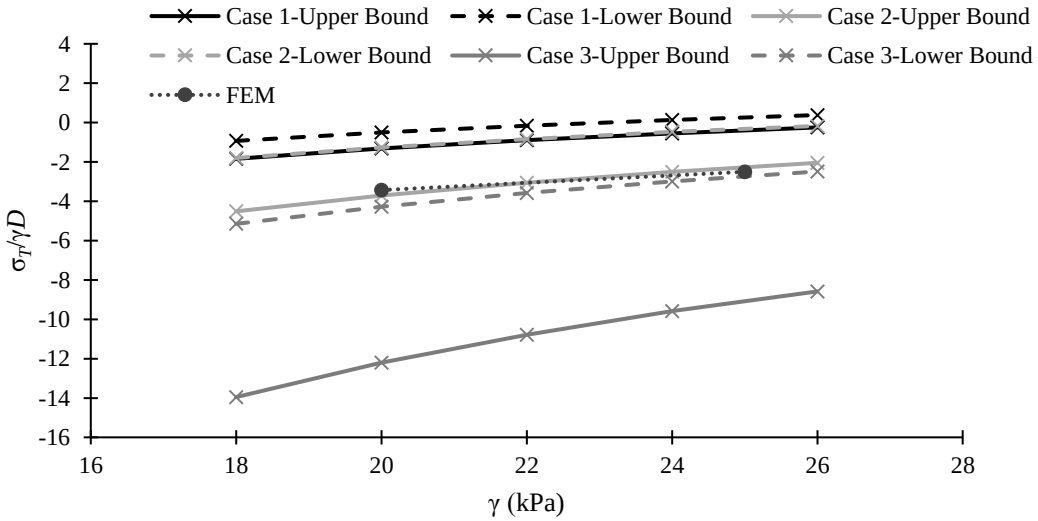


b)

Figure 3.14 Comparison of tunnel face failure pressure from undrained axisymmetric FEM and Davis et at. (1980)'s solutions for a) undrained shear strength, b) unit weight, and c) depth ratio

c)

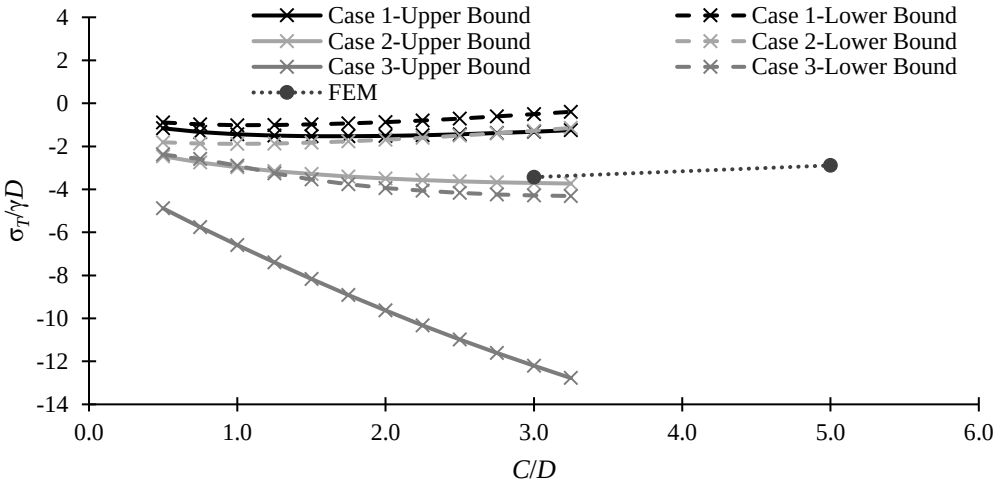


Figure 3.14 Continued

For this study $u_{N_F} = 1$ has been used for the displacement gap in the drained analysis. A smaller number, when compared to the undrained analysis, was chosen as the drained analysis typically stopped calculation at smaller displacements. Figure 3.15 shows the tunnel face failure pressure for the axisymmetric FEM and Leca and Dormieux (1990)'s solutions for a number of different parameters. The results are consistent with the comparisons above. Figure 3.15a shows the comparison for effective friction angle. It can be seen that using this failure criteria the axisymmetric FEM solution failure pressure is comparatively larger than the upper bound solution at lower effective friction angle values. Figure 3.15b shows the comparison for effective cohesion. It can be seen that the FEM results are slightly larger than the upper bound solution. They follow a similar trend. Figure 3.15c shows the comparison for unit weight. It can be seen that the FEM results are around the upper bound solution. Figure 3.15d shows the comparison for depth ratio, or confining stress. It can be seen that the FEM results are around the upper bound solution. In all the comparisons the axisymmetric FEM solution failure results are near, typically slightly larger than, the upper bound of the limit analysis solution. This is consistent with experimental results from the paper of Leca and Dormieux (1990). When comparing the failure points from the axisymmetric FEM solution to Leca and Dormieux (1990)'s solution the differences in results for variation of unit weight and confining stress, identified above,

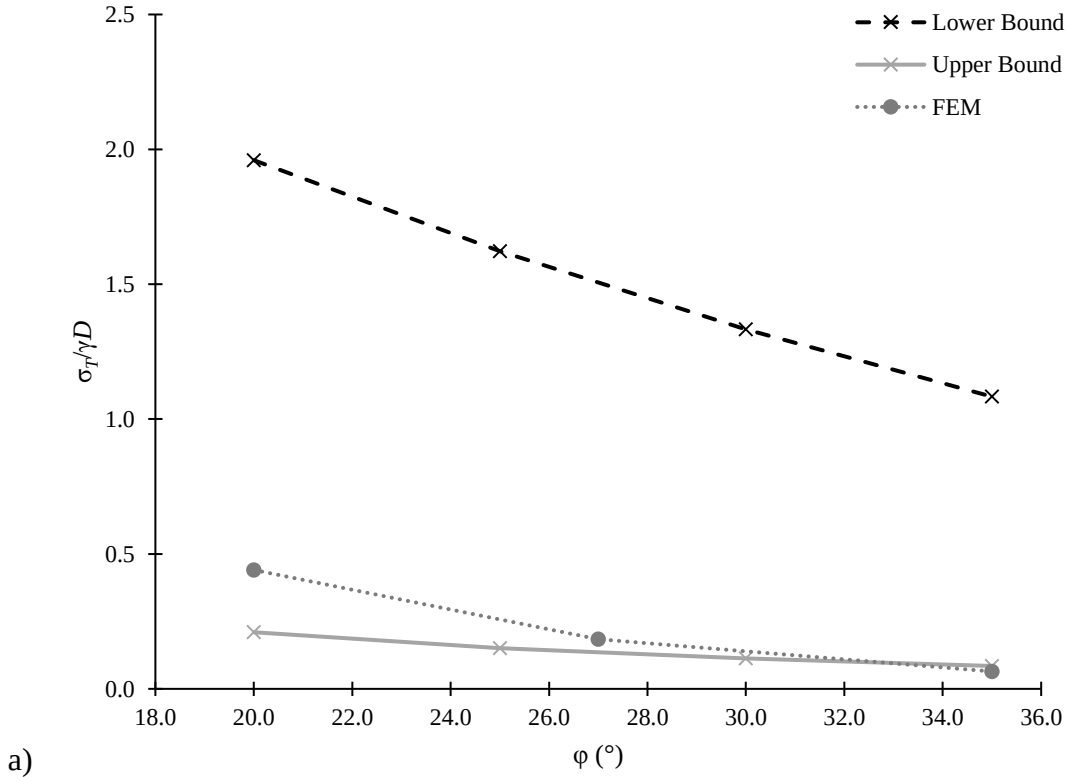


a)

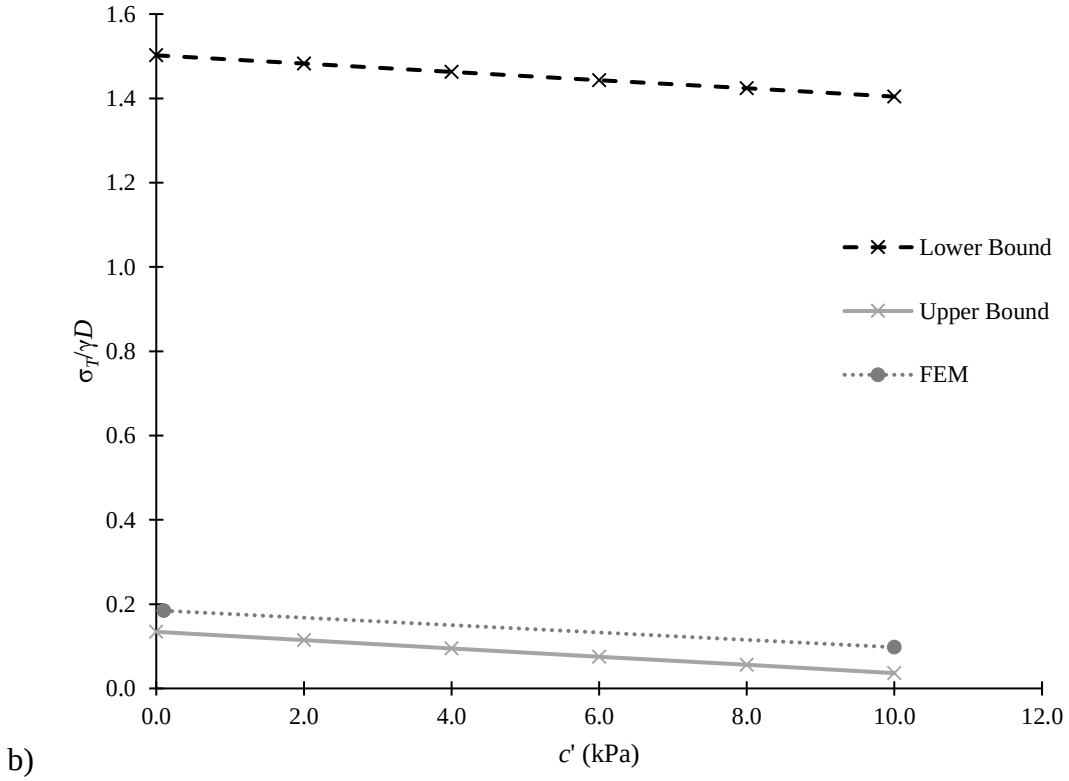


b)

Figure 3.15 Comparison of tunnel face failure pressure from drained axisymmetric FEM and Leca and Dormieux (1990)'s solutions for a) effective friction angle, b) effective cohesion, c) unit weight, and d) depth ratio

c)

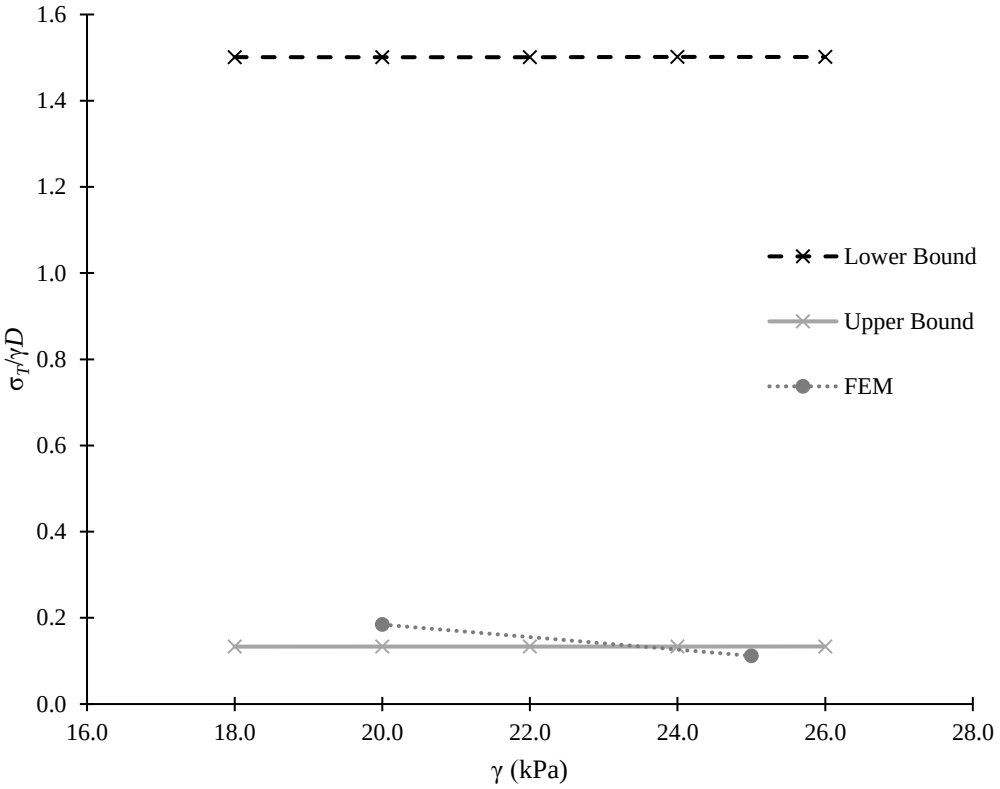


d)

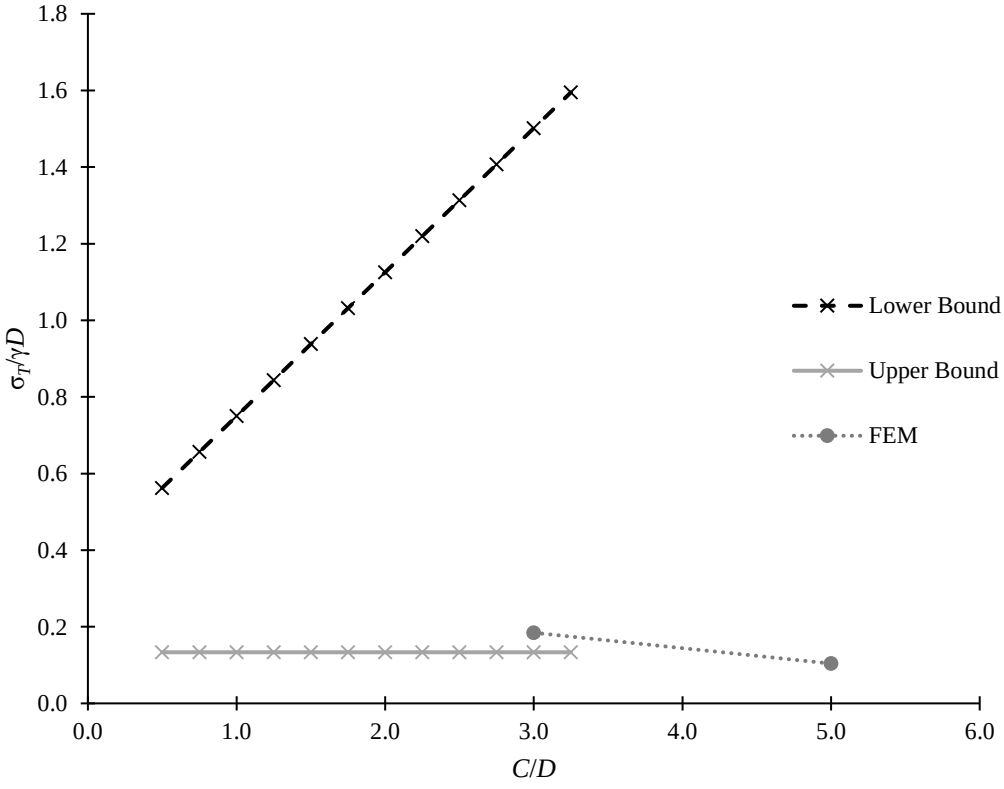


Figure 3.15 Continued

are apparent. The differences are small when compared to the range of Leca and Dormieux (1990)'s solution. They are likely due to the assumptions required to simplify the problem to an axisymmetric solution. From these comparisons the prediction of tunnel face support pressure using the drained axisymmetric FEM solution is generally consistent with Leca and Dormieux (1990)'s solution. However, there should be consideration of the slightly different trends found for variation of unit weight and confining stress when developing conclusions.

# CHAPTER 4

# ASSESSMENT OF SEISMIC TUNNEL FACE STABILITY

In this section the axisymmetric FEM model developed in section 3.2 is used to investigate the effect of seismic forces on tunnel face stability. The tunnel face support pressure required to ensure stability with respect to the seismic coefficient, $k_h$, is calculated. The application $k_h$ of is done by applying a distributed static force to the model, that is equal to the unit weight of material multiplied by $k_h$. This force approximates the effect of an earthquake without the requirement of time history analysis. The application of the pseudo static force and required changes to the model are outlined. The results of the pseudo static analysis are presented and compared to previous research. Finally, suggestions for the development of seismic design factors are made. It is important that the axisymmetric FEM model can adequately reflect tunnel face stability. Any imprecision in the static solution can erroneously impact the seismic results. Therefore, it is important that any inconsistencies found in the development and verification of the static solution are considered when discussing the seismic results.

## 4.1 Applying Pseudo Static Forces to the Axisymmetric FEM Model

The pseudo static force was applied as $k_h$ using the weight factor in PLAXIS. The weight factor was used was because the in built PLAXIS pseudo static factor does not work when the weight factor is zero (Brinkgreve *et al.*, 2017). The weight factor cannot be negative. Therefore, the orientation of the tunnel for pseudo static analysis must be such that the tunnel is advancing from the base of the model. If the tunnel is orientated to advance from the top of the model the applied weight factor would be a stabilising force. To ensure that the tunnel face support pressure was the only thing that was changing in the last phase $k_h$ was applied in the excavation phase. Five different values of $k_h$ were analysed; 0.05, 0.1, 0.2, 0.35 and 0.5. These are over a range similar to that used by Saada *et al.* (2013).

To apply $k_h$ to the model, some of the boundary parameters had to be changed. These were changed in both the excavation and tunnel face support pressure reduction phases. The normally fixed boundary at $y$-max was creating tension in the top of the model when the earthquake loading was applied. The tension failure points can be seen at the top of Figure 4.1a. To prevent this, the fixity of the $y$-max boundary was changed to free and a uniform force was added. The value of this force equals the stress in the $y$-direction along the $y$-max boundary at the end of the confining phase under static conditions. After this change the free boundary at $x$-max was failing similar to a triaxial test at the bottom of the boundary. The application of $k_h$ was creating compression in the model. These failure points can be seen in Figure 4.1b, where both. $x$-max and $y$-max boundaries are set as free with confining stress applied. To prevent this the fixity of the $x$-max boundary was changed to normally fixed. This prevented the displacement and failure as it provides additional confining pressure. Figure 4.1c shows no failure developed when the normally fixed $x$-max boundary, free $y$-max boundary and $y$-max surcharge were applied. These effects were more predominant in the undrained model and at higher values of $k_h$. The boundary changes were applied to all models, undrained and drained, so that the analysis was consistent.

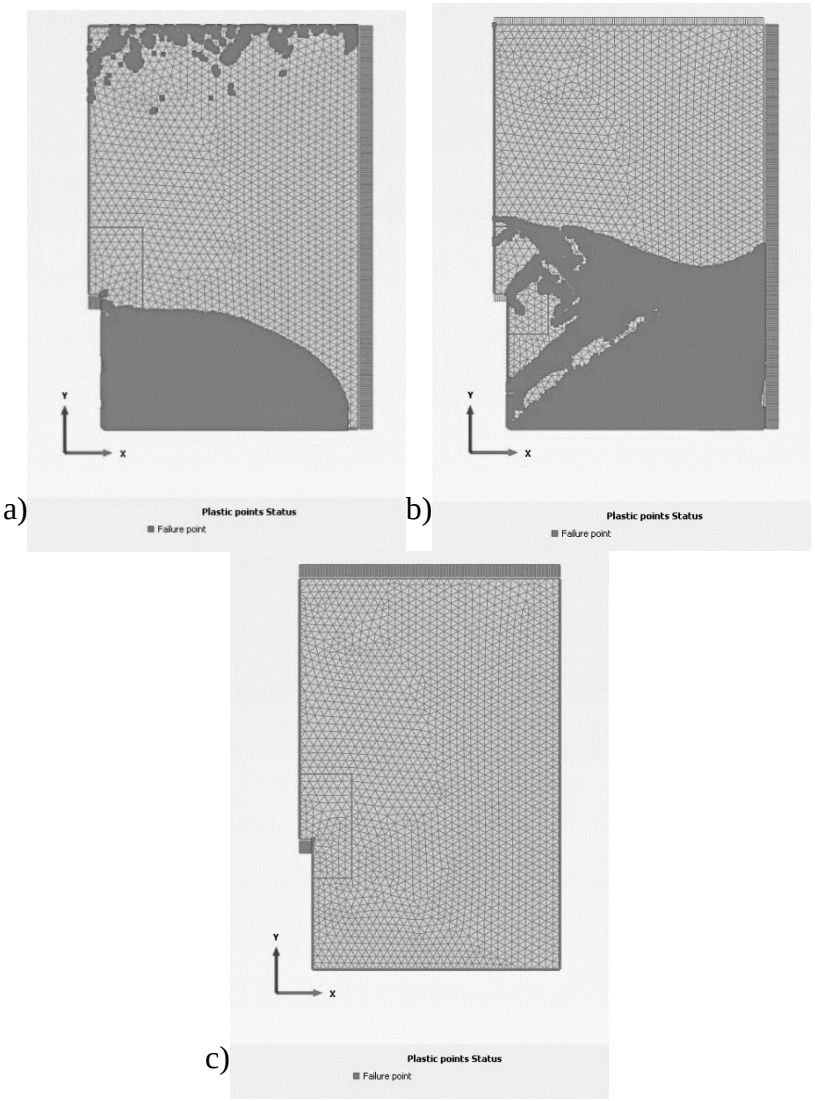


Figure 4.1 Comparison of boundary changes a ) free with surcharge *x*-max boundary and normally fixed *y*-max boundary, b) free with surcharge *x*-max and *y*-max boundaries, and c) normally fixed *x*-max boundary and free with surcharge *y*-max boundary ($k_h$=0.35 and default undrained parameters)

## 4.2 Examination of Axisymmetric Pseudo Static Results

The failure tunnel pressure has been calculated for a number of $k_h$ values between 0 and 0.5 using the axisymmetric FEM model. These results for the undrained and drained axisymmetric FEM solutions are presented below and compared to the conclusions of Saada *et al.* (2013).

In the undrained axisymmetric FEM solution significant plastic deformation was observed in the excavation phase when higher values of $k_h$ were applied to the simulations for undrained shear strength of 50kPa and 100kPa and unit weight of 25kN/m$^3$. The corresponding tunnel face failure pressure values have been excluded from the results as the start of the tunnel face failure phase cannot be considered elastic. The results of the pseudo static analysis and the effect of undrained shear strength are shown in Figure 4.2a. The analysis generally predicts a linear increase in tunnel face support pressure with $k_h$. The slope of the linear relationship was found to be between 8.8 and 9.9. This was calculated using the least-squares analysis available in Microsoft Excel. For all fitted straight lines, the $R^2$ value was greater than 0.97 indicating excellent agreement between the results and the linear model (Mendenhall, 1979). The slope for 50kPa was 9.8, 100kPa was 9.5, 200kPa was 8.8 and 400kPa was 9.7. This indicates there is no apparent relationship between undrained shear strength and slope. Figure 4.2b shows the influence of other variables on the undrained axisymmetric FEM solution. It can be seen that the behaviour is comparable to that in Figure 4.2a. Using Microsoft Excel, the slope of the linear relationship was found to be between 7.8 and 8.6. For all straight lines fitted, the $R^2$ value was greater than 0.97 indicating excellent agreement between the results and the linear model (Mendenhall, 1979). The increase in confining pressure resulted in a slope of 7.8. This is less than the prediction for default parameters. The change in unit weight had very little effect on the slope of the relationship, decreasing slightly to 8.6. These results suggest that seismic actions have a significant undesirable effect on tunnel face support pressure. Moreover, the relationship between tunnel face support pressure and $k_h$ is approximately linear in the undrained case. This is consistent with the results of Saada *et al.* (2013). The slope of the linear behaviour is not noticeably influenced by the undrained shear strength of the soil or the unit weight. The confining pressure may influence the slope, with larger confining pressures reducing the slope and thus the effect of seismic loading.

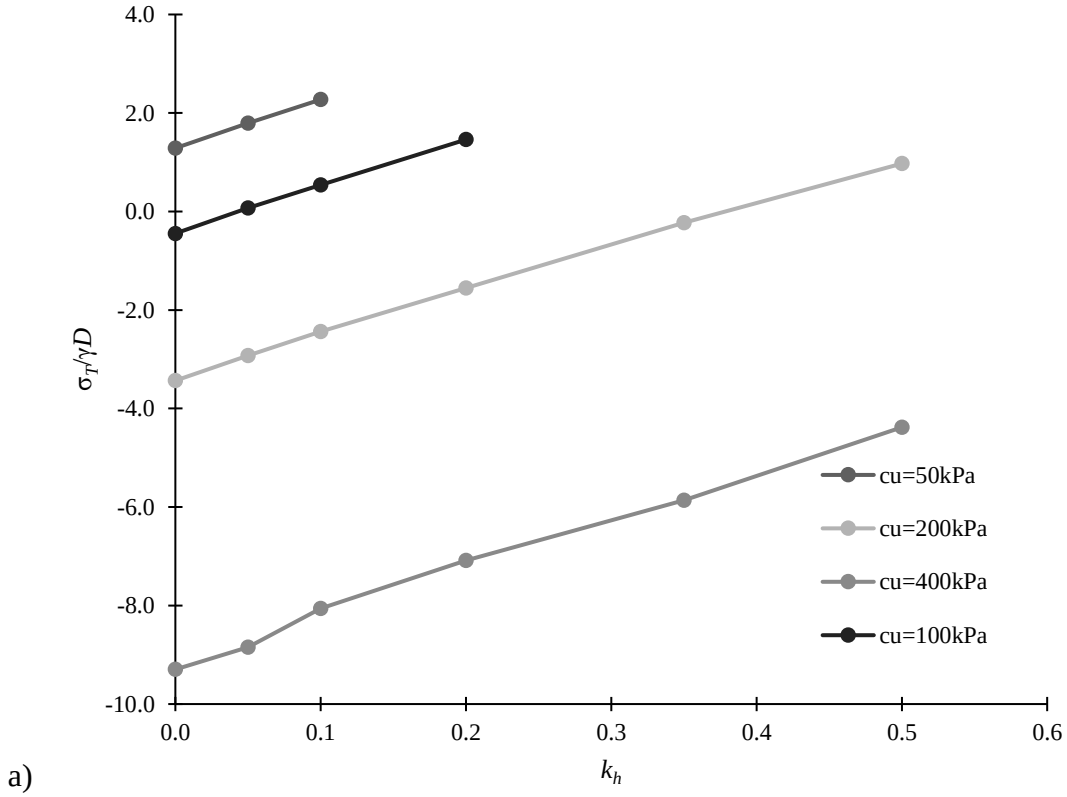


a)

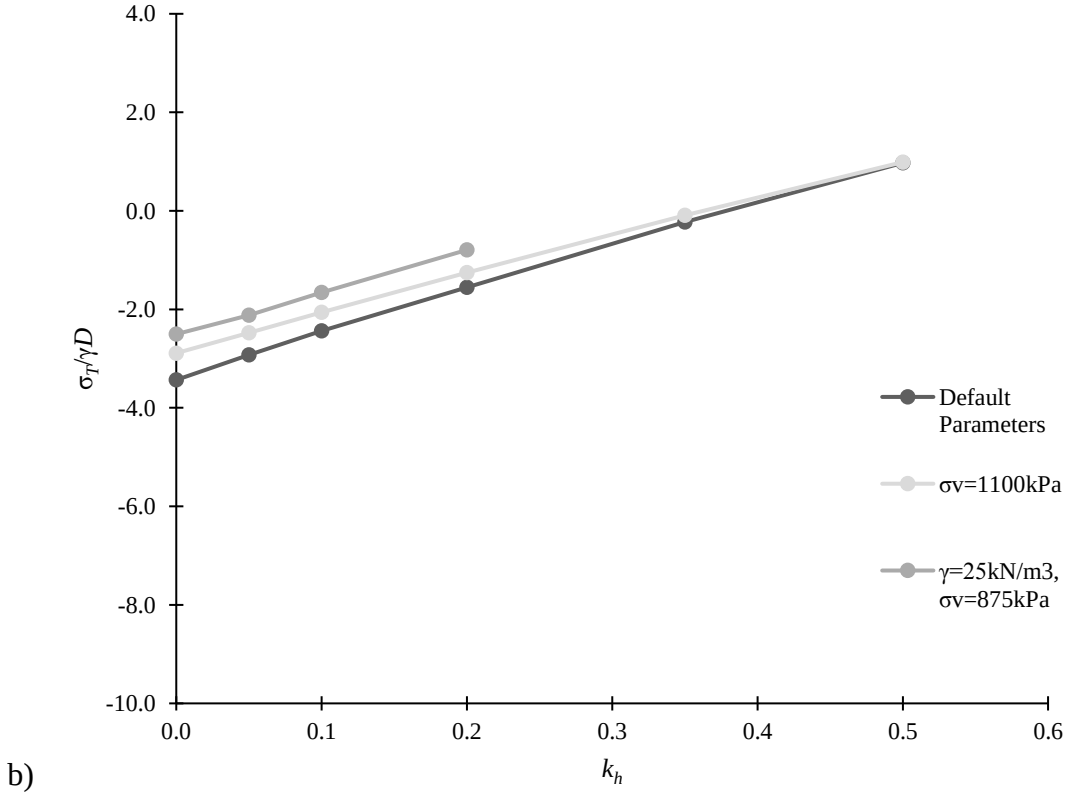


b)

Figure 4.2 Effect of a) undrained shear strength and b) other parameters, and $k_h$ on tunnel face stability using the undrained pseudo static axisymmetric FEM solution

In the drained analysis, no significant plastic deformation in the excavation phase was observed at any $k_h$ for any of the parameters investigated, so all values are presented. The results of the pseudo static analysis and the effect of effective friction angle are shown in Figure 4.3a. The analysis predicts an increase in tunnel face support pressure with $k_h$. The relationship is not perfectly linear but can be approximated using a linear model over the values of $k_h$ that are likely to be of interest. Using Microsoft Excel, the slope of the linear relationship was found to be between 0.36 and 1.15. For all linear approximations the $R^2$ value was greater than 0.97 indicating excellent agreement between the results and linear model (Mendenhall, 1979). More complex models, such as exponential, are more complicated and provide very little improvement of fit. The slope was found to be 0.35 for the analysis at 35°, 1.15 for the analysis at 20°, and 0.67 for the analysis at 27°. This indicates that decreasing the friction angle tends to increase the influence of $k_h$. Using Microsoft Excel, it was found that the slope of the linear relationship decreased by 0.05 for each degree increase in effective friction angle. The $R^2$ value was greater than 0.97 indicating the linear model is an excellent fit. Figure 4.3b shows the influence of other variables on the drained axisymmetric FEM solution. It can be seen that the behaviour is generally parallel to the line of default values, the variation in slope is comparatively smaller than that in Figure 4.3a. The slope of the linear relationship was found to be between 0.42 and 0.67 using Microsoft Excel. For all linear approximations the $R^2$ value was greater than 0.97 indicating excellent agreement between the results and the linear model (Mendenhall, 1979). The change in effective cohesion had no effect on the slope of the relationship. There was no change from the slope of the default parameters, 0.67. The increase in confining pressure resulted in a reduction of slope to 0.42. The change in unit weight had very little effect on the slope of the relationship, decreasing slightly to 0.54. These results suggest that seismic actions have a significant undesirable effect on tunnel face support pressure. Moreover, that relationship between tunnel face support pressure and $k_h$ is linear in the drained case. This is consistent with both the results of the undrained case and the results of Saada *et al.* (2013). The slope of the linear behaviour appears to be influenced by the effective friction angle of the soil. Larger values for the friction angle decrease the slope. This indicates a reduction in the effect of the seismic loading on tunnel face stability. As in the undrained case, the

slope of the linear behaviour is not noticeably influenced by the effective cohesion of the soil or the unit weight. Again, like the undrained case, the confining pressure appears to influence the slope, with larger confining pressures reducing the slope and thus the effect of seismic loading. The effects of changing the confining pressure were not found to be consistent with the limit analysis solutions in section 3.1. As the undrained solution also indicates the same reduction of seismic loading with increased depth, this is unlikely to be due to the imprecision of the model.

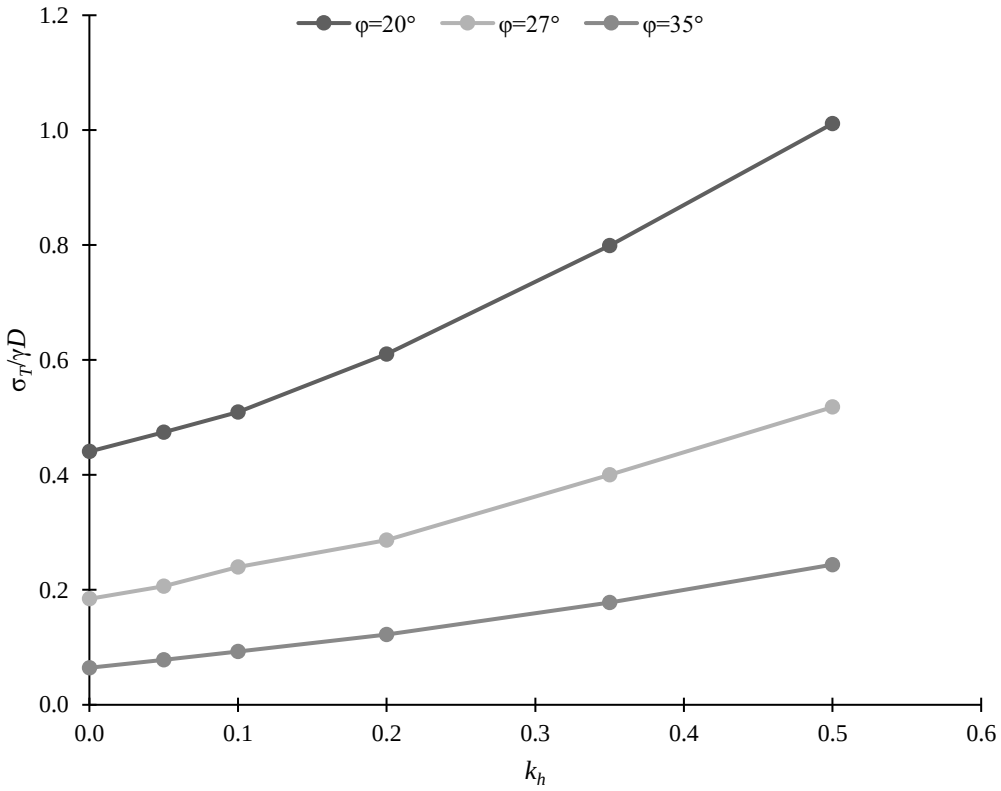


a)

Figure 4.3 Effect of a) effective friction angle and b) other parameters, and $k_h$ on tunnel face stability using the drained pseudo static axisymmetric FEM analysis

b)

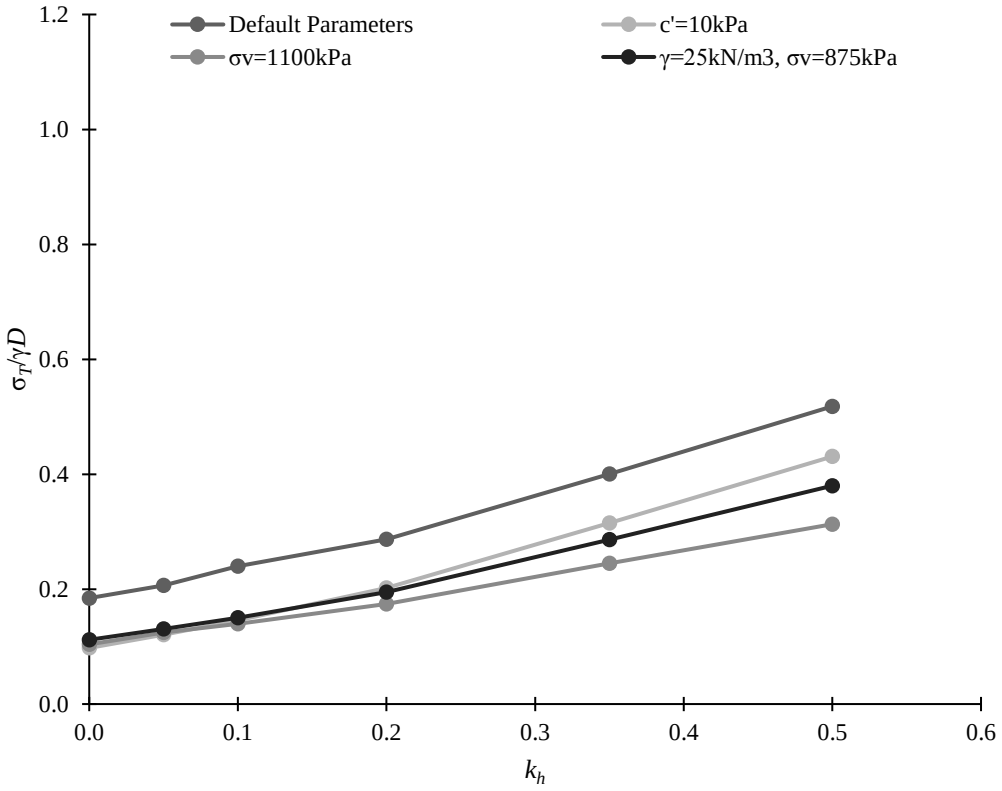


Figure 4.3 Continued

Figure 4.4 shows the effect of seismic loading compared to the uncertainties of the limit analysis. In Figure 4.4a the results from the undrained seismic axisymmetric FEM solution are compared to the case-2 and case-3 lower and upper bounds of Davis *et at.* (1980)'s solution. Only the analysis using the default parameters is shown. It is predicted that the variation with seismic loading is smaller than the uncertainty of the limit analysis solution. The static failure tunnel face support pressure is in the middle of the bounds of the limit analysis solution. For larger values of $k_h$ the seismic results are outside the bounds of the limit analysis solution. In Figure 4.4b the results from the drained seismic axisymmetric FEM solution are compared to the lower and upper bounds of Leca and Dormieux (1990)'s solution. Only the analysis using the default parameters is shown. It is predicted that the variation with seismic loading is smaller than the uncertainty of the limit analysis solution. Even for larger values of $k_{h,}$ the seismic results are within bounds of the limit analysis solution.

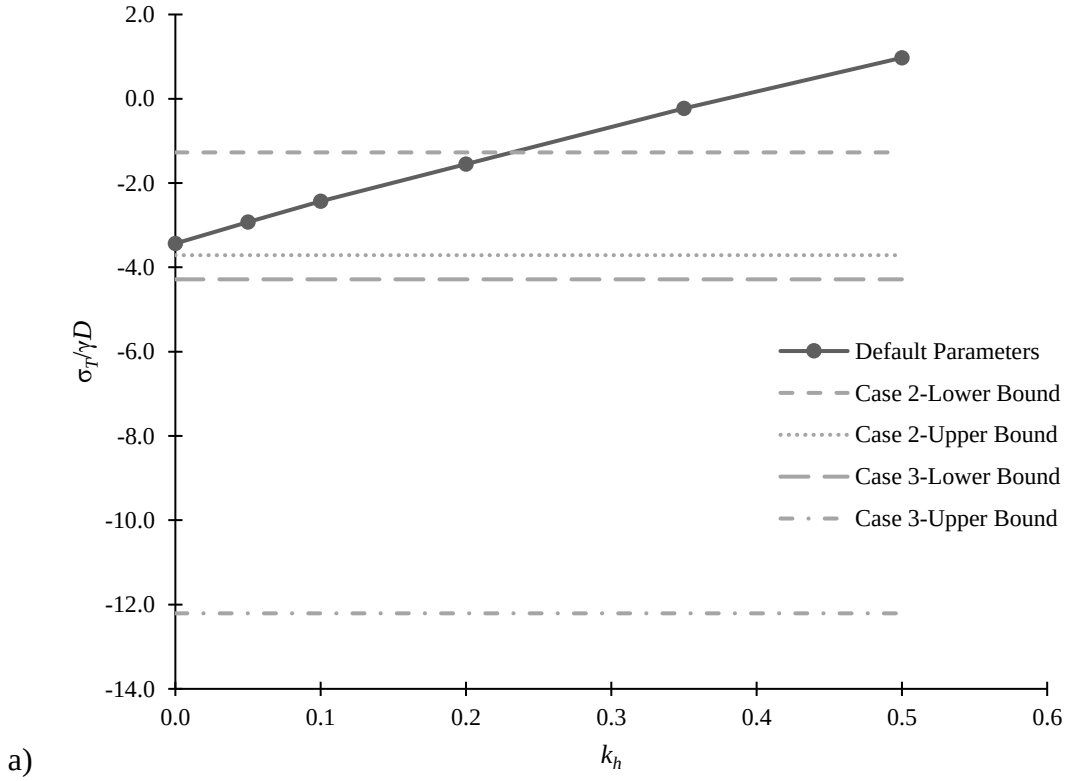


a)

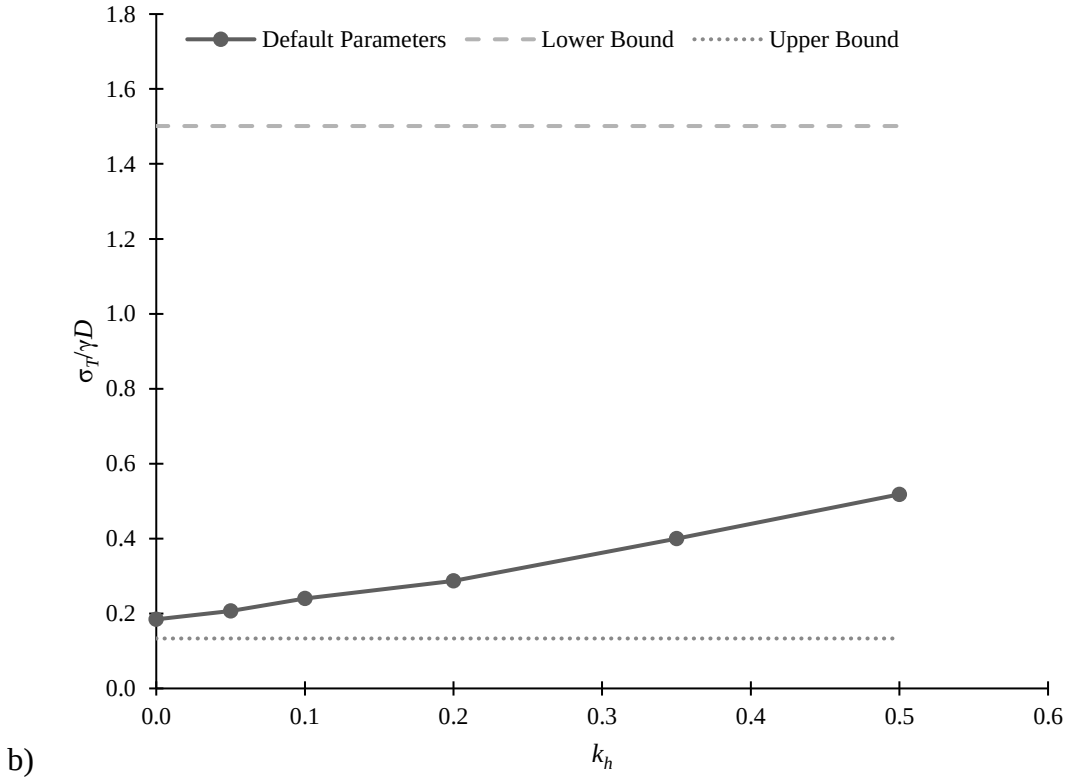


b)

Figure 4.4 Comparison of seismic effects on tunnel face stability and uncertainty between lower and upper bounds in limit analysis for a) undrained and b) drained using default parameters

## 4.3 Development of Seismic Design Factors

Both the results of this investigation and the results of Saada *et al.* (2013) suggest that the effect of seismic loading is linear. The drained axisymmetric results also indicate that the slope may be dependent on the effective friction angle of the material. The confining pressure also appears to influence the slope.

The seismic effect on tunnel stability could be accounted for by using a seismic design factor, $S_D$. This would be added to the normalised static tunnel face failure pressure to get a value for seismic design:

$$\sigma_{T_N\,Eq} = \sigma_{T_N\,Static} + S_D \qquad (\ 4.1\ )$$

$S_D$ represents the seismic portion of the loading. From the relationships discussed in section 4.2 it should be dependent on $k_h$ in undrained case and, on both $k_h$ and the effective friction angle in the drained case. The effect of confining pressure has not been included due to the limited simulations, uncertainties in the model and additional complexity required to include it. This gives two forms of $S_D$, for undrained;

$$S_D = C_S k_h \qquad (\ 4.2\ )$$

And for drained;

$$S_D = (C_S + C_\varphi(\varphi_0 - \varphi))k_h \qquad (\ 4.3\ )$$

Where;

$C_S$ is a coefficient based on the slope of linear relationship between the tunnel face support pressure and $k_h$.

$C_\varphi$ is a coefficient based on the influence of the effective friction angle on the slope. It is positive if increasing the friction angle reduces the slope.

$\varphi_0$ is the value of the effective friction angle for which $C_S$ is chosen.

Using the results discussed in section 4.2, values have been selected to compare the axisymmetric FEM solution results with the predictions using the proposed seismic design factor. The values for $C/D = 3$ have been used. This uses the larger results for

confining pressure and thus are considered conservative. The comparison is presented in Figure 4.5. For the undrained analysis only one coefficient must be selected, $C_S$. The slope was found to vary from around 7 to 10. $C_S = 9$ has been used in the prediction. This gives an undrained seismic design factor of;

$$S_D = 9k_h \qquad (4.4)$$

Figure 4.5a compares this prediction to the undrained axisymmetric FEM solution results using different values of undrained shear stress. It can be seen that the values calculated using the seismic design factor generally have good agreement with the axisymmetric FEM solution results.

For the drained analysis three coefficient must be selected, $C_S$, $C_\varphi$ and $\varphi_0$. From the results it was found that the influence of effective friction was approximately 0.05. Therefore $C_\varphi = 0.05$ has been used in the prediction. To select a value for $C_S$ first $\varphi_0$ must be selected. Most of the modelling has been done for an effective friction angle of 27°. $\varphi_0 = 27°$ has been used in the prediction. The corresponding value of $C_S = 0.7$ is used. This gives a drained seismic design factor of;

$$S_D = (0.7 + 0.05(27 - \varphi))k_h \qquad (4.5)$$

Figure 4.5b compares this prediction to the drained axisymmetric FEM solution results using different values of effective friction angle. It can be seen that the values calculated using the seismic design factor generally have good agreement with the axisymmetric FEM solution results. Although the relationship is not perfectly linear the linear model provides a good fit over the range of $k_h$ that has been considered. It is also significantly less complex than other models. These seismic design factors are preliminary. Good agreement has been found with the results from both undrained and drained axisymmetric FEM solutions. Further investigation should be done before the seismic design factors are applied in engineering practice. A large area of uncertainty is how the slope of the linear relationship between the tunnel face support pressure and $k_h$is affected by the effective friction angle in the drained case. Additionally, the effect of the confining pressure and therefore the depth of the tunnel should be investigated.

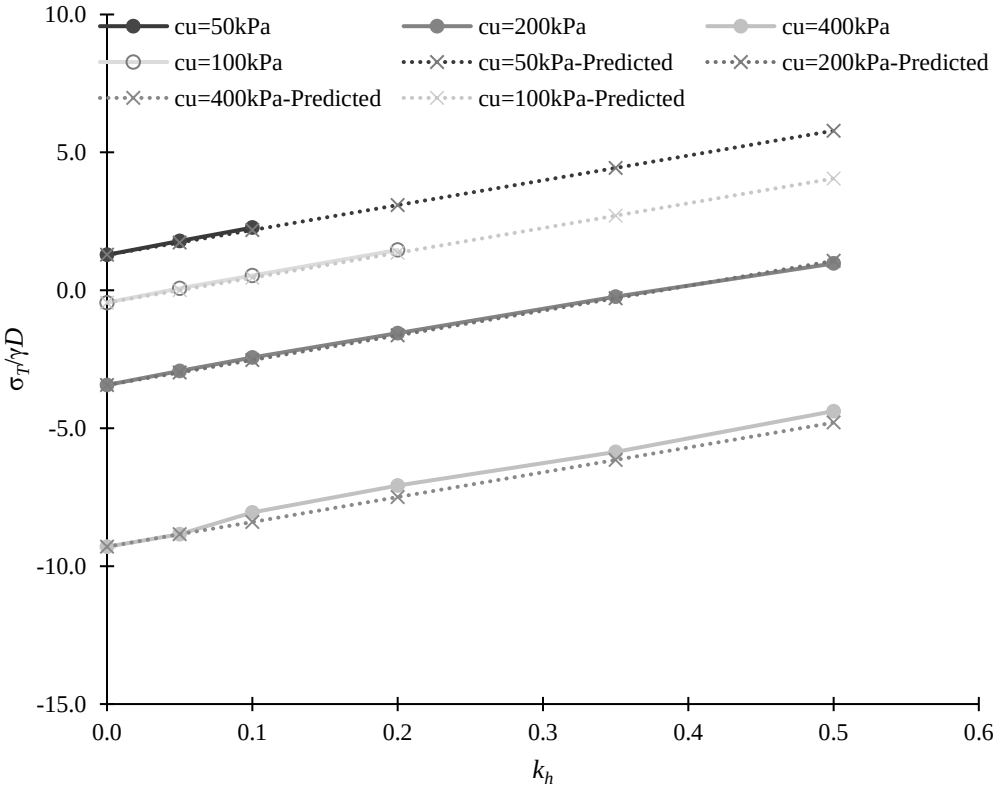


a)

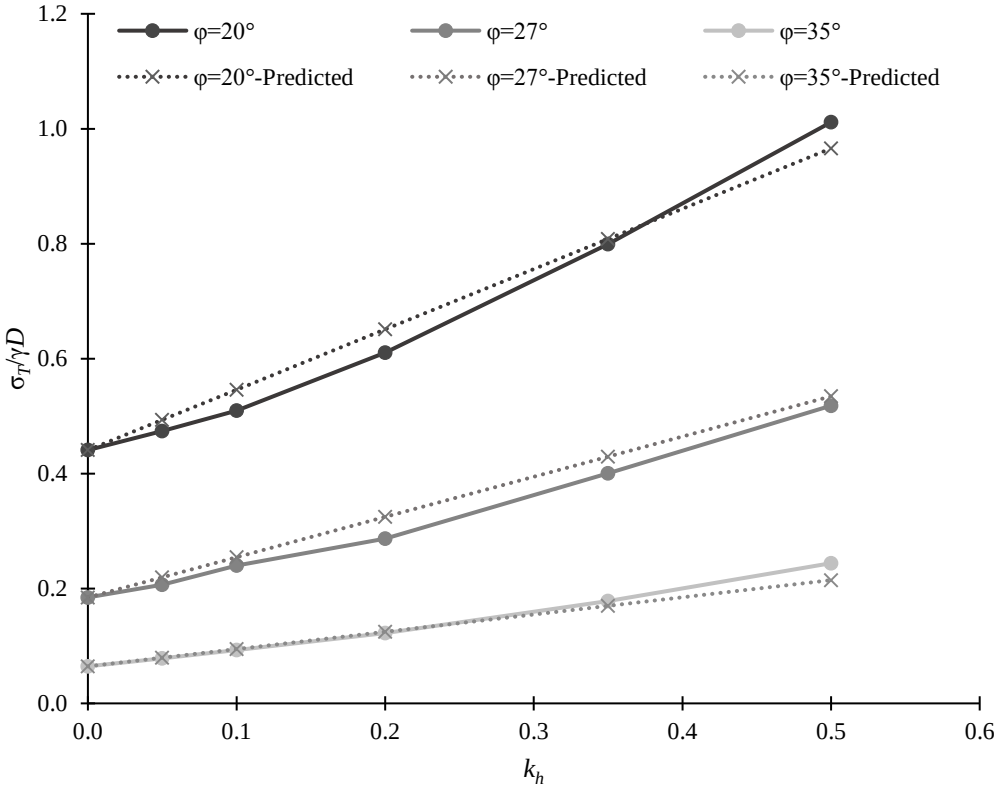


b)

Figure 4.5 Predicted tunnel face support pressure (dotted line), compared to axisymmetric results (solid line) for a) undrained and b) drained analysis

# CHAPTER 5

# SUMMARY AND CONCLUSIONS

This section sets out the summary, conclusions and recommendations for further investigation of this study.

## 5.1 Summary

This study investigated the effects of seismic loading on tunnel face stability. The static stability of tunnel faces has been widely studied, with the development of limit analysis and numerical modelling solutions. There has been some research into seismic stability of tunnels. This is generally limited to post construction and lining failure. Very little consideration of the effects of earthquakes on tunnel face stability has been undertaken.

An axisymmetric FEM model was developed in PLAXIS to investigate tunnel face stability of deep tunnels under seismic loading. Both undrained and drained conditions were investigated. The static results of the axisymmetric FEM solution were compared to selected limit analysis tunnel face stability solutions. It was found that the axisymmetric FEM solution results suggest the same behaviour as the limit analysis solutions for strength parameters. There were some inconsistencies when variations in unit weight and confining stress were compared. This is probably due to the assumptions required in setting up the axisymmetric FEM model.

Earthquake forces were applied to the axisymmetric FEM model using the pseudo static method. The effect of $k_h$ on tunnel face stability was investigated. The results suggest that seismic actions have a significant undesirable effect on tunnel face support pressure of deep tunnels. The results also suggest that relationship between tunnel face support pressure and $k_h$ can be approximated using a linear model. This is consistent with the conclusions from previous investigations of seismic tunnel face stability. The slope of the linear relationship appears to be influenced by the effective friction angle

of the soil in the drained solution. The slope of the linear relationship is not noticeably influenced by the effective cohesion of the soil, the undrained shear strength or the unit weight. In both the undrained and drained cases, the confining pressure appears to influence the slope of the linear relationship.

To account for the effects of earthquake loading during design a seismic design factor was developed using the pseudo static results. Due to the linear nature of the increase in tunnel face support pressure the seismic design factor was added to the static tunnel face failure pressure. The seismic design factor was dependant on $k_h$ in the undrained case, and both $k_h$ and the effective friction angle in the drained case. Any effect of confining pressure was not included due to uncertainty in the reliability of the model and the additional complexity required to include it. Suggestions for seismic design factors are preliminary and should not be applied in tunnel design practice.

This study is limited to deep tunnels, typically $C/D \geq 3$. It can probably be extended to $C/D \geq 2$ considering the failure mechanisms from experimental results and limit analysis solutions. It is also limited by the parameters used in the model; the effective friction angle is limited to between 25° and 35°, the effective cohesion to below 10 kPa, and the undrained shear stress is limited to below 400kPa. Unit weights of 20kN/m$^3$ and 25kN/m$^3$ have been considered and tunnel depth ratios of 3 and 5. Caution should be taken before extending the conclusions of this study.

## 5.2 Conclusions

The conclusions of this study are summarised below;

- The uncertainty between the lower and upper bounds of the limit analysis solutions is relatively large.

- When comparing the axisymmetric FEM and limit analysis solutions for tunnel face stability, similar trends in behaviour were found with variation of strength parameters: undrained shear strength, effective friction angle, and effective cohesion.

- When comparing the axisymmetric FEM and limit analysis solutions for tunnel face stability, the trends in behaviour found with variation of unit weight and confining pressure were less consistent with limit analysis results. It is likely that these inconsistencies are due to the assumptions and simplifications required for the simplification of the problem to an axisymmetric FEM model. The proposed axisymmetric FEM solution is considered appropriate for investigating the effect of seismic loading.

- Results indicate that earthquakes are likely to have significant undesirable effects on tunnel face stability of deep tunnels, independent of material parameters and tunnel depth. The effects increase with an increase in $k_h$. The relationship between tunnel face support pressure and $k_h$ is generally linear; a constant increase in tunnel face support pressure with increasing $k_h$. In drained behaviour tunnel face stability is more likely to be affected by seismic loading when the surrounding material is weaker. These findings are consistent with the study of seismic tunnel face stability using limit analysis by Saada *et al.* (2013).

- The results suggest a seismic design factor could be added to the static tunnel face support pressure for deep tunnels. For undrained analysis it is suggested that the seismic design factor be dependent on $k_h$. For drained analysis it is suggested that the seismic design factor be dependent on $k_h$ and the effective friction angle.

- Although the seismic acceleration has an effect on tunnel face stability, the uncertainty in the estimation of tunnel face stability from limit analysis solutions is larger. It is suggested that the focus should be on the design of static tunnel face stability. Seismic issues may not be of concern if sufficient safety is used in design to ensure static tunnel face stability, particularly in areas of lower seismicity. Seismic design of tunnel face stability is likely to be important in areas with high seismicity and where soil is likely to exhibit undrained behaviour under seismic loading.

## 5.3 Further Investigation

There are a number of areas where further investigation is suggested:

- The effect of unit weight and confining stress/depth on tunnel face stability in the axisymmetric FEM model should be investigated further.

- The appropriateness of the suggested seismic design parameters, particularly over a larger range of material parameters and model depths, and the slope coefficients applied.

- The relationship between effective friction angle and slope coefficient should be confirmed and quantified.

- The effect of the confining pressure and therefore the depth of the tunnel on the linear relationship between the tunnel face support pressure and $k_h$ should be investigated.

- The effect of seismic loading on shallow tunnels should be investigated to generalise the results to all tunnel design, including shallow tunnels and a wider range of parameters.

## REFERENCES


Argyroudis, S., Pitilakis, K., Boussoulas, N., Nakou, F. (2007) "Vulnerability Assessment of Shallow Metro Tunnels," Proceedings of 4th International Conference on Earthquake Geotechnical Engineering, Thessaloniki, Greece.

Atkinson, J. (2007) The Mechanics of Soils and Foundations, CRC Press, London, United Kingdom.

Brinkgreve, R., Kumarswamy, S., Swolfs, W. (2017) 2D Plaxis - Reference Manual, Plaxis, Delft, The Netherlands.

Broms, B., Bennermark, H. (1967) "Stability of clay in vertical openings," J. Soil Mech. Fdns Div. Am. Soc. Civ. Engrs, Vol. 193, pp. 71-94.

Chambon, P., Corté, J. (1994) "Shallow Tunnels in Cohesionless Soil: Stability of Tunnel Face," Journal of Geotechnical Engineering, Vol. 120, No.7, pp. 1148-1165.

Chambon, P., Corte, J. (1989) "Stabilité du front de taille d'un tunnel faiblement enterré: modélisation en centrifugeuse," Proceedings of international Conference Tunnelling and Microtunneling in Soft Ground: From Field to Theory. Paris, France, pp. 307-315.

Chen, W., Liu, X. (1990) Limit analysis in soil mechanics, Elsevier, Amsterdam, The Netherlands.

Cuvillier, A. (2001) "Aspects mécaniques du creusement d'un tunnel en milieu poreux saturé," Individual Study, Ecole Nationale des Ponts et Chaussées, France.

Davis, E., Gunn, M., Mair, R., Seneviratine, H. (1980) "The stability of shallow tunnels and underground openings in cohesive material," Géotechnique, Vol. 30, No. 4, pp. 397-416.

Hashash, Y., Hook, J., Schmidt, B., Yao, J. (2001) "Seismic Design and Analysis of Underground Structures", Tunnelling and Underground Space Technology, Vol. 16, pp. 247-293.

Hashash, Y., Park, D., Yao, J. (2005) "Ovaling deformations of circular tunnels under seismic loading, an update on Seismic design and analysis of underground structures," Tunnelling and Underground Space Technology, Vol. 20, pp. 435-441.

Hoek, E. (2001) "Big Tunnels in Bad Rock," Journal of Geotechnical and Geoenvironmental Engineering, Vol. 127, No. 9, pp. 726-740.

Hoek, E., Brown, E. (1997) “Practical estimates of rock mass strength,” International Journal of Rock Mechanics and Mining, Vol. 34, No. 8, pp. 1165-1186.

Hoek, E., Carranza-Torres, C., Corkum, B. (2002) “Hoek-Brown failure criterion-2002 edition,”. Proceedings of the North American Rock Mechanics Society Meeting, Toronto, Canada, pp. 267-273.

Huang, M., Song, C. (2013) “Upper-bound stability analysis of a plane strain heading in non-homogeneous clay,” Tunnelling and Underground Space Technology, Vol. 38, pp. 213-223.

Ladd, C., Foot, R., Ishihara, K., Schlosser, F., Poulos, H. (1997) “Stress-deformation and strength characteristics,” Proceedings of the 9th International Conference on Soil Mechanics and Foundation Engineering, Tokyo, Japan. Vol. 2, pp. 421–494

Leca, E., Dormieux, L. (1990) “Upper and lower bound solutions for the face stability of shallow circular tunnels in frictional material,” Géotechnique, Vol. 40, No. 4, pp. 581-606.

Leca, E., Panet, M. (1988) “Application du Calcul a la Rupture a la stabilitb du front de taille dun tunnel,” Revue FranGaise de Giotechnique, Vol. 43, pp. 5-19.

Lee, I., Nam, S., Ahn, J. (2003) “Effect of seepage forces on tunnel face stability,” Canadian Geotechnical Journal, Vol. 40 No. 2, pp. 342-350.

Lu, X., Wang, H., Huang, M. (2014) “Upper Bound Solution for the Face Stability of Shield Tunnel below the Water Table,” Mathematical Problems in Engineering, Vol. 2014, Article ID 727964, pp. 1-11.

Mair, R. (1979) “Centrifugal modelling of tunnel construction in soft clay,” Individual Study, University of Cambridge, United Kingdom.

Mendenhall, W. (1979) Introduction to Probability and Statistics, 5th ed, Duxbury Press., N. Scituate, MA: United States of America

Mollon, G., Dias, D., Soubra, A. (2013) “Range of the Safe Retaining Pressures of a Pressurized Tunnel Face by a Probabilistic Approach,” Geoenvironmental Engineering, Vol. 139, No. 11, pp. 1954-1967.

Pastor, J. (1978) “Analyse limite: determination numérique de solutions statistiques completes. Application au talus vertical,” J. Méc. appl, Vol. 2, No. 2, pp. 167-196.

Perazzelli, P., Leone, T., Anagnostou, G. (2014) “Tunnel face stability under seepage flow conditions,” Tunnelling and Underground Space Technology, Vol. 43, pp. 459-469.

Potts, D. M., Zdravkovic, L. (2001) Finite Element Analysis in Geotechnical Engineering: Volume two – Application, Thomas Telford Ltd., London, United Kingdom

Saada, Z., Maghous, S., Garnier, D. (2013) "Pseudo-static analysis of tunnel face stability using the generalized Hoek–Brown strength criterion," Int. J. Numer. Anal. Meth. Geomech, Vol. 37, p. 3194–3212.

Sahoo, J., Jyant, K. (2012) "Seismic stability of a long unsupported circular tunnel," Computers and Geotechnics, Vol. 44, pp. 109-1165.

Shalabi, F. (2005) "FE analysis of time-dependent behavior of tunneling in squeezing ground using two different creep models," Tunnelling and Underground Space Technology, Vol. 20, No. 3, pp. 271-279.

Shin, J., Potts, D., Zdravkovic, L. (2002) "Three-dimensional modelling of NATM tunnelling in decomposed granite soil," Géotechnique, Vol. 52, No. 3, pp. 187-200.

Sozio, L. (2005) "Analytical stability models for tunnels in soil," Proceedings of Geotechnical aspects of underground construction in soft ground: proceedings of the 5th International Conference of TC28 of the ISSMGE, Taylor & Francis, The Netherlands pp. 299-304.

Suzuki, T. (2000) "The Axisymmetric Finite Element Model developed as a Measure to evaluate Earthquake Responses of seismically isolated Tunnels," Proceedings of 12th World Conference on Earthquake Engineering, Auckland, New Zealand

Üçer, S. (2012) "Seismic Response and Vulnerability Assessment of Tunnels: A Case Study on Bolu Tunnels," Individual Study, Middle East Technical University, Ankara, Turkey.

Wilson, D.W., Abbo, A.J., Sloan, S.W., Lyamin, A.V. (2011) "Undrained stability of a circular tunnel where the shear strength increases linearly with depth," Canadian Geotechnical Journal, Vol. 48, No. 9, pp. 1328-1342.

Zhang, C., Han, K., Zhang, D. (2015) "Face stability analysis of shallow circular tunnels in cohesive–frictional soils," Tunnelling and Underground Space Technology, Vol. 50, pp. 345-357.

# APPENDIX A

## SCREENSHOTS OF SPREADSHEET

Screenshots from the spreadsheet developed for the assessment of tunnel face stability using limit analysis are presented below. Equation references are from the papers of Davis *et at.* (1980) and Leca and Dormieux (1990). An electronic copy of the spreadsheet can be obtained through personal communication with the author.

### Sheet-Input and Output

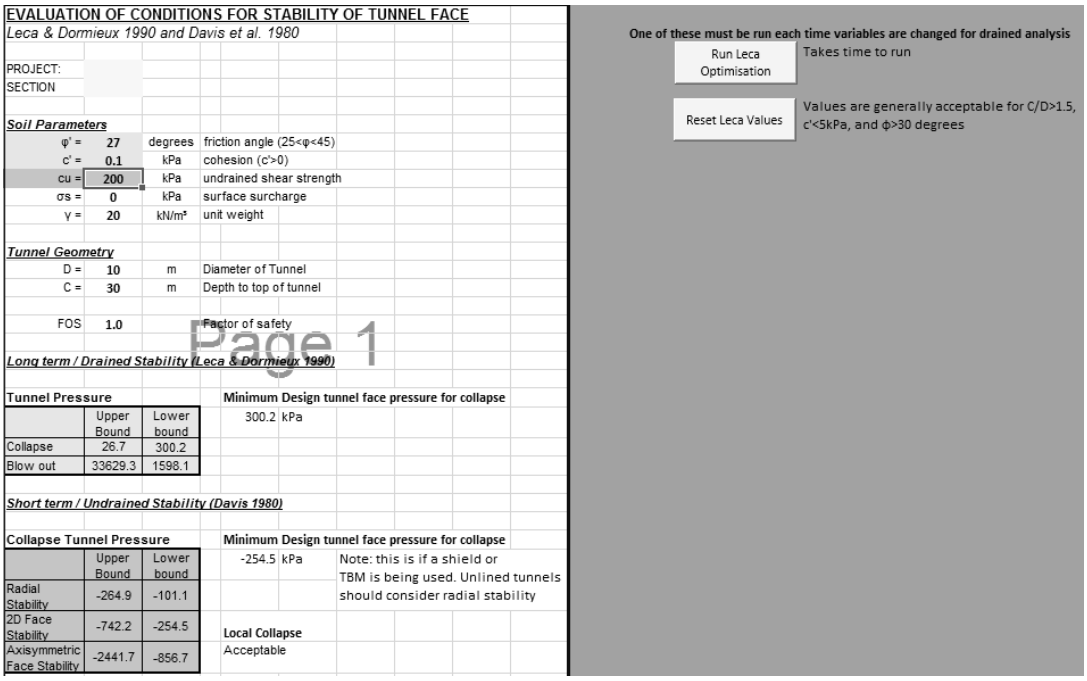

EVALUATION OF CONDITIONS FOR STABILITY OF TUNNEL FACE

*Leca & Dormieux 1990 and Davis et al. 1980*

PROJECT:

SECTION

***Soil Parameters***

| | | | |
|---|---|---|---|
| φ' = | 27 | degrees | friction angle (25<φ<45) |
| c' = | 0.1 | kPa | cohesion (c'>0) |
| cu = | 200 | kPa | undrained shear strength |
| σs = | 0 | kPa | surface surcharge |
| γ = | 20 | kN/m³ | unit weight |

***Tunnel Geometry***

| | | | |
|---|---|---|---|
| D = | 10 | m | Diameter of Tunnel |
| C = | 30 | m | Depth to top of tunnel |
| FOS | 1.0 | | Factor of safety |

Page 1

***Long term / Drained Stability (Leca & Dormieux 1990)***

**Tunnel Pressure**

| | Upper Bound | Lower bound |
|---|---|---|
| Collapse | 26.7 | 300.2 |
| Blow out | 33629.3 | 1598.1 |

**Minimum Design tunnel face pressure for collapse**

300.2 kPa

***Short term / Undrained Stability (Davis 1980)***

**Collapse Tunnel Pressure**

| | Upper Bound | Lower bound |
|---|---|---|
| Radial Stability | -264.9 | -101.1 |
| 2D Face Stability | -742.2 | -254.5 |
| Axisymmetric Face Stability | -2441.7 | -856.7 |

**Minimum Design tunnel face pressure for collapse**

-254.5 kPa

Note: this is if a shield or TBM is being used. Unlined tunnels should consider radial stability

**Local Collapse**

Acceptable

**One of these must be run each time variables are changed for drained analysis**

Run Leca Optimisation — Takes time to run

Reset Leca Values — Values are generally acceptable for C/D>1.5, c'<5kPa, and ϕ>30 degrees

# Sheet-Leca 1990 Calculation

| | | | | | | | | | | |
|---|---|---|---|---|---|---|---|---|---|---|
| **Leca Calibration** | | | | | | | | | | |
| the limits for the calibration of α are | | | | +/- | 20 | 0.34907 | | | | |
| | Reccome | min | max | | | | | | | |
| MI | 35.5 | 15.5 | 55.5 | 0.61959 | 0.27053 | 0.96866 | | | | |
| MII | 35.5 | 15.5 | 55.5 | 0.61959 | 0.27053 | 0.96866 | | | | |
| MIII | 49 | 29 | 69 | 0.85521 | 0.50615 | 1.20428 | | | | |
| **Inputs** | | | | | | | | | | |
| | | | | | | | | | | |
| ϕ' | 27 | degrees | friction angle | | | | | | | |
| c' | 0.1 | kPa | cohesion | | | | | | | |
| σs | 0 | kPa | surface surcharge | | | | | | | |
| D | 10 | m | Diameter of Tunnel | | | | | | | |
| C | 30 | m | Depth to top of tunnel | | | | | | | |
| γ | 20 | kN/m3 | unit weight | | | | | | | |
| | | | | | | | | | | |
| ϕ'rad | 0.47124 | radians | friction angle in radians | | | | | | | |
| H | 35 | m | | | eq 1 | | | | | |
| C/D | 3 | | | | | | | | | |
| | | | | | | | | | | |
| σc | 0.32637 | kPa | unconfined compr | | eq 2 | | | | | |
| Ka | 0.37552 | | Active Rankine ea | | eq 3 | | | | | |
| Kp | 2.66294 | | Passive Rankine e | | eq 4 | | | | | |
| | | | | | | | | | | |
| Qs | 1 | | | | eq 7a | | | | | |
| Qγ | 1019.05 | | | | eq 7c | | | | | |
| | | | | | | | | | | |
| **upper bound solution** | | | | | | | | | | |
| **MI** | | | | | | | min | max | | |
| α | 0.62582 | | initial guess shou | | eq 10 | 0.61959 | 0.35779 | 0.88139 | | |
| ground surface check | | | | | | 35.5 | | | | |
| 7 | <= | 1.17365 | | | eq 63 | | | | | |
| ground is not reached Rd=0 | | | | | | | | | | |
| | | | | | | | | | | |
| Rb | 0.55719 | | | | eq 42b | | | | | |
| Rd | 0 | | | | eq 42d | | | | | |
| Re | 0.49703 | | | | eq 42e | | | | | |

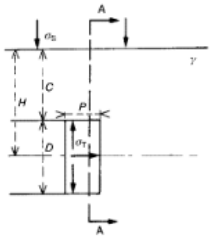


| | | | | | | | | | | |
|---|---|---|---|---|---|---|---|---|---|---|
| | 0 | | | | | | | | | |
| Ns | 0 | these need to be maximise | | | eq 61 | | | | | |
| Nγ | 0.13423 | | | | eq 62 | | | | | |
| | | | | | | | | | | |
| calculati | 0 | | | | | | | | | |
| Qt | 136.79 | | | | eq 8 | | | | | |
| σt | 26.6503 | | | | eq 7b | | | | | |
| | | | | | | | | | | |
| **MII** | | | | | | | min | max | | |
| α | 0.61047 | | initial guess shou | | eq 10 | 0.61959 | 0.35779 | 0.88139 | | |
| β | 1.09063 | | | | eq 66b | | | 62.4886 | | |
| ground surface check | | | | | | | | | | |
| 3 | <= | 0.30041 | | | eq 119 | | | | | |
| ground is not reached Re=0 | | | | | | | | | | |
| | | | | | | | | | | |
| Ra | 0.76555 | | | | eq 85 | | | | | |
| Rb | 0.57511 | | | | eq 86 | | | | | |
| Rc | 0.40177 | | | | eq 87 | | | | | |
| Re | 0 | | | | eq89 | | | | | |
| | 0 | | | | | | | | | |
| Ns | 0 | these need to be maximise | | | eq 117 | | | | | |
| Nγ | 0.13437 | | | | eq 118 | | | | | |
| | | | | | | | | | | |
| calculation of Qt and then allowable tunnel pressure | | | | | | | | | | |
| Qt | 136.926 | | | | eq 8 | | | | | |
| σt | 26.6771 | | | | eq 7b | | | | | |
| | | | | | | | | | | |
| **MIII** | | | | | | | min | max | | |
| α | 0.8544 | | initial guess shou | | eq 11 | 0.85521 | 0.59341 | 1.11701 | | |
| | | | | | | | | | | |
| Ra | 0.31157 | | | | eq 138a | | | | | |
| Rb | 0.45418 | | | | eq 138b | | | | | |
| Rc | 9.17308 | | | | eq 138c | | | | | |
| | | | | | | | | | | |
| Ns | 122.661 | these need to be minimise | | | eq 155 | | | | | |
| Nγ | 168.027 | | | | eq 156 | | | | | |

| | | | | | |
|---|---|---|---|---|---|
| calculation of Qt and then allowable tunnel pressure | | | | | |
| Qt | 171351 | | | | eq 9 |
| σt | 33629.3 | | | | eq 7b |
| | | | | | |
| **Lower bound** | | | | | |
| **SI** | | | | | |
| collapse | | | | | |
| Nsc- | 0.37552 | | | | eq 17a |
| Nγc- | 1.5021 | | | | eq 17b |
| | | | | | |
| Qt | 1531.09 | | | | eq 15 |
| σt | 300.297 | | | | eq 7b |
| | | | | | |
| Blow out | | | | | |
| Nsb- | 2.66294 | | | | eq 17c |
| Nγb- | 7.98882 | | | | eq 17d |
| | | | | | |
| Qt | 8143.68 | | | | eq 16 |
| σt | 1598.09 | | | | eq 7b |
| | | | | | |
| **SII** | | | | | |
| collapse | | | | | |
| Nsc- | 0.01477 | | | | eq 18a |
| Nγc- | 0 | | | | |
| | | | | | |
| Qt | 0.01477 | | | | eq 15 |
| σt | -0.19336 | | | | eq 7b |
| | | | | | |
| Blow out | | | | | |
| Nsb- | 8.97644 | | | | eq 18b |
| Nγb- | 0 | | | | |
| | | | | | |
| Qt | 8.97644 | | | | eq 16 |
| σt | 1.56546 | | | | eq 7b |
| | | | | | |
| **SIII** | | | | | |
| collapse | | | | | |
| Nsc- | 0.00155 | | | | eq 19a |
| Nγc- | 0 | | | | |
| | | | | | |
| Qt | 0.00155 | | | | eq 15 |
| σt | -0.19596 | | | | eq 7b |
| | | | | | |
| Blow out | | | | | |
| Nsb- | 11.3628 | | | | eq 19b |
| Nγb- | 0 | | | | |
| | | | | | |
| Qt | 11.3628 | | | | eq 16 |
| σt | 2.03381 | | | | eq 7b |
| | | | | | |
| | **Summary** | | | | |
| MI | Ns | 0 | | | |
| MI | Nγ | 0.13423 | | | |
| MI | σt | 26.6503 | | | |
| MII | Ns | 0 | | | |
| MII | Nγ | 0.13437 | | | |
| MII | σt | 26.6771 | | | |
| MIII | Ns | 122.661 | | | |
| MIII | Nγ | 168.027 | | | |
| MIII | σt | 33629.3 | | | |
| SI | Nsc | 0.37552 | | | |
| SI | Nγc | 1.5021 | | | |
| SI | σtc | 300.297 | | | |
| SI | Nsb | 2.66294 | | | |
| SI | Nγb | 7.98882 | | | |
| SI | σtb | 1598.09 | | | |
| SII | Nsc | 0.01477 | | | |
| SII | σtc | -0.19336 | | | |
| SII | Nsb | 8.97644 | | | |
| SII | σtb | 1.56546 | | | |
| SIII | Nsc | 0.00155 | | | |
| SIII | σtc | -0.19596 | | | |

| | | |
|---|---|---|
| SIII | Nsb | 11.3628 |
| SIII | σtb | 2.03381 |
| | | |
| Bracketing values | | |
| lower bo | Nsc- | 0.00155 |
| | NSc+ | 0 |
| | Nγc- | 1.5021 |
| | Nγc+ | 0.13437 |
| | Nsb- | 2.66294 |
| | Nsb+ | 122.661 |
| | Nγb- | 7.98882 |
| | Nγb+ | 168.027 |
| | | |
| | σtc- | 300.224 |
| | σtc+ | 26.6771 |
| | σtb- | 1598.09 |
| | σtb+ | 33629.3 |

# Sheet-Davis 1990 Calculation

**Davis calculation**

**Inputs** Fig 2

| | | | |
|---|---|---|---|
| cu | 200 | kPa | cohesion |
| σs | 0 | kPa | surface surcharge |
| D | 10 | m | Diameter of Tunnel |
| C | 30 | m | Depth to top of tunnel |
| γ | 20 | kN/m3 | soil unit weight |
| γD/cu | 1 | | |
| C/D | 3 | | |

**Local Collapse**

| | | |
|---|---|---|
| γD/cu ma | 5.63 | page 412 |
| | ok | |

**Case 1** fig 3

figure 15 shows all

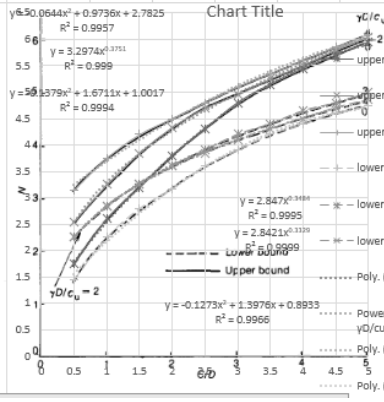


| | bound | upper | upper | upper | lower | lower | lower | |
|---|---|---|---|---|---|---|---|---|
| | γD/cu | 0 | 2 | 4 | 0 | 2 | 4 | |
| C/D | | upper - γ | upper - γ | upper - γ | lower - γ | lower - γ | lower - γD/cu=4 | |
| | 0.5 | 1.75 | 2.55 | 3.15 | 1.45 | 2.25 | 2.25 | |
| | 1 | 2.6 | 3.25 | 3.75 | 2.25 | 2.85 | 2.85 | |
| | 1.5 | 3.2 | 3.85 | 4.2 | 2.8 | 3.25 | 3.25 | |
| | 2 | 3.8 | 4.33333 | 4.5 | 3.16667 | 3.6 | 3.6 | |
| | 2.5 | 4.3 | 4.7 | 4.8 | 3.6 | 3.9 | 3.85 | |
| | 3 | 4.8 | 4.95 | 5.1 | 3.9 | 4.2 | 4.1 | |
| | 3.5 | 5.15 | 5.25 | 5.35 | 4.2 | 4.4 | 4.3 | |
| | 4 | 5.45 | 5.5 | 5.6 | 4.4 | 4.65 | 4.5 | |
| | 4.5 | 5.7 | 5.8 | 5.85 | 4.6 | 4.8 | 4.7 | |
| | 5 | 5.95 | 6.05 | 6.1 | 4.75 | 5 | 4.85 | |
| | best fit | polynom | power | polynom | polynom | power | power | |
| | | -0.13788 | -0.10606 | -0.06439 | -0.12727 | -0.08333 | -0.08409 | ax^2+bx+c |
| | | 1.67106 | 1.31788 | 0.97356 | 1.39758 | 1.04136 | 1.00735 | ax^2+bx+c |
| | | 1.00167 | 2.02 | 2.7825 | 0.89333 | 1.82833 | 1.86417 | ax^2+bx+c |
| | | 0.99935 | 0.99472 | 0.99574 | 0.99657 | 0.9974 | 0.99528 | r2 |
| | | 0.53791 | 0.37511 | 0.2851 | 0.51053 | 0.34845 | 0.33287 | ax^**b** |
| | | 2.5864 | 3.29738 | 3.76244 | 2.18914 | 2.84698 | 2.84214 | ax^b |
| | | 0.99776 | 0.99904 | 0.99503 | 0.99203 | 0.99951 | 0.99987 | r2 |

**Fig. 15. Upper and lower bound stability ratios for plane strain circular tunnels**

| | | | | | | | |
|---|---|---|---|---|---|---|---|
| 3 | 4.67029 | 4.97898 | 5.14631 | 3.83581 | 4.1748 | 4.09701 | |

| | |
|---|---|
| N+ | 4.82463 |
| N- | 4.00531 |
| σt+ | -264.927 |
| σt- | -101.061 |

**Case 2** fig 4

equations taken from fig 19

| | |
|---|---|
| N+ | 7.2111 |
| N- | 4.77259 |
| σt+ | -742.221 |
| σt- | -254.518 |

**Case 3** fig 20

equations taken from fig 21

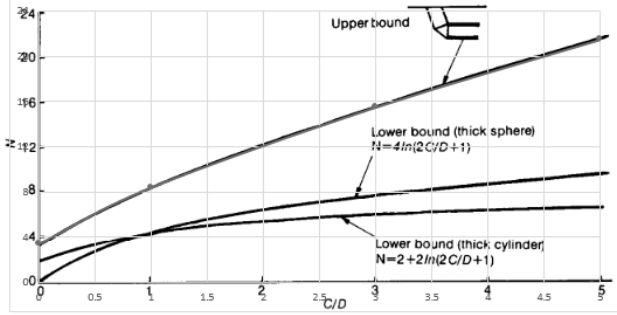


| | |
|---|---|
| | upper bound |
| C/D | N |
| 0 | 3.4 |
| 1 | 8.4 |
| 3 | 15.5 |
| 5 | 21.5 |
| | power |
| | -0.23656 ax^2+bx+c |
| | 4.75691 ax^2+bx+c |
| | 3.56683 ax^2+bx+c |
| | 0.99909 r2 |

| | |
|---|---|
| our case | |
| C/D | N |
| 3 | 15.7085 |

**Fig. 21. Stability solutions for the circular tunnel heading**

| | |
|---|---|
| N+ | 15.7085 |
| N- | 7.78364 |

| | | |
|---|---|---|
| σt+ | -2441.71 | |
| σt- | -856.728 | |
| | | |
| **Summary** | | |
| Case 1 | N+ | 4.82463 |
| Case 1 | N- | 4.00531 |
| Case 1 | σt+ | -264.927 |
| Case 1 | σt- | -101.061 |
| Case 2 | N+ | 7.2111 |
| Case 2 | N- | 4.77259 |
| Case 2 | σt+ | -742.221 |
| Case 2 | σt- | -254.518 |
| Case 3 | N+ | 15.7085 |
| Case 3 | N- | 7.78364 |
| Case 3 | σt+ | -2441.71 |
| Case 3 | σt- | -856.728 |
| | | |
| | Braketing values | |
| Radial | N+ | 4.82463 |
| Radial | N- | 4.00531 |
| Face | N+ | 15.7085 |
| Face | N- | 7.78364 |
| Wall | N+ | 7.2111 |
| Wall | N- | 4.77259 |
| Radial | σt+ | -264.927 |
| Radial | σt- | -101.061 |
| Face | σt+ | -2441.71 |
| Face | σt- | -856.728 |
| Wall | σt+ | -742.221 |
| Wall | σt- | -254.518 |
| Partial Fa | σt | 671 |